การติดตามการทรุดตัวของกรุงเทพมหานครและปริมณฑล โดยใช้เทคนิค INSAR TIME SERIES ANALYSIS

นายอนุเผ่า อบแพทย์

วิทยานิพนธ์นี้เป็นส่วนหนึ่งของการศึกษาตามหลักสูตรปริญญาวิศวกรรมศาสตรดุษฎีบัณฑิต
สาขาวิชาวิศวกรรมสำรวจ ภาควิชาวิศวกรรมสำรวจ
คณะวิศวกรรมศาสตร์ จุฬาลงกรณ์มหาวิทยาลัย
ปีการศึกษา 2555

INSAR TIME SERIES ANALYSIS FOR LAND SUBSIDENCE MONITORING IN BANGKOK AND ITS VICINITY AREA

MR.ANUPHAO AOBPAET

A Dissertation Submitted in Partial Fulfillment of the Requirements

for the Degree of Doctor of Philosophy Program in Geomatics Engineering

Department of Survey Engineering

Faculty of Engineering

Chulalongkorn University

Academic year 2012

Thesis Title	INSAR TIME SERIES ANALYSIS FOR LAND SUBSIDENCE MONITORING IN BANGKOK AND ITS VICINITY AREA
By	Mr. Anuphao Aobpaet
Field of Study	Geomatic Engineering
Thesis Advisor	Associate Professor Itthi Trisirisatayawong, Ph.D.

Accepted by the Faculty of Engineering, Chulalongkorn University in Partial Fulfillment of the Requirements for the Doctoral Degree

……Dean of the Faculty of Engineering
(Associate Professor Boonsom Lerdhirunwong, Dr.Ing.)

THESIS COMMITTEE

…….. Chairman
(Associate Professor Banjerd Phalakarn, Ph.D.)

……. Thesis Advisor
(Associate Professor Itthi Trisirisatayawong, Ph.D.)

…….. Examiner
(Associate Professor Vichai Yiengveerachon)

…….. Examiner
(Thongtit Chayakula, Ph.D.)

…….. External Examiner
(Chaowalit Silapathong, Ph.D.)

อนุเผ่า อบแพทย์ : การติดตามการทรุดตัวของกรุงเทพมหานครและปริมณฑลโดยใช้เทคนิค INSAR Time Series Analysis. (INSAR TIME SERIES ANALYSIS FOR LAND SUBSIDENCE MONITORING IN BANGKOK AND ITS VICINITY AREA)
อ. ที่ปรึกษาวิทยานิพนธ์หลัก : รศ.ดร.อิทธิ ตริสิริสัตยวงศ์, 87 หน้า.

จากข้อมูลงานสำรวจระดับตั้งแต่ต้นปี 2513 พบว่าเกิดแผ่นดินทรุดบริเวณเขตกรุงเทพมหานครและปริมณฑล ถึงแม้ว่าค่าจากการทำระดับจะมีความน่าเชื่อถือและมีความถูกต้องสูง แต่ก็มีข้อจำกัดสำคัญสองประการได้แก่ 1) สามารถตรวจสอบค่าการทรุดตัวได้เฉพาะตามแนวถนนหรือพื้นที่ที่สามารถเข้าถึงได้และ 2) เป็นเทคนิคที่ต้องใช้เวลาและกำลังคนมาก ซึ่งเป็นเงื่อนไขที่ทำให้การเพิ่มจำนวนจุดตรวจสอบทำได้ลำบาก โครงข่ายระดับตรวจสอบการทรุดตัวที่มีอยู่มีความหนาแน่นของจุดวัดน้อยกว่า 1 จุด/กม.^{2} ซึ่งต่ำเกินกว่าที่จะให้ภาพการเปลี่ยนแปลงของค่าการทรุดตัวที่แปรผันอย่างรวดเร็วทางตำแหน่งได้อย่างถูกต้อง

การวิจัยนี้ใช้เทคนิค InSAR ซึ่งเป็นเทคนิคทางเรดาร์ที่สามารถใช้เป็นเครื่องมือในการวัดระยะทางหรือการเปลี่ยนแปลงของระยะทางจากสายอากาศเรดาร์กับวัตถุที่สนใจบนพื้นดิน เพื่อใช้วัดค่าการทรุดตัวของแผ่นดิน วัตถุประสงค์หลักของงานวิจัยคือการประยุกต์ใช้เทคนิคเฉพาะของ InSAR 2 วิธีร่วมกัน ได้แก่ Persistent Scatterer (PS) และ small baseline (SB) เพื่อวัดค่าการทรุดตัวที่เกิดขึ้นด้วยการวิเคราะห์ข้อมูลจากดาวเทียมเรดาร์ โดยทั้ง 2 วิธีใช้ภาพจากดาวเทียม Radarsat-1 จำนวน 19 ภาพ ในช่วงเดือนตุลาคม 2548 ถึงมีนาคม 2553 ครอบคลุมพื้นที่ส่วนใหญ่ของกรุงเทพมหานครและพื้นที่บางส่วนของจังหวัดนนทบุรี ปทุมธานี และสมุทรปราการ ผลการวิจัยได้จุดตรวจสอบมากกว่า 300,000 จุด และความหนาแน่นของจุดประมาณ 120 จุด/กม.^{2} ซึ่งจำนวนจุดที่ได้จาก InSAR มีความหนาแน่นมากพอที่จะใช้แก้ปัญหา under-sampling และความลำเอียงของข้อมูลระดับได้

ผลลัพธ์จาก InSAR แสดงให้เห็นว่าอำเภอเมือง จังหวัดสมุทรปราการและอำเภอลำลูกกา จังหวัดปทุมธานี มีการทรุดตัวอย่างรวดเร็วในอัตรา 20-30 มม./ปี ส่วนใจกลางกรุงเทพฯ ด้านตะวันออกของแม่น้ำเจ้าพระยามีลักษณะการทรุดค่อนข้างช้ากว่าในอัตราประมาณ 10 มม./ปี ในขณะที่บริเวณชานเมืองทางทิศเหนือและทิศตะวันตกพบอัตราการทรุดตัวอยู่ที่ 10-20 มม./ปี นอกจากนี้ InSAR ยังแสดงให้เห็นการทรุดตัวอย่างรวดเร็วในเขตสะพานสูงและลาดกระบัง กรุงเทพฯ ซึ่งเป็นพื้นที่ที่ไม่มีข้อมูลจากงานระดับ การทดสอบทางสถิติ (t-test) เพื่อเปรียบเทียบอัตราการทรุดตัวที่ได้จากการสำรวจระดับและ InSAR ในพื้นที่ 71 แห่ง พบว่าใน 52 จาก 65 บริเวณ มีอัตราที่สอดคล้องกัน นอกจากนี้ยังมี 10 พื้นที่ที่อัตราการทรุดตัวที่ได้จากข้อมูล InSAR มีขนาดใหญ่กว่า ซึ่งพบในบริเวณชานเมืองที่มีความหนาแน่นของสิ่งปลูกสร้างน้อย และมีช่องว่างระหว่างอาคารค่อนข้างกว้าง ทำให้มีโอกาสที่จะมีการสะท้อนของเรดาร์ในแบบ double-bounce จากตึกไปสู่พื้นดิน ซึ่งจะทำให้ได้อัตราการทรุดตัวที่เร็วกว่า นอกจากนี้ยังพบว่าพื้นที่ 3 แห่งที่ InSAR มีอัตราการทรุดตัว ที่ช้ากว่านั้นสามารถอธิบายได้ด้วยปัญหา phase unwrapping ผลการวิจัยนี้สามารถสรุปได้ว่า InSAR สามารถใช้เป็นเครื่องมือทางด้านยีออเดติก สำหรับตรวจสอบและติดตามแผ่นดินทรุดได้เป็นอย่างดี อย่างไรก็ตามยังมีความจำเป็นที่จะต้องคงหมุดระดับบางส่วนไว้สำหรับเป็นจุดตรวจสอบ และสำหรับเป็นข้อมูลเพื่อวิเคราะห์การทรุดตัวในบางพื้นที่ที่ InSAR ยังมีข้อจำกัดและให้ผลลัพธ์ที่ไม่น่าเชื่อถือ

ภาควิชา วิศวกรรมสำรวจ ลายมือชื่อนิสิต .....

สาขาวิชา วิศวกรรมสำรวจ ลายมือชื่อ อ. ที่ปรึกษาวิทยานิพนธ์หลัก .....

ปีการศึกษา 2555 .....

5071876521 : MAJOR GEOMATIC ENGINEERING

KEYWORDS : INSAR, TIME SERIES ANALYSIS, LAND SUBSIDENCE, STAMPS-MTI

ANUPHAO AOBPAET : INSAR TIME SERIES ANALYSIS FOR LAND SUBSIDENCE MONITORING IN BANGKOK AND ITS VICINITY AREA.

ADVISOR : ASSOC. PROF. ITTHI TRISIRISATAYAWONG, Ph.D., 87 pp.

Since early 1970s, leveling data has revealed land subsidence occurring in Bangkok and surrounding provinces. Though leveling is reliable and accurate, serious drawbacks of the technique are that 1) it measures only places that accessible by roads and 2) it is time-consuming and labor-intensive. Consequently, the density of measuring points is less than one point/km^2 which is far too low to capture short wavelength phenomena like land subsidence.

This research applies InSAR, a space-based radar technique which can accurately measure distance or change of distance from radar antenna to objects of interest on the ground, to measure land subsidence. A main objective is to apply a combination of two specific methods of InSAR namely Persistent Scatterer (PS) and Small Baseline (SB) to measure occurring subsidence from radar data. PS and SB were employed to analyze 19 images of Radarsat-1, the footprint of which covers most of Bangkok and certain areas of Nothaburi, Pathumthani and Samutprakarn, for the period October 2005 until March 2010. More than 300,000 points, yielding the density of 120 points/km^2 are detected as stable which can be treated like survey benchmarks. Thus, the number of points provided by InSAR and its density has largely overcome the under-sampling and bias problem of leveling data.

InSAR reveals that Muang, Samutprakarn and Lam luk ka, Pathumthani have been subsiding rapidly at the rate of 20-30 mm/yr. Central Bangkok on the east of Chao Phraya river appears to be subsiding slowly at rates around 10 mm/yr or slower while in northern and western suburban areas are found to subside at rates between 10-20 mm/yr. InSAR also shows fast subsiding areas in Saphansung and Ladkrabang district, Bangkok which have been missed by leveling due to its under sampling problem. At 71 locations where leveling and InSAR data of the same period are available, statistical test (t-test) of subsidence rates obtained from both methods found that 52 of 65 locations where InSAR results available within radius 100 m around leveling benchmarks are identical. Most of the 10 places where InSAR rates are larger are found to be in suburban areas where building density are low. Larger opening between buildings make it more likely for double-bounce of radar echo from building to ground slab to occur and so faster subsiding ground slab contaminated into that of building. The 3 areas where InSAR rates are slower can be explained by phase unwrapping problem. The research result leads to a conclusion that InSAR can be utilized as a geodetic tool to monitor land subsidence but a certain number of leveling points are still required as check points and for certain places where limitations of InSAR may provide unreliable rates.

Department : Survey Engineering Student's Signature .....

Field of Study : Geomatic Engineering Advisor's Signature .....

Academic Year : 2012

ACKNOWLEDGEMENTS

The positive thinking throughout the journey is the best solution for life. This thesis is the result of five years of work whereby I have been accompanied and supported by many people. It is a pleasure that I have now the opportunity to express my gratitude to all of them.

The first person I would like to thank is my advisor Assoc.Prof.Dr. Itthi Trisirisatayawong. I have been working under his supervision since the end of the year 2007 when I started my PhD study. He also gives me many best solutions in another path of my life. I would also like to thank the others members of my PhD committees who monitored my work and took effort in reading and providing me with valuable comments on this thesis: Assoc. Prof. Dr. Banjerd Phalakarn, Assoc. Prof. Vichai Yiengveerachon, Dr. Chaowalit Silapathong, and Dr. Thongtit Chayakula. I am also grateful to the members of Department of Survey Engineering at Chulalongkorn University for their cheerful assistance and nice comments.

In May 2008, I got the partial scholarship from the Alaska Satellite Facility of the Geophysical Institute at the University of Alaska Fairbanks for SAR/InSAR training course which made me have a chance to join SAR community and gain more knowledge/experience. I thank Dr. Nettie La Belle-Hamer, Dr. Franz Meyer, Dr. Rudi Gens, Wade Albright, and ASF team for their friendship and support when I stayed in Alaska.

I would like to thank people of InSAR group, Delft University of Technology, Netherlands namely Dr. Ramon F. Hanssen, Dr. Andrew J. Hooper, and Miguel Caro Cuensa, for their teaching and support. Thank you the European Union for funding my two visits to TUDelft through the joint Thailand_EU research project - GEO2TECDI and GEO2TECDI-SONG. The DORIS software package that is used in this research for generating interferograms is developed by the InSAR group of TUDelft. Special thanks go to Dr. Andrew Hooper for providing StaMPS-MTI software that has been used for time series analysis of land subsidence.

A special thanks goes to Royal Thai Survey Department for the support data of subsidence measurement from leveling. I would like to personally thank to Col.Dr. Ekkapop Panumastrakul and Lt.Col. Sarayut Yousamran for their kindly cooperation, suggestion on the leveling survey data used in this thesis.

I thank Dr. Chaiyapon Keeratikasikorn and Pattama Pordee who shared parts of my memorable time working, discuss, and experiencing InSAR together during my PhD period.

Finally, I am forever indebted to my mother, my father, and my brother for their constant support, encourage, and guidance. Thank you my wife and my daughter for their love and patience during the PhD period.

CONTENTS

Page

Page

LIST OF TABLES

Page

LIST OF FIGURES

Page

Page

Page

Page

LIST OF ABBREVIATIONS

3D	three-dimensional
AIT	Asian Institute of Technology
ALOS-PALSAR	Advanced Land Observing Satellite-Phased Array type L-band Synthetic Aperture Radar
AOE	Atmosphere and Orbit error phase
ASI	Italian Space Agency
BMA	Bangkok Metropolitan Administration
COSMO-SkyMed	Constellation of small Satellites for the Mediterranean basin Observation
CSA	Canadian Space Agency
DEM	Digital Elevation Model
DGR	Department of Groundwater Resources
DInSAR	Differential Interferometric Synthetic Aperture Radar
DLR	German Aerospace Center
DMR	Department of Mineral Resources
DORIS	Delft object-oriented radar interferometric software
ENVISAT	Environmental Satellite
ERS	European Remote Sensing Satellite
ESA	European Space Agency
GISTDA	Geo-Informatics and Space Technology Development Agency
GPS	Global Positioning System
INSAR	Interferometric Synthetic Aperture Radar
JAXA	Japan Aerospace Exploration Agency
JERS	Japanese Earth Resources Satellite
JICA	Japan International Cooperation Agency
LOS	Line of Sight
NASA	National Aeronautics and Space Administration
PGS	Product Generation System
PSI	Persistent Scatterer Interferometry
RADARSAT-1	Canadian synthetic aperture radar satellite 1

RMS	Root Mean Square
ROI_PAC	Repeat Orbit Interferometry Package
RTSD	Royal Thai Survey Department
SAR	Synthetic Aperture Radar
SB	Small Baseline
SCLA	Spatially Correlated Look Angle
SCP	Spatial correlated phase
SDFP	Slowly-decorrelating filtered phase
SIR-B	Shuttle Imaging Radar B
SLC	Single Look Complex
SNAPHU	Statistical-Cost, Network-Flow Algorithm for Phase Unwrapping
SNR	Signal to Noise ratio
StaMPS-MTI	Stanford Method for Persistent Scatterers with Multi-Temporal InSAR
TERRASAR-X	German Earth observation satellite
WGS84	World Geodetic Coordinate System 1984

CHAPTER I

INTRODUCTION

1.1 Background

The province of Bangkok, Thailand, is under a continuous threat of flooding. This region has a very low elevation, with height ranging from 0.5 to 1.50 m above mean sea level, and is situated on a river delta (figure 1.1). The area was already affected by major floods in 1983 and 2011. Monitoring of subsidence in Bangkok is therefore crucial, particularly as the city of Bangkok is the most populated metropolitan area of Thailand and the economical and political heart of the country. Subsidence in Bangkok and the surrounding areas was first detected in the late 1960s and early 1970s (Haley and Aldrich Inc., 1970; Brand et al., 1971; and Edward, 1976). However, surface subsidence was not measured quantitatively until 1978 (Nutalaya, 1981). Monitoring of land subsidence has been performed since then using leveling. Leveling benchmarks were installed in the late 1970s by Thai authorities, and their heights have been re-measured since then by the Royal Thai Survey Department (RTSD), which has also performed annual campaigns since 1978.

Leveling surveys revealed very high subsidence rates of up to 120 mm/yr from 1978 to 1981. Bontebal (2001) and Phien-wej et al. (2006) reported a decrease in the rates for later periods with values of around 35 mm/yr between 1985 and 1988 and 30 mm/yr between 1988 and 1991. The reduction in subsidence rates was caused by new laws, which were introduced in the late 1980s to decrease groundwater pumping. The maximum subsidence occurred around Ramkamhaeng University in the Bang Kapi district and the industrial area in the eastern part of Bangkok and Samut Prakarn province, (locations can be found in figure 1.1). The total subsidence measured in these areas reached maximum values of 950 mm from 1978 to 2000.

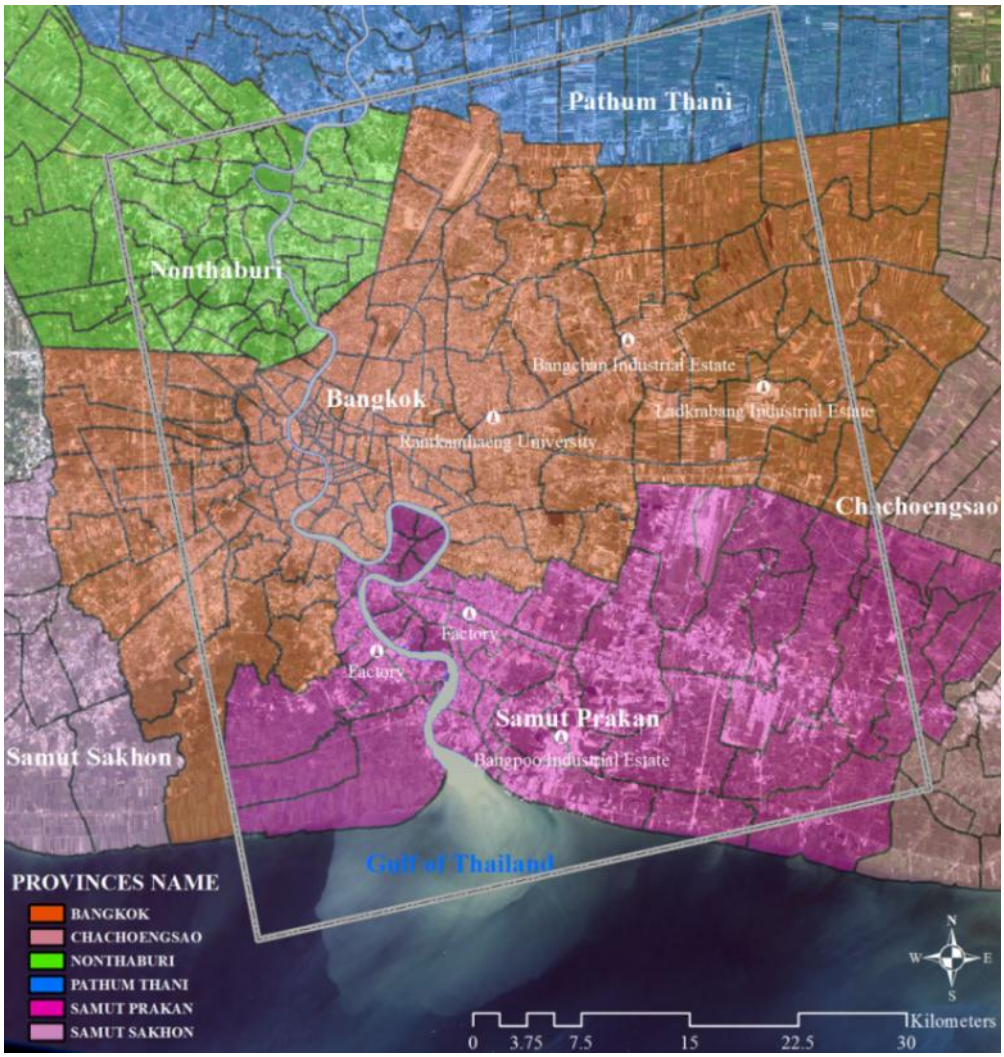

Figure 1.1 Bangkok and its vicinity area maps with the footprint of Radarsat-1 SAR imagery used in this thesis including locations of the past maximum subsidence area (Ramkamhaeng University, Bang kapi) and the industrial estate growth in the eastern part of Bangkok and Samut Prakarn province.

1.2 Research Motivation

Currently, the surveying technique for land deformation by using the space-borne Synthetic Aperture Radar (SAR) instrument has extensively increased the more interest for the scientist worldwide. The methodology of SAR Interferometry (InSAR) can detect ground displacement such as land subsidence, earthquake, land slide, etc. with relatively high precision. InSAR provides measurements of ground motion with high spatial and temporal resolution depending on the condition of available data.

In the case of land subsidence monitoring in Bangkok area, the leveling survey has been applied to measure subsidence rates, but this tool provides point measurements that are spatially and temporally limited. The temporal resolution depends on the yearly campaigns monitoring which is quite low. InSAR time series analysis, on the other hand, is employed in this study to provide the measurements of land subsidence at a significantly improved spatial resolution with millimeter-level accuracy covering large areas (2,500 km²). The more densely observation points from the technique can alleviate the under sampling problem of small scale phenomena like land subsidence.

Thus, the different characteristics of leveling and InSAR data can be integrated for subsidence monitoring, possibly resulting in more efficient monitoring strategies as complementary measurement techniques. This is very interested to perform land subsidence using InSAR time series analysis and compare the results with leveling survey in order to substantiate subsidence rate for the valuable practice.

1.3 Problem Statement

As reported in Phien-wej (2006), the land subsidence still continues with the average rates of approximately 20 mm/yr inside Bangkok. The geological setting of Bangkok further complicates the study of subsidence from leveling data. Features such as roads, pavement, and walkways lie on the soft clay ground surface, while most of buildings and bridges rest on piles standing on the deeper and less compressible sand layer 20-50 m beneath the surface. As a result of differing water content and physical properties, the subsidence rates of the soft clay layers are faster than those of the sand layer. This effect is exposed in figure 1.2(*a*) and figure 1.2(*b*) where the ground appears to subside faster than the buildings. The same situation can be found in other parts of the city. Most leveling monuments are metal plates fixed to bridges and public buildings. Ground monuments do exist, but they are usually destroyed or moved in a short time due to development and construction. As such, leveling data provide mainly subsidence rates of the sand layer, not those of the ground surface. These estimates are however of great value for many applications such as drainage and flood protection.

(*a*) (*b*)

Figure 1.2 Gaps opened due to differences between subsidence of the ground surface and buildings whose foundations rest on the sand layer found at earth observation center located near Ladkrabang district, Eastern Bangkok.

In the past, differential InSAR has been applied to the Bangkok metropolitan area; Kuehn et al. (2004) demonstrated that the maximum subsidence rate was 30 mm/yr in the southeast and southwest alongside Chao Phraya River during the time spanning February 1996 to October 1996. However, this result may not reflect accurately the actual deformation rates, because of the short time span and limited number of images used. InSAR time series analysis methods, namely persistent scatterer interferometry (PSI) (Ferretti et al., 2001; Hooper et al., 2006) and small baseline (SB) techniques (Berardino et al., 2002), were developed to address the limitations of differential InSAR such as atmospheric delay and loss of coherence. For this technique, the phase evolution of pixels is used to detect those that remain coherent within the time span covered by the data set. As a result, it is possible to detect and measure millimeter variations in the satellite line-of-site (Perissin, 2008). Moreover, the technique can provide a network of observations with a density of 100 observations per square kilometer, or more for urban areas compare to the leveling network. The precision of InSAR time series techniques can be on up to 1 mm/yr (Marinkovic et al., 2008).

Worawattanamateekul (2006) applied the PSI technique for deformation estimation in Bangkok using data acquired by ERS-1 and ERS-2, which covered the time period of 1992-2000. However, the study was limited by the coverage area which due to two adjacent tracks of data from the satellite giving the small area in eastern side of Chao Phraya river only up to 100 km^2 to be investigated. Thus, in this contribution, we will apply the Stanford Method for Persistent Scatterers (StaMPS) algorithm (Hooper et al., 2007) combined with a small baseline approach (Hooper, 2008) to the dataset of Radarsat-1 satellite using full scene basis. These algorithms can produce reasonable results, even for small number of images (Hooper et al., 2007).

1.4 Study Objectives

The goal of this research is to determine the subsidence rate in Bangkok and its vicinity area using InSAR time series analysis and to perform the validation of the results with leveling survey technique. The Stanford Method for Persistent Scatterers (StaMPS) algorithm combined with the application of a multi-temporal InSAR approach (MTI) is explored. Thus, the objectives of this work can be summarized as follows:

1. Evaluation of the performance of InSAR time series analysis technique to monitor land subsidence in Bangkok and its vicinity area.
2. Investigation of InSAR time series analysis technique developed and implemented in public domain software.
3. Evaluation on the potentialities and benefits of the integration of InSAR and leveling approaches.

1.5 Study Area and data description

The 19 Radarsat-1 images in F1N beam mode with nominal azimuth resolution 8.9 m and nominal range resolution 6.0 m in slant range are employed. The images cover an area approximately 2,500 km^2 centered in Bangkok (lat 13° 33' 44.37"N, long: 100° 38' 47.76"E). The footprint of scene location can be found in figure 1.1. The images were acquired between October 2005 and March 2010 in ascending orbit (Path-Row: 2-60). From the available radar images, fine beam mode is the best spatial resolution available for the Radarsat-1 system. Each original fine beam position can either be shifted closer to or further away from Nadir by

modifying timing parameters and adding 10 new positions with offset ground coverage. The resulting positions are denoted by either an N (Near) or F (Far). The swath width is 50 km to keep the downlink signal within its allocated bandwidth. All production requests were submitted through a Product Generation System (PGS) interface at GISTDA Earth observation center. The data employed in this research were single look complex (SLC) products, which are pre-processed in CEOS format.

1.6 Synopsis

This dissertation is composed of six chapters. The introduction and the objectives are presented in Chapter I. Reviews of basic SAR Interferometry for measuring land deformation are presented in Chapter II with the historical review and brief discussion of applications. Chapter III provides the background of land subsidence in Bangkok and its vicinity areas including the leveling and InSAR measurements for subsidence monitoring. Chapter IV presents the InSAR time series analysis with combined data set processing called Multi-temporal InSAR approach. The discussions of land subsidence rate comparing with leveling survey have been performed in Chapter V. The last chapter, Chapter VI summarizes the research results and suggests avenues for future work with the discussion on the potential for successful use of InSAR approaches to land subsidence and possibility to apply for the others land deformation.

CHAPTER II

SAR INTERFEROMETRY FOR MEASURING LAND DEFORMATIONS

2.1 Introduction

Essentially, there are two main characteristics which made InSAR technique very interesting to the scientific community and more effective than other widely used deformations measurement techniques. The first one is that it represents a line-of-sight deformation of the imaged terrain. Furthermore, a SAR image usually has the coverage area over ten kilometers in both azimuth and range directions, allowing the detection and monitoring of different land deformation regimes possible. Secondly, the most important factor is the high accuracy of measuring phase differences, so the results are then a two-dimensional high resolution image of the ongoing deformations measured with accuracies of a few millimeters and several kilometers wide.

The results of InSAR application have been achieved by analyzing a single differential interferogram derived from one pair of SAR images (2-pass DInSAR). This is the simplest configuration due to the limited data availability in the study area. However, this technique is suitable for monitoring a high magnitude deformation signals compared to the errors sources in areas that do not continue from significant temporal surface changes. Though, in areas with slow deformation rates, the estimation of the error sources such as atmospheric disturbances is necessary to obtain an acceptable accurate and reliable deformation estimates. Furthermore, the losses of coherence due to temporal decorrelation areas of vegetation limit the application of InSAR. A significant improvement in the quality of the results was obtained with the new methods using large stack of SAR images acquired over the same area with the same beam mode and look angle. These advanced techniques so call InSAR time series analysis represent an outstanding advance with respect to the standard method in terms of deformation modeling capabilities and quality of the deformation estimations. In this study, Persistent Scatterer Interferometry (PSI) and Small baseline approach is combined using StaMPS-MTI processor, which enables the detection of the slow earth surface deformation such as land subsidence monitoring at the millimeter level (Ferretti et al., 2000, 2001).

2.2 Historical Review

2.2.1 SAR missions and State-of-the-Art

The exploitation of imaging radar is able to be considered as one of the most remarkable remote sensing development tools. Graham (1974) was the first to introduce InSAR for topographic mapping using a military airborne SAR system configured as a cross-track interferometry. By employing two vertical separated antennas to receive backscattered signals from the terrain, he showed that the data extracted from the interferometer channel during system test and topographic map are within map accuracy standards. He also pointed out that there will be widely supplementary of improved capability for other methods of acquiring such data in the future.

Zebker and Goldstein (1986) presented the first practical results of InSAR topographic measurements by using an along-track interferometric SAR configured to measure radial velocity. Practically, they mounted two horizontal SAR antennas on an aircraft with a baseline of 11.1 m length. One antenna transmitted the radar signals, and the backscattered signals were received by the two antennas. The complex images are generated from this experiment which approximately 10 m resolution, but the accuracy was quite limited with elevation deviations of 2-10 m Root Mean Square (RMS) error over the ocean and with larger RMS values over the land. Nevertheless, the experiment showed the promise of the interferometric approach.

Gabriel and Goldstein (1988) first demonstrated single-antenna by adapted the existing interferometric technique to the cross-orbits using the Shuttle Imaging Radar (SIR-B) repeat-pass data. They are able to obtain an altitude map of the imaged region even the orbits were not parallel making the complicate refocusing and image registration. Thus, this applied technique was computationally complicated and required precise knowledge of orbit parameters. Afterward, Gabriel et al. (1989) introduced the differential interferometric approach by using two interferograms generated from repeat-pass SEASAT data to produce a double difference interferogram. The result was approved that InSAR could detect land deformation on the order of sub-centimeter accuracy. The study on using multiple baselines to detect topography was first presented by Li and Goldstein (1990). They found that the height measurements sensitivity is relative to the length of baseline. On the other hand, the phase error will be increased when baseline increased.

From July 1991, the data sets from C-band ERS-1 satellite by the European Space Agency (ESA) have been acquired for interferometry purpose on a routine basis. It was the first operational space borne system allowed comprehensive studies of land deformations, atmospheric effects, and temporal decorrelations in InSAR data. The applications were greatly extended following the launch of the ERS-2 satellite in April 1995 for the tandem mission of the ERS-1 and ERS-2 satellites acquired InSAR data within 24 hours interval. The tandem data sets facilitate to investigate the optimal performance in terms of temporal decorrelation and atmospheric effects. Since then, numerous papers covering InSAR limitations and its potential applications have been published from scientific group around the world. Usai and Hanssen (1997) remark that some radar targets maintain stable backscattering characteristics for a period of months or years and the phase information from these stable targets can be used, even over a long time period. This is a very important basis for further exploitation of existing SAR scene archives and the establishment of long time series of SAR images.

Currently, there are several space borne missions available for the applications of InSAR, and the satellite SAR systems commonly work in one of the following microwave bands:

- C band - 5.3 GHz (ESA's ERS and ENVISAT, the Canadian RADARSAT, and the US shuttle missions);
- L band - 1.2 GHz (the Japanese JERS and ALOS-PALSAR);
- X band - 10 GHz (TerraSAR-X by German Aerospace Center (DLR), and COSMO-SkyMed by the Italian Space Agency (ASI)

Figure 2.1 resumes the most important SAR missions, showing their launching date and operating band.

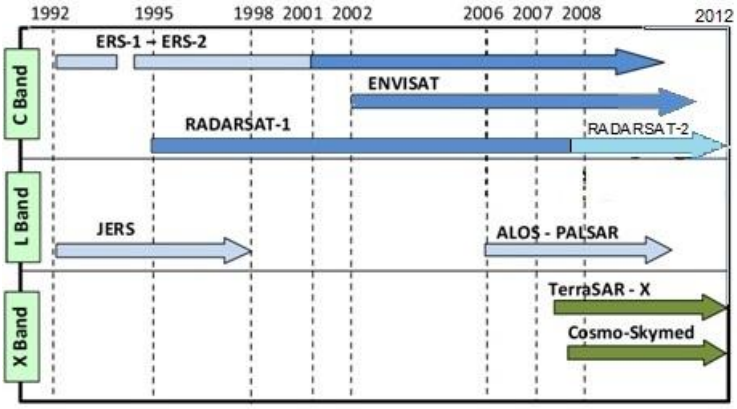

Figure 2.1 Space-borne SAR missions.

The accessibility of InSAR data, open-source and commercial InSAR processing packages lead to an interesting geodetic tool for earth observation study.

2.2.2 Applications for land deformations

2.2.2.1 Earthquakes

The co-seismic deformation of Landers earthquake in 1992 can be found on (Massonnet et al., 1993 and 1994; Zebker et al., 1994a; Massonnet and Feigl, 1995a; Hernandez et al., 1997; Price and Sandwell, 1998). The results from these studies agreed with the modelled scheme of earthquake deformation in many similar details. Some InSAR studies provided more insights into modelling of the earthquake motion (Pletzer et al., 1994; Massonnet and Feigl, 1995b). For post-seismic, the subsidence of about 3 cm was observed in the area of the destructive fault three years after the main shock of Bam earthquake (Iran) (Fielding et al., 2009). TerraSAR-X observations of post-seismic deformation indicate various processes in the first two months after the Darfield earthquake including shallow deformation on the Charing Cross reverse fault and a small amount of after-slip on the Greendale Fault (Beavan et al., 2011). Cetin et al. (2012) study the post-seismic surface deformation of the Mw 6.8, 2003 Zemmouri earthquake (northern Algeria) using InSAR time series analysis technique reveal sub-cm coastline ground movements between Cap Matifou and Dellys.

2.2.2.2 Volcanoes

The first use of InSAR to study volcanoes was reported by Evans et al. (1992). They used TOPSAR airborne data to assess damage caused by lava flaws and the inter-comparison of the volcano morphology. Later on, Massonnet et al. (1995) applied ERS data to investigate volcanic deformation of Mount Etna. A lot of volcanoes across the world have been studied using InSAR such as Hawaiian volcanoes (Rosen et al., 1996), Alaskan volcanoes (Lu et al., 1997), localized inflation on Izu Peninsula, Japan (Fujiwara et al., 1998a), deformation of the active Yellowstone Caldera (Wicks et al., 1998), and volcanic deformation in the Long Valley (Thatcher and Massonnet, 1997). Zebker et al. (2000) reported sixteen active volcanoes detected with SAR interferometry. Hooper et al. (2004) introduced a new method for measuring deformation on volcanoes and other natural terrains using InSAR Persistent Scatterers. Lu et al. (2005) study Okmok volcano, located in the central Aleutian arc, Alaska using 88 SAR images from ERS-1, ERS-2, Radarsat-1 and JERS-1 satellites. The results provide insights into the post-emplacement behaviour of lava flows for the interpretation of inflation patterns at active volcanoes. Wadge et al. (2010) report the 1995-99 eruption of Soufriere-Hills volcano, Montserrat. They found that the volcano became a more accessible target when applying InSAR. The thickness of deposits on the slope can be mapped in this way. Though, the summit lava dome did not become coherent, so it could not be measured by InSAR.

2.2.2.3 Landslides

Landslides typically degrade the ground surface very quickly reducing the interferometric coherence. They commonly deform the ground surface in excess of the high slope limit. For the study of landslides, a very accurate DEM is required as they usually occur in areas of rough topography (Massonnet and Feigl, 1998). These factors in fact limit the use of InSAR to study most of landslides on many sites. Singhroy et al. (1998) studied landslide characterization in Canada using InSAR. Rott et al. (2003) investigated the InSAR techniques and applications for monitoring landslides. Another study for landslide monitoring using ground-based SAR interferometry was reported by Tarchi et al. (2003). Colesanti et al. (2003) applied the Permanent Scatterer interferometric technique to monitor landslides and tectonic motions. Hilley et al. (2004) addressed the dynamics of slow-moving landslides using the Permanent Scatterer analysis.

2.2.2.4 Land subsidence

A number of land subsidence studies using InSAR have increased significantly. Carnec et al. (1996) applied the techniques to detect land subsidence of coal mining near Gardanne, France. Massonnet et al. (1997) observed land subsidence over a geothermal field in California. Fielding et al. (1998) generated a subsidence map of the Lost Hills and Belridge oil fields as a result from oil and gas extraction. Galloway et al. (1998) studied land subsidence in the Lancaster area, California. Amelung et al. (1999) mapped subsidence in Las Vegas, Nevada. Hoffmann et al. (2001) studied seasonal affect on the subsidence and rebound in Las Vegas Valley, Nevada, using synthetic aperture radar interferometry. Buckley et al. (2003) measured successfully urban land subsidence in Houston, Texas, using conventional SAR interferometry. Dixon et al. (2006) studied land subsidence in New Orleans by using the Permanent Scatterer technique. Teatini et al. (2006) investigated land subsidence in the Venice coastland by integrating five monitoring method, i.e. leveling survey, Differential Global Positioning System (DGPS), Continuous GPS (CGPS), Interferometric Synthetic Aperture Radar (InSAR), and Interferometric Point Target Analysis (IPTA) into a Subsidence Integrated Monitoring System (SIMS). The result exhibits the subsidence rates in averaging 3 to 5 mm/yr in the northern and southern of the city. The subsidence rates increase up to 10-15 mm/yr in the southern coastland. Chatterjee et al. (2006) apply InSAR for detecting slow land subsidence phenomenon in Kolkata City occurring primarily due to piezometric fall and then groundwater over pumping. The results indicate that the subsidence rates are up to 6.5 mm/yr in an area of Kolkata City during the period of 1992-1998. Ng et al. (2008) select six cities from Australia and China, and divided into 2 groups. Group 1 consists of Brisbane, Sydney, Newcastle and Canberra. Group 2 concentrates on the cities where groundwater over extraction including Perth in Western Australia and northern China. The PSI technique is applied using the data from ERS-1, ERS-2, and ENVISAT satellite. The results show that the subsidence rates less than 5 mm/yr are observed in Brisbane, Canberra and Sydney and less than 10 mm/yr is measured in Newcastle. While the subsidence rates are up to 50 mm/yr in Pert (Australia) and a city in China. Friedrich et al. (2010) used the InSAR stable points network to improve land subsidence mapping in Semarang, Indonesia. For the results, the land subsidence rates vary from 1 mm/yr to 100 mm/yr between 2002 and 2006. Wang et al. (2011) carried out a combination of permanent scatterer and quasi permanent scatterer time series InSAR analysis to extract the deformation over the Three Gorges Dam. The results demonstrated that the deformation was influenced by the changing level of the Yangtze River. In terms of

vertical deformation, the subsidence of the dam basement has ceased and there has been some rebound. While, in terms of horizontal deformation, there is the displacement of the dam in 175 m upriver direction.

2.3 SAR Interferometry

Topographic information can be derived from the difference in the phase (ϕ) between two images (Massonnet and Feigl, 1998) called the interferogram. In particular, Figure 2.2 shows a simplified figure of the difference in phase due to ground movement. The change in the distance (R) of the SAR images between two acquisitions at any point on the ground along the look direction is simply determined from the interferogram phase $(\phi_2 - \phi_1)$ with half of the radar wavelength (λ). In order to interpret the direction and magnitude on the change, the conversion from the look direction to the actual ground movement relies on the knowledge of the study area.

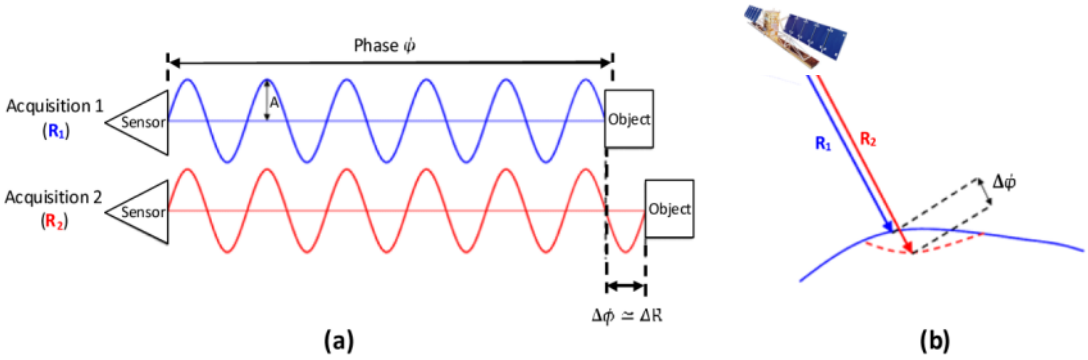

Figure 2.2 Phase difference measurement (Modified from Woodhouse, 2006). (*a*) Relation between a phase differences, $\Delta\phi$, and the difference in the distance between sensor and object, ΔR (*b*) Satellite measurements on the ground deformation.

SAR Interferometry (InSAR) is a powerful tool to take advantage of the phase information by combining two SAR images of the same beam mode acquired from slightly different positions (Madsen et al., 1993; Massonnet, 1993; Prati et al., 1994). InSAR uses phase difference observations between two radar acquisitions for estimating of surface deformation. In addition, the deformation signal of interest also contains contributions due to atmospheric signal delay, (residual) topography, and orbital errors (Hanssen, 2001). Thus, the only fractional phase is

observed in form of wrapped phase, which implies that the number of integer cycles from satellite to the Earth's surface is unknown. The InSAR methodology is aiming for a continuous coherent phase different image (interferogram) refers to conventional InSAR. In this work, we will focus on the repeat-pass interferometry which requires only one antenna, and it is suitable for space-borne systems.

2.3.1 The Interferometric Phase

Figure 2.3a shows the difference between point P' on the reference surface $(H_{P'} = 0)$ and point P at the same range but at height (H_P). The repeat-pass InSAR configuration present in Figure 2.3b. The distances between two antennas to point P' are R_1 and R_2 and for orbit$_1$ and orbit$_2$. Two SAR antennas are separated by a baseline vector B, which can be decomposed into either parallel/perpendicular components $(B_{\parallel}$ or $B_{\perp})$ or horizontal/vertical components $(B_h$ or $B_v)$. The change in look angle $(\delta\theta)$ can be determined from the interferometric phase. Thus, the range R_1 and the height H_{sat} of the platform can be used to determine the height H_P of point P.

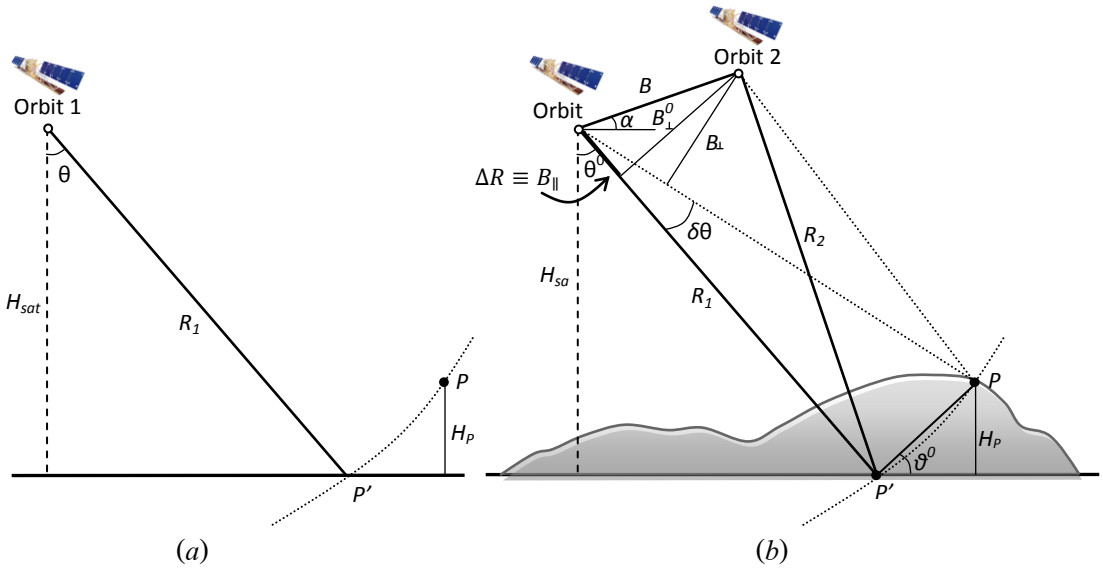

Figure 2.3 Repeat-pass interferometric configuration for a height H_P (Modified from Baran, 2004). (*a*) The difference between point P' and point P. (*b*) Interferometric configuration.

The physical and the geometrical relationships between the two phase observations to obtain topographic height and estimates surface deformation can be derived using the interferometric configuration drawing in Figure 2.3b. Both SAR images are composed of a regular grid with complex values, y_1 and y_2, which can be decomposed in amplitude and phase component as follows:

$$y_1 = |y_1|\exp(j\phi_1)$$
$$y_2 = |y_2|\exp(j\phi_2) \tag{2.1}$$

The observed phases values ϕ_{1p} and ϕ_{2p} in the two images for resolution cell *P* are:

$$\phi_{1p} = -\frac{2\pi 2R_1}{\lambda} + \phi_{scat,1p}$$
$$\phi_{2p} = -\frac{2\pi 2R_2}{\lambda} + \phi_{scat,2p} \tag{2.2}$$

Where R_1 and R_2 are the geometric distances and $\phi_{scat,1p}$ and $\phi_{scat,2p}$ are the contributions of the scattering phases in both images. If the terrain characteristics have not changed between both acquisitions, backscattering terms should be very similar, e.g.:

$$\phi_{scat,1p} \approx \phi_{scat,2p} \tag{2.3}$$

Then, if the phases from both acquisitions are subtracted, we obtain the well-known interferometric phase:

$$\phi_p = \phi_{1p} - \phi_{2p} = -\frac{4\pi(R_1 - R_2)}{\lambda} = -\frac{4\pi\Delta R}{\lambda} \tag{2.4}$$

The phase derivative is therefore:

$$\delta\phi_p = -\frac{4\pi}{\lambda}\delta\Delta R \tag{2.5}$$

If the range, R, is much larger than the baseline, B, we can assume that both ray paths are approximately parallel. Therefore, using this approach, known as the far field approximation, introduced by Zebker and Goldstein (1986), the path difference $(\Delta R = B_{\parallel})$ can be approximated by:

$$\Delta R \approx B\sin(\theta - \alpha) \tag{2.6}$$

Due to orbit inaccuracies and the 2π phase ambiguity, it is not possible to derive $(\Delta R = B_{||})$ directly from the geometry. However, the relation between changes in ΔR and in θ can be described as:

$$\delta B_{||} = B\cos(\theta^0 - \alpha)\delta\theta \tag{2.7}$$

where θ^0 is the initial value obtained for the reference surface (e.g. ellipsoid).

Combining the physical phase observations in Equation 2.5 with the geometric configuration expressed in Equation 2.7, the relation between an interferometric phase change and the change in the look angle θ is found to be:

$$\delta\phi = -\frac{4\pi}{\lambda}B\cos(\theta^0 - \alpha)\delta\theta \tag{2.8}$$

The interferometric phase change can be defined as the difference between the measured (unwrapped) phase ϕ and the expected phase for the reference body,ϑ, derived from the orbit geometry, thus:

$$\delta\phi = \phi - \vartheta \tag{2.9}$$

The height of the satellite above the reference body is known, and can be expressed as follows:

$$H_{sat} = R_1\cos\theta \tag{2.10}$$

The derivative for a resolution cell P with range R_{1p} gives the relationship between changes in look angle θ due to a height difference δH_{sat}:

$$\delta H_{sat} = -H_P = -R_{1p}\sin\theta_p^0\,\delta\theta \tag{2.11}$$

Where R_{1P} is the range from the satellite to the resolution cell P, determined in the configuration of the master image (acquired from orbit 1 – Figure 2.3), B is the baseline and θ_P^0 is the initial value found for an arbitrary reference surface, for instance an ellipsoid.

Finally, the height H_P of the pixel location above the reference surface and the phase difference $\delta\phi_P$ can be defined using the relation:

$$H_P = -\frac{\lambda R_{1p}\sin\theta_P^0}{4\pi B_{\perp,P}^0}\delta\phi_P \quad \text{where: } B_{\perp,p}^0 = B\cos(\theta_P^0 - \alpha) \tag{2.12}$$

Rearranging Equation 2.12, the functional relationship between the absolute interferometric phase ϕ_P and the terrain height H_P above a reference surface can be defined as:

$$\phi_P = -\frac{4\pi H_P B_{\perp,P}^0}{\lambda R_{1P}\sin\theta_P^0} \tag{2.13}$$

A recursive scheme is used to determine a new value at a specific height above the arbitrary reference surface. The component $\delta\phi_P$ in Equation 2.12 can be replaced by 2π that yields the height ambiguity. In other words, it is the linear interval that corresponds to a 2π phase shift:

$$h_{2\pi} = \left|\frac{\lambda R_{1P}\sin\theta_P^0}{2B_{\perp,P}^0}\right| \tag{2.14}$$

To conclude this estimation, the influence of the topography, H_P, and the surface displacement, D_P, are combined on the interferometric phase differences, relative to the reference body. Using Equations 2.5, 2.7 and 2.12 the following relation can be obtained:

$$\delta\phi_P = -\frac{4\pi}{\lambda}\left(D_P + \frac{B_{\perp,p}^0}{R_{1p}\sin\theta_p^0}H_P\right) \tag{2.15}$$

Since the measured interferometric phase is the sum of the expected reference phase ϕ_{R_P} and the deviations, with the reference phase expressed as:

$$\phi_{R_P} = \frac{4\pi}{\lambda}B\sin(\theta_P^0 - \alpha) \tag{2.16}$$

we find:

$$\phi_P = \frac{4\pi}{\lambda}\left(B\sin(\theta_P^0 - \alpha) - D_P - \frac{B_{\perp,P}^0}{R_1\sin\theta_P^0}H_P\right) \tag{2.17}$$

Thus, the final interferogram contains both the interferometric phase that represents a map of the relative terrain elevation with respect to the slant range direction and deformation (D_P).

If the ground is flat, the achieved fringe pattern is very uniform. However, if the surface has variable topography, the point $P(x, y)$ moves in the range and azimuth directions, as well as up and down, causing path differences in 3D. Thus, terrain height disrupts the uniform fringe pattern. The interferometric fringes do not directly represent the surface height because phases are wrapped discontinuities. Therefore, the unwrapping process can be performed to find the correct number of whole plane cycles scaled by the height ambiguity value. The different unwrapping approaches and algorithms are described by several authors (Goldstein et al., 1988; Spagnolini, 1995; Ghiglia and Pritt, 1998; Loffeld and Krämer, 1999; Fornaro and Sansosti, 1999; Stramaglia et al., 1999 and Hooper, 2006).

2.3.2 Interferometry for Surface Deformation mapping

The surface deformation caused by natural and human activities observed using InSAR generates a local phase shift in the result. The technique called Differential Interferometry (DInSAR) can detect local and relative motions in the slant range direction (line-of-sight). Ground displacement has a direct impact on the interferogram phase shift, and it is independent of the satellite separation. The quantity of surface displacement can be estimated directly as a fraction of a wavelength. The ideal condition occurs when the satellites are in the same position in space during both acquisitions to make sure that only deformation phase contains in the interferogram. However, it is technically impossible to ensure such a condition and the non-zero perpendicular baseline $(B_{\perp} \neq 0)$ will cause interferometric fringes, due to the surface topography as well as deformation.

There are several approaches to generate a differential interferogram, but commonly all techniques involve the construction of two interferograms: one spanning some surface change and topography, the other indicating only the surface topography. The topography related to the interferogram could either be calculated from a conventional DEM (2-pass differential interferometry), or from an independent interferometric pair (three and four-pass differential interferometry). Finally, the topography interferogram is used to subtract the topographic phase from the interferogram. Franceschetti and Lanari (1999) used a given DEM with 30 m accuracy for ERS-1 with 100 m perpendicular baseline, and they get 1 cm accuracy on the displacement.

Figure 2.4 shows the two-pass DInSAR configuration geometry. D_P indicates the displacement of point P that took place between two radar acquisitions. The range in the second pass (slave) is indicated by $R_{SP'}$, while R_{SP} is the range in the absence of displacement. The interferometric phase is given by:

$$\phi_P = \frac{4\pi}{\lambda}(R_{SP'} - R_{MP}) \tag{2.18}$$

By rearranging Equation 2.18, the contributions to the path difference due to the target displacement (D_P) and the topographic height (H_P) can be distinguished (Franceschetti and Lanari, 1999).

$$\frac{\phi_P \lambda}{4\pi} = (R_{SP'} - R_{SP}) + (R_{SP} - R_{MP}) = D_P + H_P \tag{2.19}$$

If the baseline is null $(B = 0)$, the topographic contribution will be zero and the interferometric phase would be related only to the displacement (D_P).

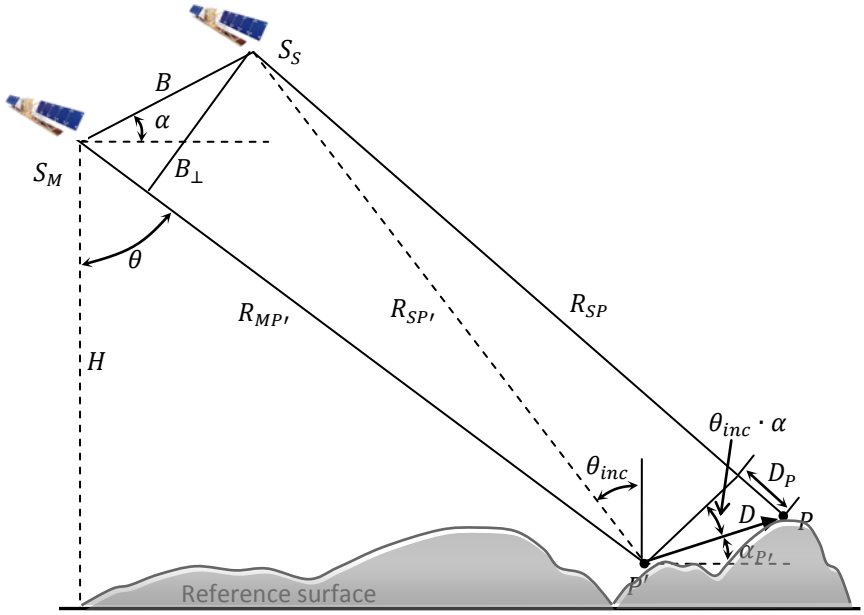

Figure 2.4 Two-pass DInSAR geometry in the plane orthogonal to the satellite trajectories. (Modified from Baran, 2004)

Using the far field approximation, a parallel look direction can be assumed. Thus, the displacement vector D in the α_P direction will create a slant range deformation component, D_P, as follow:

$$D_P = |D| \sin(\theta_{inc} - \alpha_P) \tag{2.20}$$

In practice, this situation is very difficult to obtain because of the satellite navigation complexity. Thus, topographic influence usually has to be removed. However, in order to reduce the topographic influence, radar images with the smallest possible perpendicular baseline $(B_\perp \rightarrow \text{min})$ are preferred if the study focuses on the surface deformation detection.

Figure 2.5 shows the example of differential interferogram formation for co-seismic displacement of March 24, 2011 Mw 6.8 Mong Hpayak Earthquake, Myanmar using two ALOS-PALSAR images in ascending orbit (Trisirisatayawong et al., 2011).

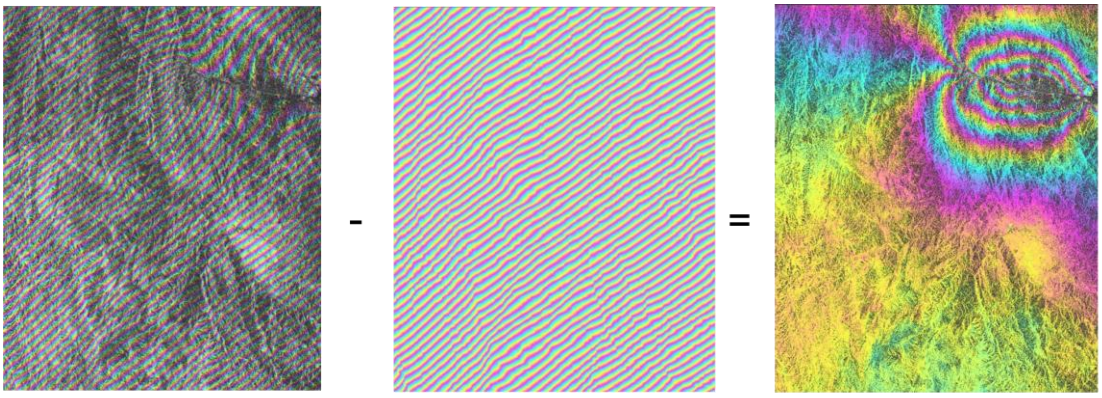

Figure 2.5 the differential interferogram formation using 2-pass differential interferometry. (Trisirisatayawong et al., 2011)

2.4 Interferometric Decorrelation and Limitations

The different errors affecting the surface displacement measurement is very important in order to interpret the measured quantitatively displacement. The most important error sources can be found in-depth discussion on (Hanssen, 2001) who has done a comprehensive study of error sources in SAR interferometry. Most of the errors by using InSAR are not only due to the ability to estimate the interferometric phase correctly but also the separation and analyze of the different phase contributions coming from surface topography, deformation, atmospheric delay, and refractivity changes in the scattering object. Sensor parameters such as the radar frequency, spatial resolution, and incidence angle have a strong impact on the feasibility of InSAR for surface deformation mapping.

2.4.1 Phase noise

The phase accuracy of SAR interferograms is primarily affected by phase noise and decorrelation. The interferometric radar relies on the coherence of two signals, so incoherent signals can lead to the improper results. Phase noise in interferograms will make the visual effect worse, and the fringes would be ambiguity and disappear in speckles obstructing phase unwrapping. In order to reduce phase noise, the interferograms has to be filtered using an adaptive band-pass filtering (Goldstein, 1998) by averaging window with a size of several resolution elements in both range and azimuth.

2.4.2 Decorrelation source

The decorrelation mainly affected phase accuracy of SAR interferograms. There are many different sources of decorrelating contribution, resulting in a total loss of coherence (Zebker and Villasenor, 1992; Hanssen, 2001). Spatial baseline decorrelation occurs when the interferometric baseline is not exactly zero. Since the radar receives the coherent sum of all independent scatterers within the resolution cell, these contributions are added slightly different due to the different geometry. The baseline decorrelation is related to the different look angles of the two SAR acquisitions, and leads to a critical baseline.

Temporal decorrelation is the most problematic to characterize theoretically. It is due to geometrical or electrical changes in the properties of the surface as a function of time between the acquisitions. These changes may be caused by moving parts of vegetation, erosion on the land surface, or agricultural activity. Terrain containing variable liquid water, such as e.g., areas covered with flooding in rainy season, will also have different scattering properties from one observation to the next. Forest is shown to have a generally low coherence, even for a temporal baseline as short as one day, while urban and arid areas show high coherence also for acquisition time intervals longer than one year. Since temporal decorrelation is due to changes of the surface mainly at the scale of the radar wavelength, temporal decorrelation is highly dependent on the operating frequency of the radar (Zebker and Villasenor, 1992). InSAR data acquired with longer wavelengths, for example L-band, exhibits a lower temporal decorrelation (Strozzi et al., 2003).

Thermal decorrelation is due to system noise, and it can be related to the SNR of the radar system (Zebker and Villasenor, 1992). Doppler centroid decorrelation is caused by the differences in Doppler centroid for the two acquisitions. It is the azimuth equivalent of the spatial decorrelation component. Volumetric decorrelation is caused by penetration of the radar wave through the scattering medium. It depends highly on the radar wavelength and the dielectric properties in the scattering medium.

2.4.3 Orbital errors

Since an interferogram is a difference measurement between the two SAR acquisitions, it is highly important to know the accurate relative positions of the two orbits. The differential SAR interferogram is obtained by subtracting the topographic phase. This differential interferogram will show the deformation field. In practice, there will still be phase left from topography, atmospheric contributions and decorrelation. Errors in the estimation of the interferometric baseline affects the scaling of the topography related phase, and the removal of the flat earth phase of the interferogram.

For SAR interferometry, an error in the baseline estimate can create a phase trend referred to as orbital fringes, which usually have a gradient in a certain direction. These fringes will still be present in the interferogram, creating confusion in interpreting the phase. In order to remove orbital fringes completely, an orbital accuracy on the order of 1 mm is required, which is

far below the current precision orbit vectors having Root Mean Square (RMS) accuracy on the order of 10 cm (Scharroo and Visser, 1998). The errors in the orbital state vectors can be represented as errors in the along-track, across-track, and the radial direction. The along track errors are usually corrected in the coregistration process in SAR interferometry. It is therefore only the radial and across-track errors that will propagate as systematic phase errors in the interferogram, and the problem can be considered two-dimensional (Hanssen, 2001). The orbital effects can be separated in a nearly instantaneous phase trend in the range direction, with a slow time dependent component in the azimuth direction. Errors in the radial direction produces fringes parallel to the flight direction, while the fringes perpendicular reveal an error in the radial or across-track velocities, respectively.

2.4.4 DEM errors

Any inaccuracies in the Digital Elevation Model (DEM) will directly translate into errors in the displacement measurement. Since the sensitivity of the phase errors to the DEM error is directly proportional to the perpendicular baseline, the effect of DEM errors can be minimized by using image pairs having small perpendicular baselines. Another issue that must be considered, particularly for large baseline interferograms, is the difference in the measured scattering center compared to the reported topography height. The elevation reported in the DEM is the land surface height, while the surface imaged by the radar may differ by many meters from the land surface. This can be a problem in urban areas due the scattering from high buildings, or in areas with tall vegetation due to scattering from the canopy (Askne et al., 1997). A difference between the elevation reported in the DEM and the elevation seen by the radar causes a phase error in the interferogram.

2.4.5 Atmospheric errors

An often mention advantage of radar remote sensing over optical remote sensing is that the radar will penetrate trough the clouds. Therefore, the SAR instrument can be used in all weather conditions and even day or night time. However, the transmission of an electromagnetic wave through any medium, such as the atmosphere, is highly dependent on the refractive index (Ishimaru, 1978; Ulaby et al., 1982; Tsang et al., 2000).

The atmosphere is a disperse medium with randomly distributed aerosols and hydrometeors, and as electromagnetic waves propagate in the atmosphere, wave energy is absorbed and scattered by these liquid or solid particles. Aerosols are particulate matter suspended in the atmosphere, such as smoke, haze, clouds, fog and fine soil particles (Tsang et al., 2000). Hydrometeors are solid or liquid water particles such as for example, mist, rain, freezing rain, ice pellets, snow, hail, ocean spray, clouds and fog (Tsang et al., 2000). Spatial or temporal changes of the refractive index between the two SAR acquisitions composing the interferogram modify the propagation velocity of the electromagnetic wave. The relative propagation delay effects within one SAR image are not of such magnitude that they are visible. This is because the relative delay differences are much smaller than the range resolution of the radar system. A radar interferometer, in contrast, measures the phase difference on the order of a fraction of the wavelength, more than accurate enough to be influenced by atmospheric path delay. The presence of atmospheric effects represents a serious issue since it may reduce the accuracy on the detected deformations, or even masks them out, see (Goldstein, 1995; Zebker et al., 1997; Hanssen, 1998; Hanssen, 2001). Cycle ambiguity problems in conventional InSAR can be overcome by carrying out InSAR measurements on InSAR time series analysis, exploring a long temporal series of SAR acquisitions for the same area (Ferretti et al., 2000, 2001; Colesanti et al., 2003).

2.5 InSAR times series analysis

Multi-temporal InSAR techniques are the extensions of conventional InSAR aimed to addressing the problems caused by decorrelation and atmospheric delay. Currently, multi-temporal InSAR algorithms can be generally categorize into two approaches called persistent scatterer (PS) and small baseline (SB) methods. Each method is designed for a specific type of scattering mechanism (see more details in chapter 4). However, these techniques involve the simultaneous processing of multiple SAR acquisitions over the same area to allow for the correction of uncorrelated phase noise terms and consequently reducing errors associated with the deformation estimates.

2.5.1 The PSI Technique

If one of the scatterers in the resolution element is brighter than the others, the interference from other scatterers is minimal, the received signal is stable, and the motion of the dominant scatterer can be determined from the interferometric phase. Persistent scatterer techniques take advantage of pixels dominated by a single scatterer to reduce the influence of atmosphere and decorrelation. First algorithms were developed by Ferretti et al. (2000) and (2001). Similar processing strategies have been developed by Crosetto et al. (2003), Lyons et al. (2003), Werner et al. (2003) and Kampes (2005). These methods have been very successful for InSAR analysis of radar scenes containing large numbers of man-made structures. One of the limitations of these methods is the PS selection strategy, which relies heavily on amplitude variation to detect a network of stable. These algorithms may fail to detect PS when the number of images is limited (less than 20) or when the PS has low amplitude.

In contrast, StaMPS (Hooper et al., 2007) overcomes this limitation by using both amplitude and phase analysis to determine the PS probability for individual pixels. Firstly, an initial selection based only on amplitude analysis is performed, and then the PS probability is refined using phase analysis in an iterative process. Once selected, the signal due to deformation in the PS pixels is isolated. This method does not require any a priori assumptions about the temporal nature of the deformation for PS selection. This is achieved by using the spatially correlated nature of deformation rather than requiring a known temporal dependence. Thus, StaMPS can provide reliable deformation measurements even when applied to mountainous areas.

2.5.2 Small Baselines technique

If all the scatterers are comparable strength, then the interferometric phase realizations are randomly distributed in the interval $(-\pi, \pi)$. In this case, we can improve the signal-to-noise ratio (SNR) by averaging the Interferometric signal from adjacent resolution elements. This forms the basis of small baseline (SB) methods. Stacking (Sandwell and Price, 1998) is one of the simplest forms of SB methods. It determines an average velocity model by averaging many interferograms with short orbital baselines to mitigate atmospheric effects. Later on, algorithms based on singular value decomposition and temporal models (Berardino et al., 2002) have since been developed to estimate non-linear deformation from a stack of interferograms.

In small baseline methods (Berardino et al., 2002 and Schmidt et al., 2003), a network of interferogram pairs is created with small temporal and geometrical baselines to limit decorrelation noise. Noise is further reduced by applying range and azimuth filters (Just et al., 1994) and spatial multilooking. However, filtering reduces spatial resolution, which can result in failure to detect some stable isolated pixels. The method from Hooper and Zebker (2007) differs in that it operates on single-look images to identify single-look slowly-decorrelating filtered phase pixels directly. Thus, we can process the data at the highest possible resolution with the ability to unwrap the phase more robustly in three dimensions.

2.5.3 Combined PSI and Small Baseline

Hooper (2008) proposed a combination of PSI and SB algorithms to take full advantage of both techniques. The combination of the two sets of pixels increases the number of observations with useable signal and also increases the signal-to-noise ratio for pixels selected by both methods. The PSI and SB data sets are combined before the phase-unwrapping (unfolding the phase out its natural range of $-\pi$ to π maximize the reliability of the unwrapped phase. A combined data set of SB interferograms phase is created from pixels selected by both the PSI and SB methods. A weighted mean value for the phase is calculated when a pixel occurs in both data sets by summing the complex signal from both data sets with the amplitude of each set to an estimate of the signal-to-noise ratio for the pixel in that data set. The combined observations are then "unwrapped" using a statistical-cost approach (Hooper, 2009). After phase unwrapping, spatially-correlated DEM errors are estimated from their correlation with perpendicular baseline. The phase is then re-unwrapped with the DEM error subtracted, to improve unwrapping accuracy for larger baselines.

CHAPTER III

LAND SUBSIDENCE IN BANGKOK AND ITS VICINITY AREAS

3.1 Introduction

Land subsidence in Bangkok and its vicinity areas has already been recognized for several decades. However, the magnitude, temporal, and spatial patterns of the land subsidence are not well defined due to several factors such as natural sediment compaction, building weight, and especially groundwater extraction. The increasing of population density in the area leads to a significant rate of groundwater pumping which accelerated land subsidence rate. The most common subsidence monitoring technique to measure absolute subsidence through leveling survey is able to describe variation in elevation of points with respect to a permanent point. For that reason, the monitoring of Bangkok subsidence from this technique started in 1978 and it has been carried out on an annual basis by the Royal Thai Survey Department (RTSD). Based on the leveling data from RTSD, most studies focus on the relationship between land subsidence and groundwater extraction rather than the assessment of subsidence rates.

Alternatively, InSAR provides temporal height differences for coherent resolutions whilst leveling measure subsoil deformations characteristic. InSAR can derive height changes subjected to deformations of surface, subsurface soils, or buildings depending on the dominant sources of radar backscatter, so it is suitable for deriving spatial extent of land subsidence information while leveling is a very precise technique for local point measurement. Therefore, to measure land subsidence analysis integrated between leveling survey and InSAR techniques could be the more efficient approach benefiting from each advantages for monitoring strategy according to their different in measuring characteristics.

3.2 History on the study of land subsidence in Bangkok

3.2.1 Bangkok subsidence

Bangkok subsidence was firstly reported by Cox (1968). He pointed out the problem of land subsidence in Bangkok region resulting from groundwater extraction. A finite difference mathematical model for the simulation of the phenomenon of land subsidence due to groundwater withdrawal was successfully developed and used to simulate land subsidence for Bangkok by Premchit (1978). Akagi (1979) reviewed the development and conditions of land subsidence in three Japanese cities in order to apply for Bangkok land subsidence. The study illustrated that groundwater pumping was a direct cause of land subsidence. Afterwards, the first systematic study on investigation of Bangkok land subsidence due to deep well pumping was conducted by researchers at the Asian Institute of Technology (AIT) during 1978-1981 (Asian Institute of Technology [AIT], 1981). The study revealed that the land subsidence rate was 100 mm/yr in eastern Bangkok and 50-100 mm/yr in central Bangkok.

A full scale field test of artificial recharge carried out in 1995, involved recharging to the shallow wells penetrating to the upper Bangkok aquifer (AIT, 1995). A more comprehensive study on management of groundwater and land subsidence was conducted by (Japan International Cooperation Agency [JICA], 1995). They stated that groundwater level in central Bangkok was recovered from the year 1983 but it has continued to drop in the vicinity area. Subsidence magnitude in central Bangkok was about 20 mm/yr while it reached 50 mm/yr in the vicinity, e.g. Samut Prakarn and Pathumthani. Ramnarong et al. (1998) stated the groundwater crisis and land subsidence in Bangkok and its vicinity area. She reported the water supply condition, ground water layer's characteristic and qualification, groundwater situation such as level of groundwater and groundwater utilization since the beginning of the year 1997 (groundwater over demand). Duc (1999) found that intensive pumping of groundwater has caused the compression of soils in the first 150 m depth zone. The average subsidence rate varied from about 15-50 mm/yr (1978-1986) to about 10-35 mm/yr (1986-1997).

The study on Thailand's groundwater situation by DGR (2004) reports that public and private sector have pumped and developed groundwater to use for three reasons; consumption, industrialization, and agriculture. This leads to land subsidence and salt water intrusion into freshwater resources. To solve this problem, the correction plan and suitable resource management measure are required. Worawattanamateekul (2006) concluded that the rate of land subsidence in Bangkok was higher than 100 mm/yr in the period during 1979-1981 at Ramkamhaeng University area. The subsidence decreased almost steadily to 85 mm/yr during 1981-1985, 35 mm/yr during 1985-1988 and 30 mm/y during 1988-1991. The subsidence rate increased again in 1997 to 4 mm/yr during 1991-1994 and 55 mm/yr during 1995-1997), and later on slowed down to the rate of approximate 35 mm/yr in 1997-2000.

The example of land subsidence maps generated through the investigations and surveys of various government agencies are presented below. Figures 3.1(*a*) shows the land subsidence in the central, east, south-eastern, and western parts of Bangkok in 1997 where the locations were still in the critical zone. From 2001 to 2003, land subsidence in these areas has been reduced to about 10 mm/yr. The land subsidence problem was observed as well as the suburbs of the city and into the surrounding provinces such as Samut Prakan, Pathumthani, Nonthaburi, Samut Sakhon, and Nakhon Pathom. In the industrial province of Samut Prakan, land subsidence at rates of 20-50 mm/yr was observed in 2003, as well as in Samut Sakhon located southwest of Bangkok (figures 3.1(*b*)-3.1(*d*)).

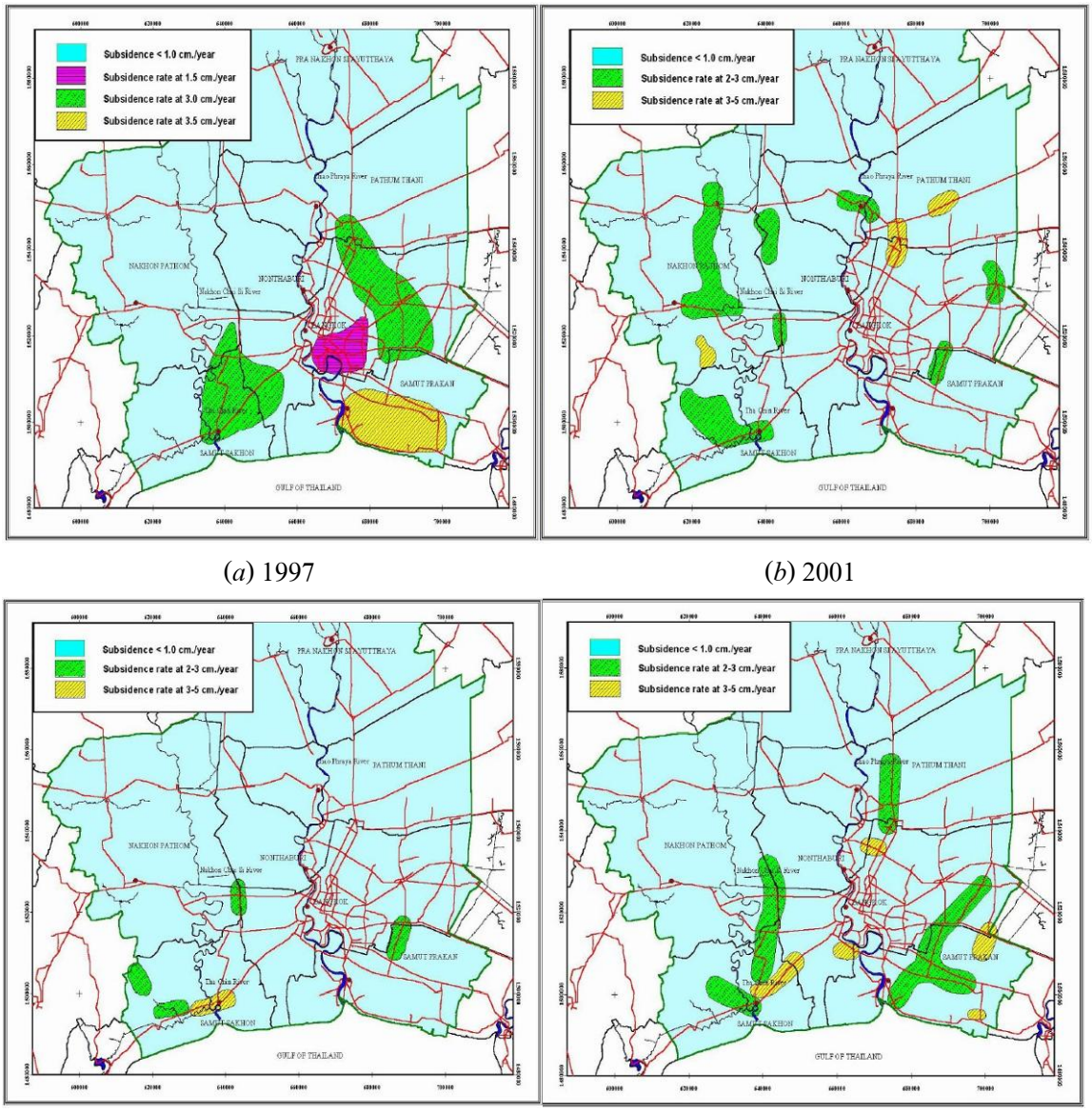

(*a*) 1997 (*b*) 2001

(*c*) 2002 (*d*) 2003

Figure 3.1 Land subsidence rate in Bangkok and the surrounding provinces in 1997, 2001, 2002, 2003. (modified from DGR to English version by Saejeng (2007))

The land subsidence situation between 2004-2005 in figure 3.2 present the subsidence rates from 30-50 mm/yr occurred in Samut Sakorn, Patum Thani, Samuth Prakarn and Ladkrabang, Bangkok. While in Bangboutong Nonthaburi, Ban Paew Samuth Sakorn, Mouang and Bangpli Samuth Prakarn, Bangcare Bangkok and the eastern side of Bangkok such as Houmark, Prakhanong, Clongsamwa, Bangchak and Minburi, the subsidence rates was between 20-30 mm/yr. The lowest rates seem to happen in the mid-town of Bangkok.

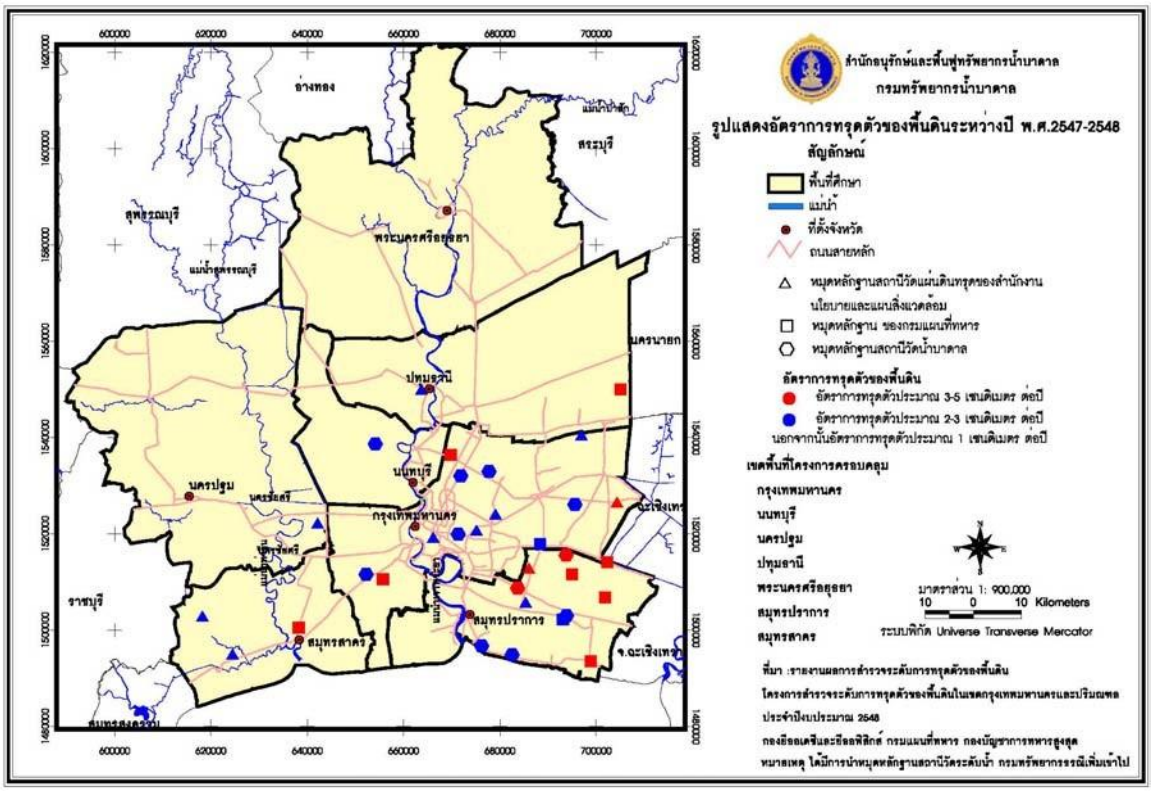

Figure 3.2 Land subsidence rate in Bangkok and the surrounding provinces in 2004-2005.

Source: Original version from DGR

3.2.2 Differential settlement

Phien-wej (2006) summarized the problem of land subsidence in Bangkok for the past 35 years. He mentioned that the land subsidence still continues in the Bangkok area, although its rate has decreased due to mitigation measuring. He also pointed out that the southeast and southwest along coastal zone is the most affected areas where the subsidence rates up to 30 mm/yr. As by the previous reports and publications, the most critical area is the eastern zone of the city which experienced the largest subsidence rate of up to 120 mm/yr in the past 25 years ago. This area still continues to subside at 20 mm/yr. Another important issue indicated in the paper is the land subsidence in different soil layer effected the buildings settlement. Figure 3.3 show the differential settlement of the building built on different pile depths.

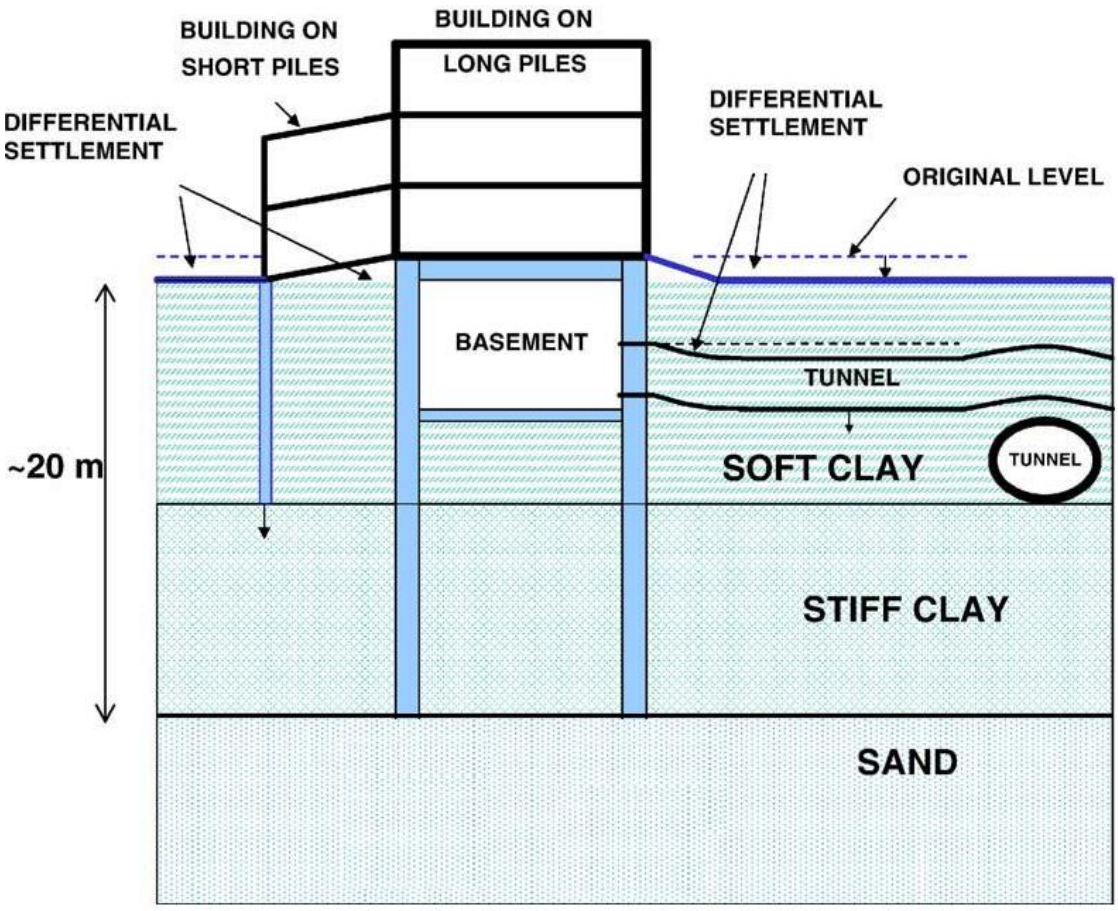

Figure 3.3 Schematic patterns of differential settlements caused by land subsidence in Bangkok areas modified after Phien-wej (2006).

Apart from Phien-wej (2006) mentioned above, the subsidence of man-made feature that rest on natural surface (e.g. pave way) subside faster than that the structure are supported by piles (e.g. bridge, building). The cracking of buildings, irregular sidewalk, and strong bumpy of the wayside are presented in figure 3.4 to figure 3.6 captured at Ladkrabang district, the eastern part of Bangkok in 2010 and 2012. They actually can be found all over Bangkok.

(*a*) (*b*)

Figure 3.4 (*a*) shows the side step of the building separated from the ground. (*b*) shows cracks on the sidewall of the same building.

(*a*) (*b*)

Figure 3.5 (*a*) show the irregular sidewalk surface and (*b*) the collapse on sidewalk and Ladder Bridge.

(*a*) (*b*)

Figure 3.6 (*a*) and (*b*) show the strong bumpy of the wayside found several places in the study area.

3.3 Groundwater extraction and mitigation measures

The available information base on the data of groundwater use in Bangkok demonstrated that the extensive use of groundwater in the region began in the mid-1950s when surface water supplies became insufficient to meet rapidly increasing of water demands. Groundwater was primarily used to supplement surface water supply for public. In the city of Bangkok and its surrounding provinces, the negative effects of groundwater over pumping lead to land subsidence in many places over the last sixty years. The problems related to groundwater use activities in Bangkok encouraged Thai government to enforce the Groundwater Act B.E. 2520 (1977) in 1978 (JIID, 1999). Afterwards, the act has been amended twice in 1992 with Groundwater Act (No.2) B.E. 2535 (1992) and again in 2003 with Groundwater Act (No.3) B.E. 2546 (2003).

In 1959, groundwater levels in the deep zones were reduced by a maximum of 9 m (AIT, 1981). When more wells were being installed in mid-1960s the rate of decline increased. Information on groundwater quantity and quality in Bangkok has been collected since 1965 (Ramnarong, 1999). By 1974, water levels in the Nakhon Luang Aquifer (see figure 3.7) had declined to 30 m below the ground in Central Bangkok and eastern suburbs. March 1983, the Cabinet issued a solution entitled 'Mitigation of Groundwater Crisis and Land Subsidence in Bangkok Metropolis' based on the results of the jointly research conducted by the DMR and AIT from 1978 to 1982. The solution was aimed to control groundwater pumping and slow down land subsidence rate for four provinces of Bangkok, Nonthaburi, Pathumthani, and Samut Prakan (Ramnarong and Buapeng, 1991). The areas were divided into three critical zones as follow; Critical Zone 1 for areas where the subsidence rate is greater than 100 mm/yr, Critical Zone 2 (50-100 mm/yr) and Critical Zone 3 (less than 50 mm/yr). Figure 3.8(*a*) shows the areas where the locations of 3 Critical Zones were set up. The more details can be found in 'the report of the groundwater and land subsidence and guidelines for the management of groundwater in the Bangkok metropolitan area' (DGR, 2007).

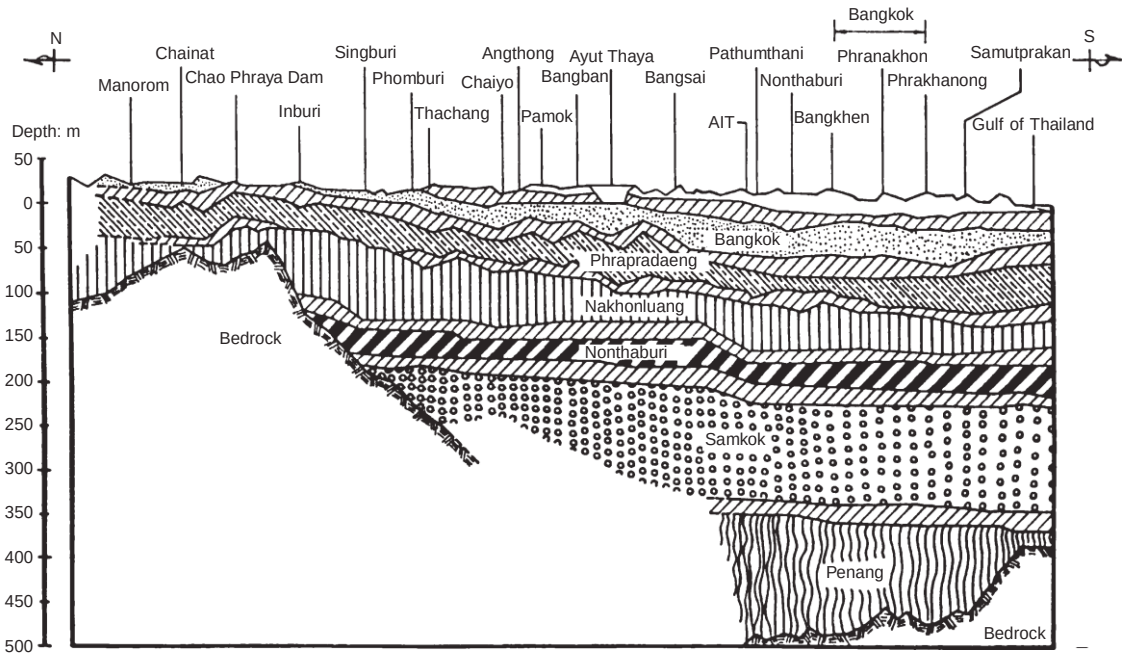

Figure 3.7 Hydrological profile of Bangkok aquifer system in north-south direction.

(Balasubramaniam et al., 2005)

The Critical Zones were expanded in 1995 (see figure 3.8(*b*)). The criteria such as monthly groundwater levels, number of pumping and wells annual recording, annual measurement of land subsidence, using pricing systems to discourage groundwater use, conducting studies about groundwater recharging, and launching public information campaigns for water conservation are considered to achieve the goal. The expanded Critical Zones in 1995 were categorized as follows; Critical Zone 1, where the subsidence rate is greater than 30 mm/yr, and/or water levels decline at more than 3 m/yr, Critical Zone 2, subsidence rates are 10-30 mm/yr and/or water levels decline 2-3 m/yr, and Critical Zone 3, for areas where subsidence is 10 mm/yr and/or water levels decline 2 m/yr.

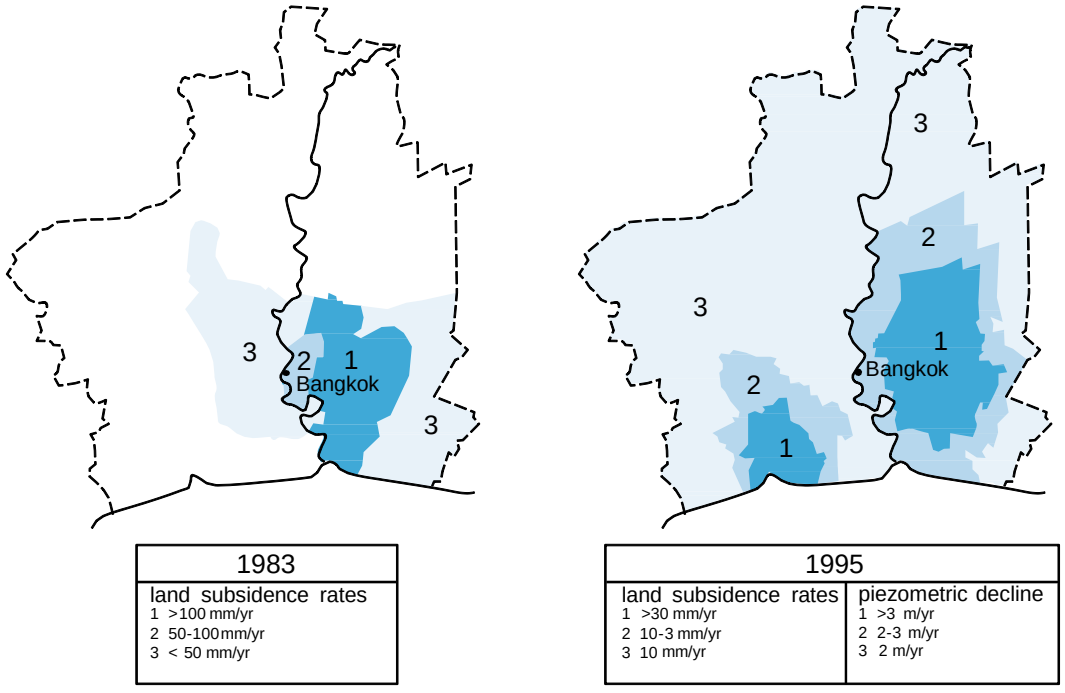

(*a*) (*b*)

Figure 3.8 Revised definitions of 'critical areas' as regards land subsidence control in Bangkok.

source : Buapeng and Foster (2008) modified after DGR.

3.4 Measurement of land subsidence

An increasing demand for regular monitoring and accurate measuring of the rates and patterns of land subsidence in the area are particularly important to gain a broad understanding of the phenomenon and to provide decision makers with useful information for integrated development and sustainable use of groundwater. Leveling survey is the most common method for measuring vertical displacement of benchmarks in subsidence monitoring while InSAR is ideally suited to measure the spatial extent and magnitude of subsidence rate. Two main methods in this study can be summarized in table 3.1.

Table 3.1 Leveling survey and InSAR methods of measuring land subsidence

(Modified from Galloway et al., 2000)

Method	**Component displacement**	**Resolution[1] (mm)**	**Spatial density[2] (samples/survey)**	**Spatial scale**
Leveling survey	Vertical	0.1-1	10-100	line-network
InSAR time series analysis	line-of-sight	1	variable[3]	map pixel[4]

[1]Measurement resolution obtained under optimum conditions. [2]Number of measurements generally necessary to define the distribution and magnitude of land subsidence at the scale of survey. [3]Depends on presence of permanent scatterers. [4]A pixel (picture element) on an InSAR displacement map based on existing space-borne sensors.

3.4.1 Subsidence Monitoring using leveling measurement

The magnitude of land subsidence may be measured in terms of absolute subsidence; compression of the soil layers, and pore water pressure. Measurement of absolute subsidence through leveling survey is the most common subsidence monitoring technique that can show a difference in elevation of points with respect to a reference point. For Bangkok, it was in 1978 when absolute subsidence was determined through the first-order leveling survey by the Royal Thai Survey Department (RTSD) to measure the magnitude of land subsidence in the area (see figure 3.9). The Bangkok Metropolitan Authority (BMA) also occasionally conducts leveling surveys with benchmarks that the agency constructed around Bangkok Metropolis. Some of these BMA benchmarks are also used by the RTSD in annual leveling surveys. The DMR constructed benchmarks near its groundwater monitoring stations and conducted leveling surveys through its Survey Division. BMR.5 of Ko Lak from national network which is placed on a stable rock is employed as referenced.

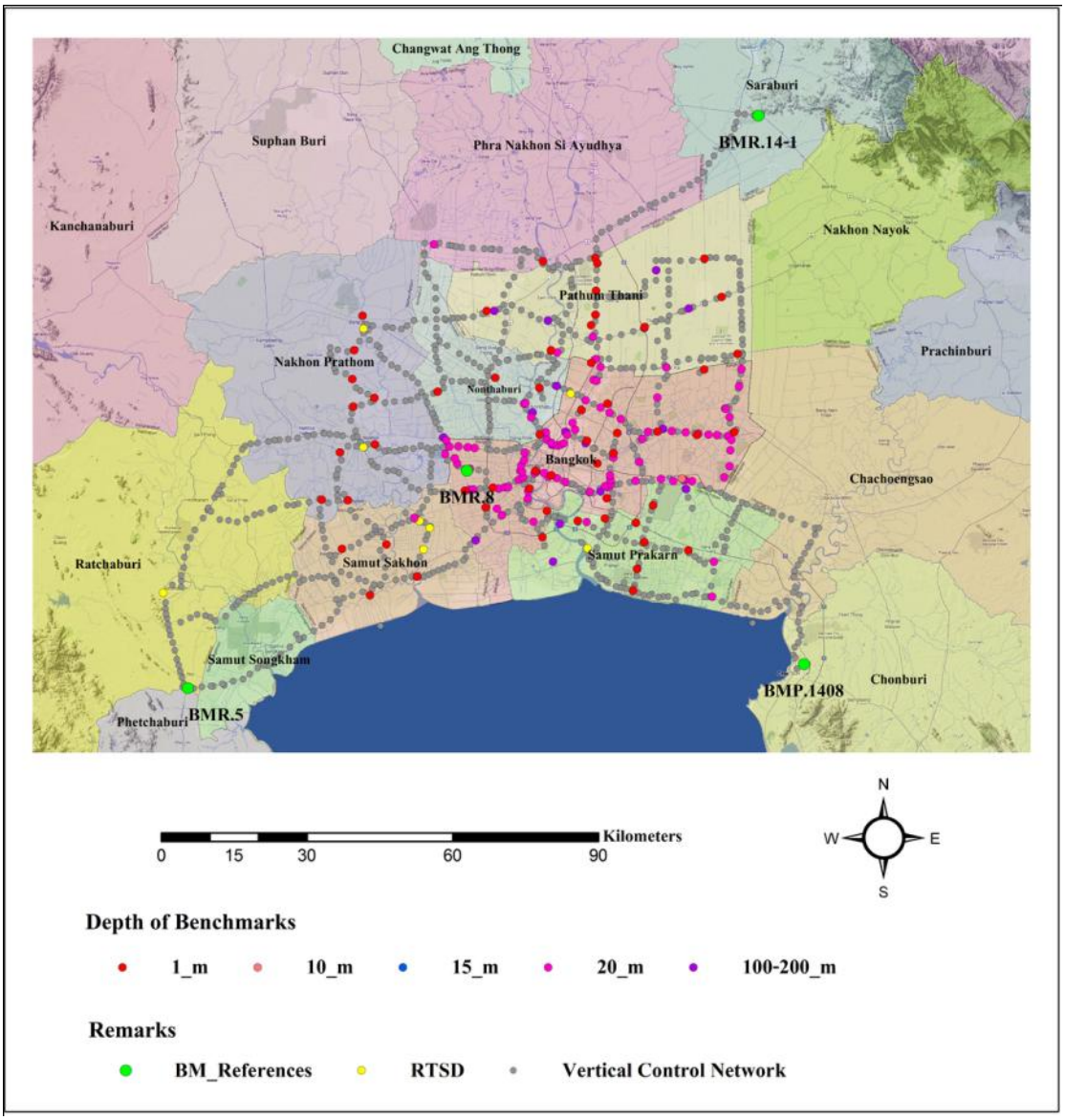

Figure 3.9 The leveling survey network of Bangkok and its vicinity area plus the depth of benchmarks.

The limitation of leveling survey network is the conditions of benchmarks which often require maintenance to prevent a natural loss of benchmarks in time. The observations are become more difficult due to urban growth increasing the building density, so the most benchmarks are usually pointed to the easily accessible area. The financial restriction and time consuming are also resulting in the limited number of monitoring points and difficult to maintain monitoring frequently. The reference benchmark is necessary to monitor and maintain. Nevertheless, by using InSAR, some of the problems listed above can be overcome, and the explanation is provided in the next section.

3.4.2 Subsidence monitoring using InSAR measurement

InSAR has the potential to provide subtle surface deformation measurements at a significantly improved SAR resolution with millimeter-level accuracy and over large areas (approximately 2,500 km² for Radarsat-1 satellites). Numerous researches have successfully applied radar interferometry to measure land subsidence. The references can be found on 2.2.2.5 in chapter two while the applications to Bangkok area have limited number due to the lack of time series data available and the new processing approaches fit to the application were just developed in recent year. Kuehn et al. (2004) reported that the maximum subsidence rate was 30 mm/yr in the southeast and southwest alongside Chao Phraya River during the time spanning from February 1996 to October 1996 using DInSAR. However, this result can not reflect accurately the actual land subsidence rates, because of the short time span and limited number of images used (see figure 3.10).

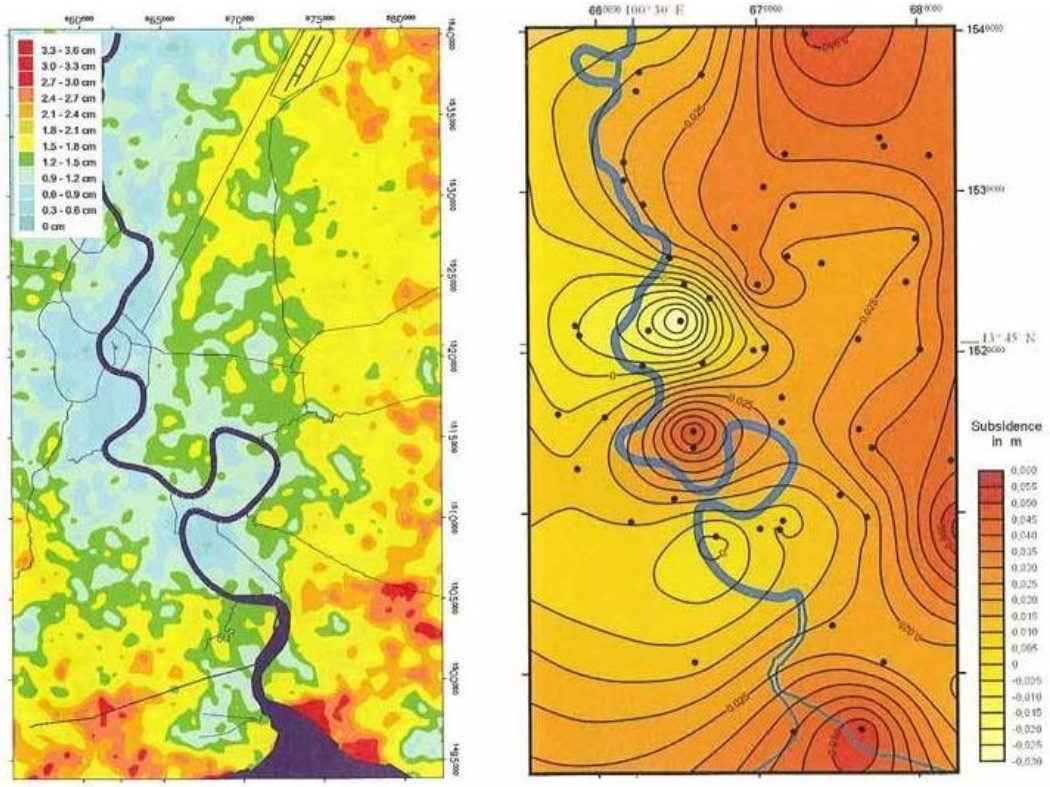

(*a*) (*b*)

Figure 3.10 InSAR-based land subsidence map showing subsidence between 20 February and 23 October 1996 (*a*) versus the land subsidence map derived from conventional leveling for 1995/1996 (*b*). (Kuehn et al., 2004)

Worawattanamateekul (2006) applied PSI using 20 radar acquisitions from ERS-1/2 C-band data to quantify surface subsidence rates covering the time period between 1996 and 2000 with PS density of around 28 PS/km^2. Figure 3.11 presented the maximum subsidence rate was found at the northeast of the intersection between Srinakarin and Teparak roads of up to 42 mm/yr. The differences between subsidence rates estimated from PSI and leveling data showing temporally linear subsidence agreed within ±1.5 mm/yr for 6 out of 10 benchmarks.

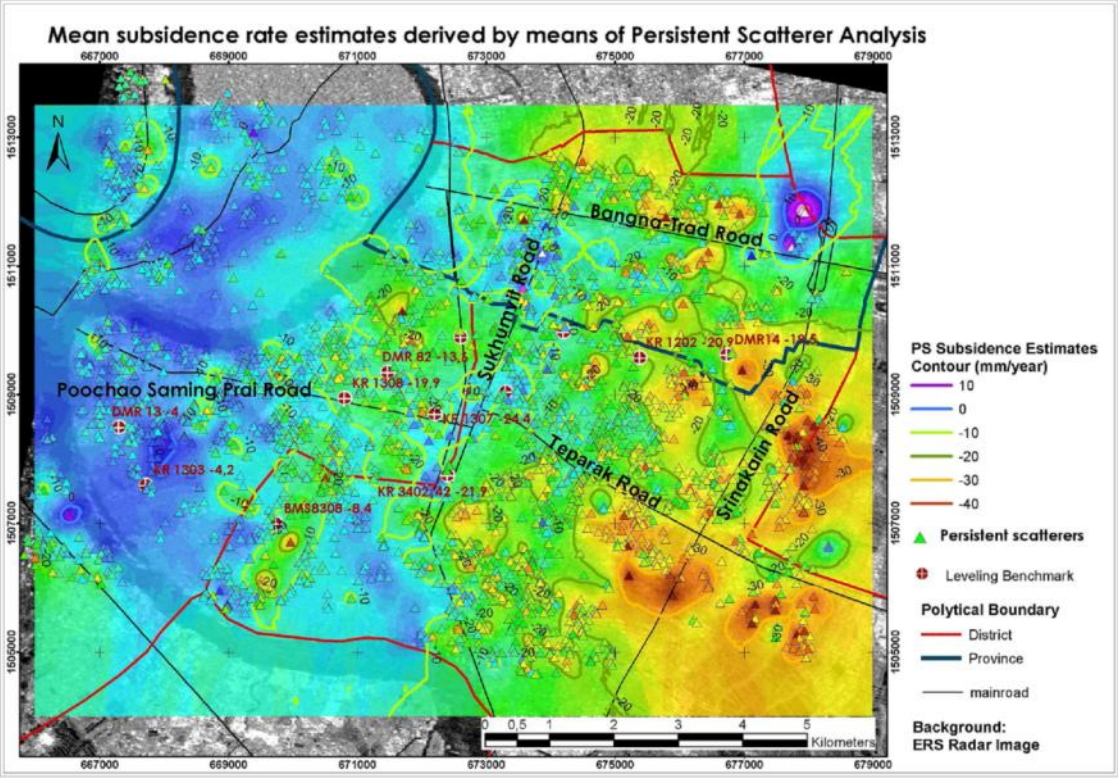

Figure 3.11 Mean subsidence rate estimates derived by means of Persistent Scatterer Analysis using ERS-1/2 C-band data to quantify surface subsidence from 20 radar acquisitions covering time period between 1996 and 2000. (Worawattanamateekul, 2006)

The study itself was limited in the coverage area about 100 km^2 due to two adjacent tracks of data from ERS-1/2. The number of image scenes acquired were 20 and 16 for the left (Track 018) and the right stacks (Track 247) with no single frame covering whole Bangkok area. Therefore, the area located in the scene-overlapping (cyan rectangle) as shown in figure 3.12 was selected as test area.

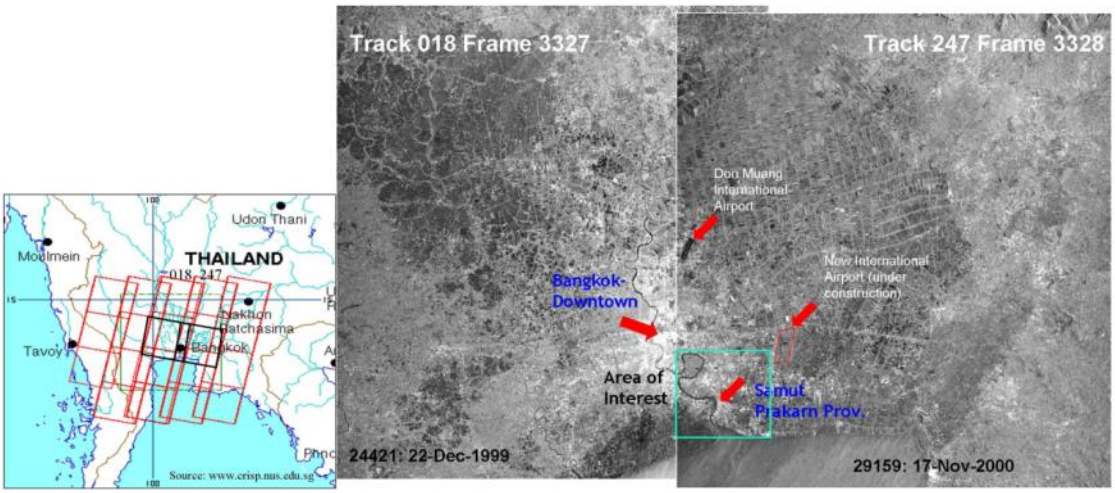

(*a*) (*b*)

Figure 3.12 (*a*) ERS-1/2 coverage over Bangkok and its vicinity. Two adjacent tracks (the left and the right tracks represented by black frames) were acquired for this study.

(*b)* The corresponding amplitude images depict AOI (cyan rectangle) - situated in the overlapping area of these two scenes- and other important locations.

(Worawattanamateekul, 2006)

CHAPTER IV

INSAR TIMES SERIES ANALYSIS - THE StaMPS-MTI APPROACH

4.1 Introduction

InSAR time series analysis is a geodetic tool for deformation measurements to identify single pixel that is coherent over long time intervals. Therefore, the principle behind the technique is the search for permanent dominant scatterers. Figure 4.1(*a*) (Hooper, 2006) can clearly that the phase strongly varies with every other acquisition. In case of a strong dominant scatterer such as a rock, buildings, bridges etc., a phase characteristic is less varies from acquisition to acquisition. This simulation result is shown in figure 4.1(*b*) indicate that the PS pixels do not decorrelated in time.

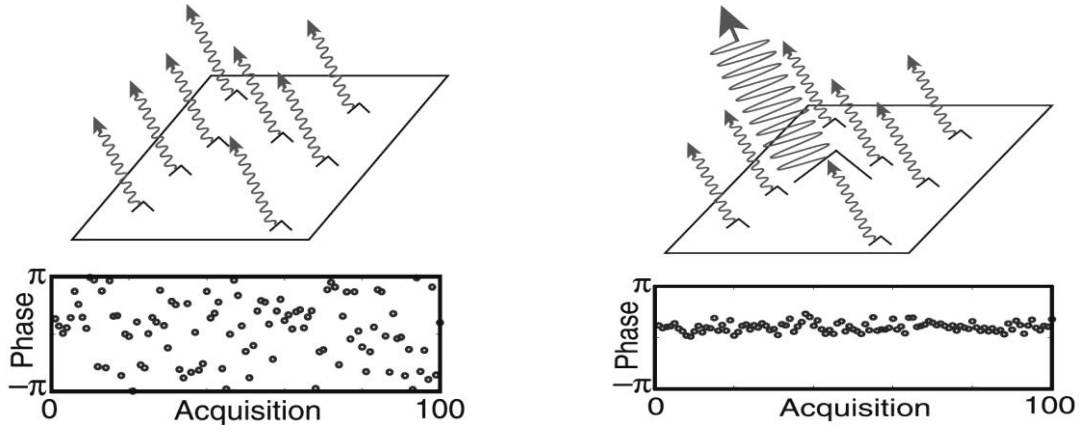

(*a*) Distributed scatterer pixel (*b*) Persistent scatterer pixel

Figure 4.1 (*a*) Hooper (2006) gives a simulation of the phase in case of varying distributed scatterers and for the case a dominant scatter. (*b*) Indicates that the phase remains stable, and do not decorrelated in time.

There are two methods of PS processing searching for the same PS pixels. The first method will search for the pixels having stable phase in time (Ferretti et al., 2001; Kampes, 2006). The second method can be found on (Hooper et al., 2004; Van der Kooij et al., 2006), it searches for the pixels whose phases are correlated in space.

For the first method, the initial step is to select the bright PS pixels (high SNR) based on amplitude dispersion as a proxy for phase stability. After that, candidate pixels selected by amplitude dispersion are then further tested by some phase stability technique, which requires phase to be unwrapped first. PS developed by Ferretti et al. (2001) solve this by assuming that phase change smoothly according to some model (linearly steady or periodic) and use 'expected phase values over time' to guide for phase unwrapping. The unwrapped phases can then be tested if the pixel phase change are random (rejected) or gradually evolve over time (accepted as permanent scatterer). The method has proved to be suitable for urban areas where man-made structures result in stable scatterers. However, the method is not well applicable when phase evolution is episodic (e.g. volcanic motion) rather than smooth.

Alternatively, there is no requirement for a priori information on the second method. The pixels having coherent phase are selected based on the statistical relations between the amplitude dispersion and the phase stability. The PS selection procedure has been changed resulting in a better applicability in all areas (urban and suburban areas). Hooper et al. (2007) developed a method called Stanford Method for Persistent Scatterer (StaMPS) which requires a minimal amount of 12 interferograms for identification of reliable scatterers while a minimum of five acquisitions can be possible using combined method (Hooper, 2008).

4.2 Master Selection

The master is chosen by maximizing the (predicted) total coherence of the interferometric stack, based on the perpendicular baseline $(B_\perp)$, temporal baseline (T), the mean Doppler centroid frequency (f_{DC}) difference and thermal noise (Hooper et al., 2007):

$$\gamma^m = \frac{1}{N}\sum_{n=0}^{N} g\left(B_\perp^{k,m}, B_{\perp,cri}\right) \cdot g\left(T^{k,m}, T_{cri}\right) \cdot g\left(f_{dc}^{k,m}, f_{dc,cri}\right) \cdot \rho_{thermal} \tag{4.1}$$

Where N is the number of images, $B_\perp^{k,m}$ is the perpendicular baseline between images m and k, $T^{k,m}$ is the temporal baseline, $f_{dc}^{k,m}$ is the Doppler baseline and the subscript cri represents the critical value for the sensor used. The function g is given by:

$$g(x,c) = \begin{cases} 1 - |x|/c & if\ |x| < c \\ 0 & \text{otherwise} \end{cases} \tag{4.2}$$

Interferograms are formed between the selected master and every slave image.

4.3 PS candidates Identification

The StaMPS approach requires both amplitude and phase analysis to estimate the PS probability for each pixel in the series of interferograms. Initially, we have to analyze the amplitude to select PS candidates, and then estimate the PS probability of each candidate pixel through phase analysis by processing in a series of iterations. The flow diagram of StaMPS framework is shown in the figure 4.2.

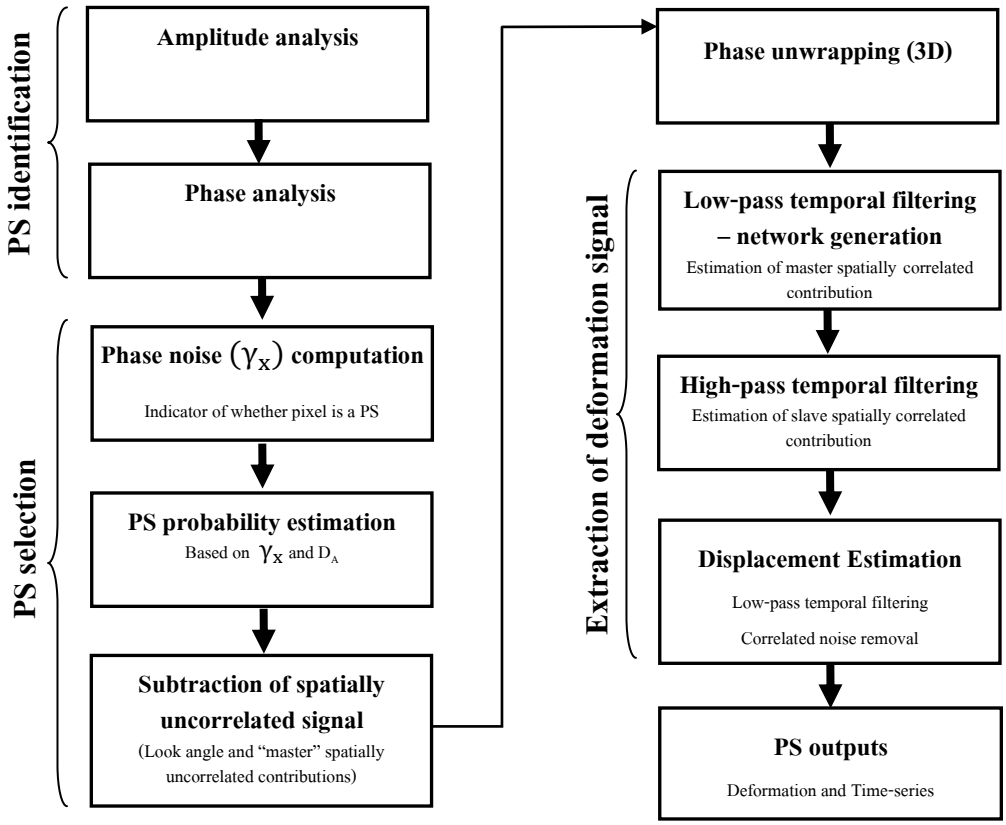

Figure 4.2 Flow diagram of StaMPS framework.

4.3.1 Amplitude Analysis

We use amplitude dispersion simply because all phases are wrapped in the initial step, and we don't know where the PS pixels are. Thus, it is used to 'guess' the locations of these PS which will be refined in later steps. This amplitude dispersion index, D_A, is defined by Ferretti et al. (2001) as:

$$D_A \equiv \frac{\sigma_A}{\mu_A} \tag{4.3}$$

Where σ_A and μ_A are respectively the standard deviation and the mean of a series of amplitude values.

4.3.2 Phase Analysis

Phase stability for each initial candidate will be estimated using phase analysis. The phase stability is analysed under the assumption that deformation is spatially correlated, and then phase observations of neighbouring PS candidates are filtered by those with the lowest residual noise are selected. The wrapped phase $\varphi_{int,x,i}$, of the x^{th} pixel in the i^{th} flattened and topographically corrected interferogram can be written as the wrapped sum of 5 terms:

$$\varphi_{int,x,i} = W\{\varphi_{defo,x,i} + \varphi_{atmo,x,i} + \Delta\varphi_{h,x,i} + \Delta\varphi_{orbit,x,i} + \varphi_{noise,x,i}\} \tag{4.4}$$

where $\varphi_{defo,x,i}$ is the phase change due to movement of the pixel in line-of-sight (LOS) direction, $\varphi_{atmo,x,i}$ the atmosphere phase between passes, $\Delta\varphi_{h,x,i}$ the topographic phase, $\Delta\varphi_{orb,x,i}$ the orbital error and $\varphi_{noise,x,i}$ represents the phase noise term, and $W\{\cdot\}$ is the wrapping operator.

Any variation in the first four terms of Equation 4.4 should dominate the noise term. Assume that $|\varphi_{noise,x,i}|$ is small enough which does not make the complicate PS identification. Then, these four terms are estimated and subtracted, giving an estimate for the noise component$(\hat{\varphi}_{noise,x,i})$, which is accessed statistically using an iterative approach. In fact, the variations in atmosphere delay between passes are spatially correlated in azimuth while the orbital error term leads to spatial correlation in both azimuth and range direction. Topographic error is partly spatial correlated on look angle error. Thus, the first four terms can be estimated by calculating the mean of surrounding pixels which assumed to be PS pixel in the initial step. The

number of pixels included in the mean calculation will be reduced using iteration as confidence in ruling out pixels as PS increases. This is accomplished applying a band-pass filtering method that adapts to any phase gradient present in the data. In StaMPS, the band-pass filter is implemented as an adaptive phase filter combined with a low-pass filter, applied in the frequency domain (see Hooper et al., 2007).

4.4 PS candidates selection

As explained in previous section, StaMPS uses the statistical relationship between amplitude stability and phase stability, so amplitude can reduce the initial number of pixels for phase analysis. However, the threshold value used is higher, typically in the region of 0.4, which leads to most of the selected pixels not being PS pixels. Nevertheless, prior to this initial selection, a digital elevation model (DEM) will be used to remove most of the topographic phase signature from the interferograms. StaMPS use a functional model based on spatial assumptions to identify and extract the deformation signal. The spatial smoothness assumption is supposed to be less affected by variations in the deformation rates, but may miss the detection of a single scatterer which behaves anomalously with respect to its surroundings. Consequently, depending on the deformation characteristics, StaMPS has been successfully applied even in suburban areas and mountainous areas (Hooper et al., 2007).

4.4.1 Phase noise estimation - Gamma (γ_x)

The spatially-correlated contribution to the interferometric phase of a pixel is estimated by band pass filtering of surrounding pixels. This assumed to include the phase due to deformation, atmospheric delay, orbital inaccuracies and topographic error. The phase error from uncertainty in the DEM is proportional to the perpendicular component of the baseline, $B_\perp$:

$$\Delta\varphi_{\varepsilon,x,i} = B_{\perp,x,i} \cdot K_{\varepsilon,x}$$
$$\text{With } \left(k = \frac{4\pi}{\lambda\, R_i^m \sin\theta_i^m}\right) \tag{4.5}$$

Using all the available interferograms will allows us to estimate K for pixel x in a least square sense, as this is the only term that would correlate with baseline.

A phase stability indicator, which is a measure of closeness between the phase of the pixel (corrected for DEM error) and the spatially-correlated phase, is defined based on the temporal coherence and can be used to evaluate whether the pixel is a PS.

$$\gamma_x = \frac{1}{N}\left|\sum_{i=1}^{N} exp\{j(\varphi_{int,x,i} - \bar{\varphi}_{int,x,i} - \Delta\hat{\varphi}_{h,x,i})\}\right| \tag{4.6}$$

Where N is the number of interferograms and $\Delta\hat{\varphi}_{n,x,i}$ is the estimate of $\Delta\varphi_{h,x,i}$. The bar in $\bar{\varphi}_{int,x,i}$ denotes the estimated spatial correlated phase (SCP) from filtering patch. For each PS candidate selected using D_A the SCP will be subtracted as:

$$\varphi_{int,x,i} - \bar{\varphi}_{int,x,i} = B_{\perp,x,i} \cdot K_{\varepsilon,x} + \varphi_{n,x,i} - \bar{\varphi}'_{n,x,i} \tag{4.7}$$

Where $\bar{\varphi}'_{n,x,i}$ is the sum of $\bar{\varphi}_n$ plus the differences between the patch mean values and the pixel values of φ_{defo}, φ_{atmo} and $\Delta\varphi_{orbit}$. Subsequently, $K_{\varepsilon,x}$ is estimated and γ_x calculated.

4.4.2 PS probability estimation

From a statistical point of view, pixels with higher γ_x are more likely to be PS, so candidates with lower γ_x will be down-weighted. Then, an iterative approach is used to recalculate the patch means using all the candidates (after each loop, γ_x is recalculated for every candidate). Generally, the values of $\bar{\varphi}'_{n,x,i}$ will be smaller than before after few iterations. The contribution of $\bar{\varphi}'_{n,x,i}$ is gradually reduced. Finally, PS are selected based on the calculated values of γ_x. Note that, PS are selected in a probabilistic way because any pixel with random phase has a finite chance of having a high γ_x.

In general, a correlation between γ_x and the probability that pixel (x, y) is a PS is expected. By normalizing the values of γ_x the probability density $p(\gamma_x)$ can be estimated. Two groups of pixels are defined: one containing only PS pixels and the other contains only non-PS pixels. $p(\gamma_x)$ is the weighted sum of the probability density for the PS pixels ($p_{PS}(\gamma_x)$) and non-PS pixels ($p_R(\gamma_x)$):

$$p(\gamma_x) = \alpha p_{PS}(\gamma_x) + (1-\alpha)p_R(\gamma_x) \tag{4.8}$$

where $0 \leq \alpha \leq 1$.

After processing the pixels with low amplitude dispersion, StaMPS uses an optional step to calculate γ_x by using the threshold function to select PS from high amplitude dispersion pixels. Then, after many iterations, the RMS change in γ_x is calculated. It was found that a threshold of 3×10^{-2} is in general sufficient (Hooper, 2006). In that case, pixels can be selected based on the PS probability. This probability can be more accurate considering both the amplitude dispersion of the pixels and the ensemble coherence.

4.4.3 Subtraction of spatially uncorrelated signal

Even when the sampling density is high, the contribution to the absolute difference in phase between neighboring PS pixels can still be greater than π due to the spatially uncorrelated part of the signal. The contribution of the master to the spatially uncorrelated part of the signal was also already estimated, so both master and look angle contributions to the spatially uncorrelated part of the signal will be subtract just before unwrapping.

$$W\{\varphi_{int,x,i} - \Delta\hat{\varphi}_{\theta,x,i} - \varphi_x\} = W\{\varphi_{defo,x,i} + \varphi_{atmo,x,i} + \Delta\varphi_{\theta,x,i}^{corr} + \Delta\varphi_{orb,x,i} + \Delta\varphi_{n,x,i}\} \quad (4.9)$$

where $\Delta\varphi_{\theta,x,i}^{corr}$ is the spatially correlated part of $\Delta\varphi_{\theta,x,i}$ and $\Delta\varphi_{n,x,i}$ is the residual spatially uncorrelated noise term.

4.5 Extraction of deformation signal

Once we have selected our PS, we remove all other pixels and return to the original wrapped interferogram phase ($\varphi_{int,x,i}$). Now, the phase must be unwrapped and other nuisance terms estimated in order to retrieve the phase due to deformation ($\varphi_{def,x,i}$).

4.5.1 Phase Unwrapping (3D)

Fully 3D phase-unwrapping algorithms are commonly based on the assumption that the phase difference between neighboring sample points in any dimension is generally less than half a phase cycle (the Nyquist criteria). However, in the case of InSAR time series, the signals are correlated spatially, but uncorrelated over the repeat time due to changes in atmospheric delay. This can vary by several phase cycles across an interferogram, leading to most phase differences

in the time dimension being greater than half a cycle. Deformation can lead to phase jumps greater than half a cycle. On the other hand, the phase difference of a sample point with respect to a neighboring sample point is likely to vary by less than half a cycle between acquisitions, because the contribution from spatially-correlated signals between points close in space is usually small. In StaMPS, this fact is used to set up the InSAR time series phase-unwrapping problem as a series of maximum a posteriori probability (MAP) estimation problems (Hooper, 2009). First, the temporal evolution of the phase difference between neighboring samples is estimated by unwrapping the phase difference under the assumption that it consists of a smooth deformation signal plus random noise. These estimates are used to build a probability density function for the phase difference between each pair of neighboring sample points in every interferogram. In order to take advantage of efficient optimization routines that exist for regularly gridded data, the phase measurements are resample to a grid using a nearest-neighbor interpolation routine. Then the optimization routines of SNAPHU (Chen, 2001) are applied. SNAPHU uses a generalized cost function approach to search for the most likely positions of phase jumps (phase changes between adjacent pixels of more than π in magnitude) within an interferogram. In StaMPS 3D unwrapping algorithm, they are set externally that the phase jumps cannot be placed between grid cells interpolated from the same sparse value and the probability of phase jumps between other cells depends on the evolution of the phase difference between the cells with time. The algorithm can be applied to single master time series of interferograms and interferograms generated from multiple master images that cover overlapping time periods. Hence, it is applicable for both PSI and SB methods. More details about this 3D unwrapping method can be found in Hooper (2009).

4.5.2 Low-pass temporal filtering and High-pass temporal filtering

After unwrapping, the spatially uncorrelated part can be modeled as noise, but the spatially correlated parts can bias the results. For that reason, those terms must be estimated and removed. Spatially correlated nuisance terms will be separated into two parts; one part will correspond to the master contribution to $\Delta\varphi_{orb,x,i}$ and $\varphi_{atmo,x,i}$, and the other part consists of the remaining spatially correlated terms. The low-pass filter in time by Gaussian function will be then used to estimate the master contribution after forming a spatial network connecting for all the PS using Delaunay triangulation. Slave contributions to the spatially correlated phase, which are expected not to be temporally correlated, will be estimated by high-pass filter in time (Hooper, 2006).

4.5.3 Displacement Estimation.

In practice as comments in (Hooper, 2006), it is possible that the spatially correlated nuisance terms may also be correlated temporally, so they will not be correctly estimated by the procedure above. For the orbital error term, we can estimate phase ramps in interferograms where the orbital error term is visible, and remove them, before estimating the other spatially correlated terms. For the atmospheric term where tropospheric moisture content is seasonally variable, the further processing is required. Finally, the estimation of the deformation will be given by:

$$\varphi_{defo,x,i} \approx \varphi_{uw,x,i} + \hat{\varphi}^{m}_{atmo,x} - \hat{\varphi}^{s}_{atmo,x,i} + \hat{\varphi}^{m}_{orb,x} - \hat{\varphi}^{s}_{orb,x,i} - \Delta\varphi^{corr}_{\theta x,,i} - \Delta\varphi_{n,x,i} - 2k_{x,i}\pi \tag{4.10}$$

4.6 Slowly-decorrelating filtered phase (SDFP) pixels Selection (SB)

For Small Baseline technique, Slowly-decorrelating filtered phase (SDFP) pixels are defined by their phase characteristics. For the data presented in this thesis a threshold value of 0.6 was used to reduce the data set size. SDFP pixels are identified among the candidate pixels in the same way as PS pixels using the algorithm of Hooper et al. (2007), which differs from standard PS identification algorithms. Note that although the same algorithm is used to select both PS and SDFP pixels, but the different sets of pixels are chosen due to the different sets of interferograms: single master with no spectral filtering vs. multiple masters with spectral filtering (Hooper, 2008).

4.7 Combined dataset processing (PSI+SB)

The PSI and SB data sets are combined before phase unwrapping step to maximize the reliability of the unwrapped phase. A combined data set of SB interferogram phase is created from both PS and SDFP pixels. When a pixel occurs in both data sets, a weighted mean value for the phase is calculated by summing the complex signal from both data sets, with the amplitude of each set to an estimate of the signal-to-noise ratio (SNR) for the pixel in that data set. The SNR is estimated as in equation 4.11 (Hooper, 2007):

$$\widehat{SNR} = \frac{1}{\gamma_x^{-1} - 1} \tag{4.11}$$

γ_x is re-estimated for PS pixels from the resulting from SB interferogram phase. This is usually lower than the value calculated from PSI interferogram phase, where the master contribution to the decorrelation term is present in every interferogram. Phase unwrapping of SB interferograms cover short time intervals while PSI interferograms has the advantage of reducing spatial-aliasing in the case of high deformation rates.

CHAPTER V

RESULTS AND DISCUSSION

5.1 Introduction

This chapter describes InSAR processing chain, performed on the data covering Bangkok from data available to interpretation of the results. From the beginning, the others SAR data from GISTDA such as ERS-1/2 C band was clarified that it was not possible to generate products from the data archive due to the problem on product generation system. JERS-1 L band has no repeated data in the study area, and all data has been transformed to geotiff format without phase contains in each pixel. ALOS is actually the first considering for this study. Though, the unexpected conditions when making a planning for acquisition; it is difficult to expect the amount of data due to many emergency cases at that time. At last, the Japan Aerospace Exploration Agency (JAXA) announced that the 5 year old ALOS satellite abruptly lost power on 22nd April 2011. Nevertheless, the data available in the study area are 13 images in FBS and FBD mode from November 2007 to December 2010.

As by the reason given above, the choice of data is constrained by time series data availability in the area. This is the most important step for using this technique; although data choice can be a simple step for some others area. In the case of Bangkok, the available of Radarsat-1 data in 2005 and 2009 are collected for the initial processing. However, the large time gap for 2 years of the data has been considered because of the lag in continuing acquired the data in 2006 and 2007. Another acquisition has been made to increase time series data and finally achieve 19 images up to 2010 for the period of 5 years interval.

In this thesis, The 19 images of Radarsat-1 in fine beam mode acquired during the period of October 2005 and March 2010 in ascending orbit are shown in ‘table 5.1’.

Table 5.1 Perpendicular ($\boldsymbol{B}_{\perp}$) and temporal ($\boldsymbol{T}$) baselines, all interferograms are relative to the master of 27 July 2008 (Beam: F1N, Incidence Angle: 38°, Orbital Sense: Ascending, Path/Row: 2/62).

DATE	$\boldsymbol{B}_{\perp}$ (m)	$\boldsymbol{T}$ (days)
23-October-2005	-479	-1008
10-December-2005	-31	-960
10-February-2008	-622	-168
5-March-2008	525	-144
29-March-2008	-768	-120
22-April-2008	774	-96
16-May-2008	-769	-72
3-July-2008	-475	-24
27-July-2008	0	0
31-October-2008	-546	96
18-December-2008	-597	144
11-January-2009	-80	168
4-February-2009	-324	192
2-October-2009	-114	432
19-November-2009	658	480
13-December-2009	-569	504
6-January-2010	-702	528
30-January-2010	125	552
19-March-2010	136	599

5.2 InSAR Processing Strategies

There are several steps based on InSAR time series analysis which the end goal is to estimate the subsidence rate. All required processing steps are visualized as a processing flowchart in figure 5.1. The Radarsat-1 data are generated to SLC processing level using MDA product generation system. The interferometric computations and the PS analysis correspond to DORIS and StaMPS-MTI blocks respectively.

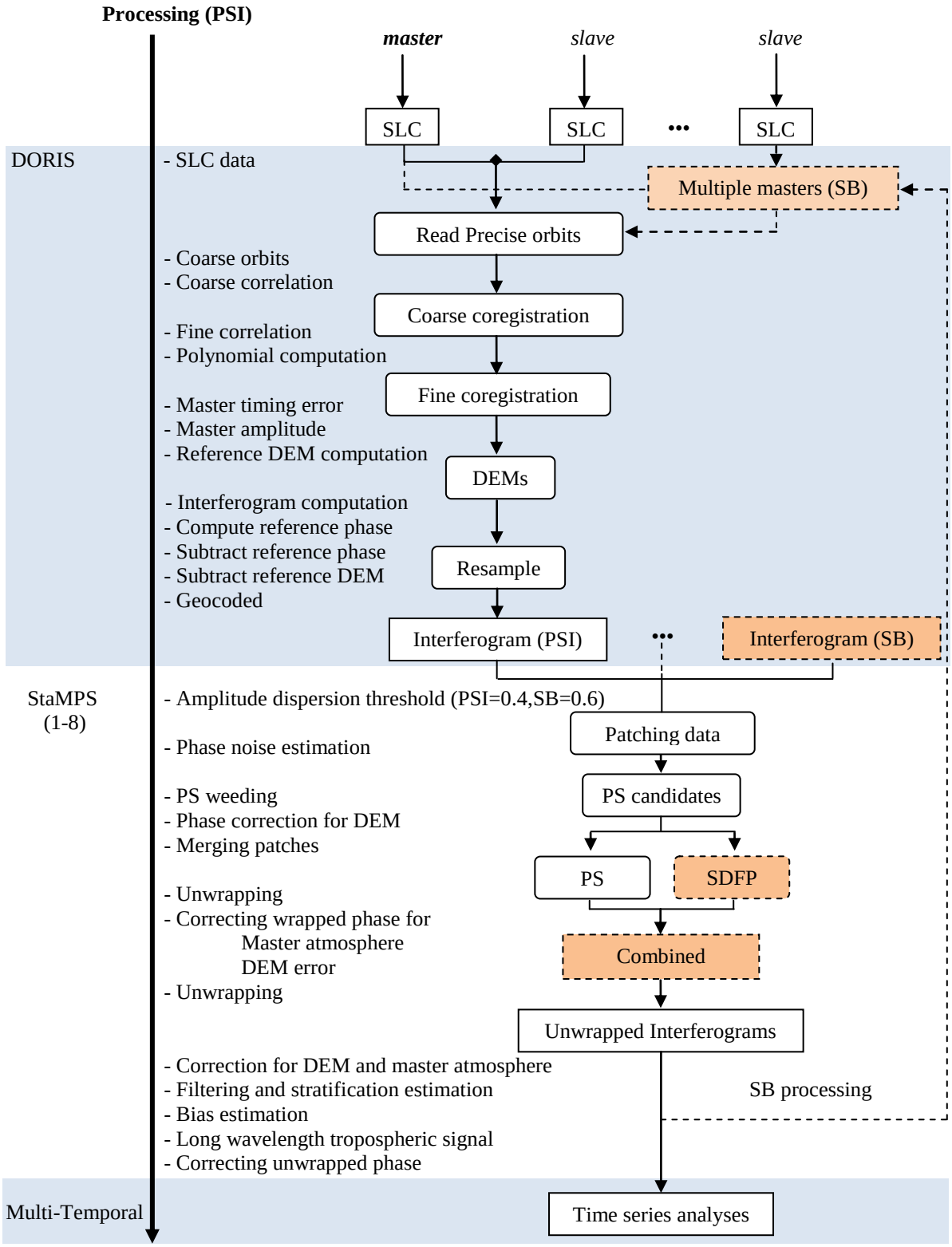

Figure 5.1 Processing flow chart (Modified from Bekaert, 2010). A distinction is made between processing using DORIS (interferograms) and StaMPS-MTI software.

DORIS

InSAR time series analysis can be started from converting CEOS format into DORIS format and cropping data for the study area. The PSI technique requires that all interferograms respect to the same image, referred to as the master. The master data in 27 July 2008 is chosen by minimizing the temporal and perpendicular baseline (see section 4.2), so 18 interferograms are possible for this circumstance of Radarsat-1 data available. For the small baseline processing, the interferograms can be formed by adding more connections using multiple master to ensure that there are no isolated clusters of images, creating a total of 57 interferograms. Figure 5.2(*a*) and 5.2(*b*) give the perpendicular and temporal baselines of each interferograms for the single master network and multiple master images.

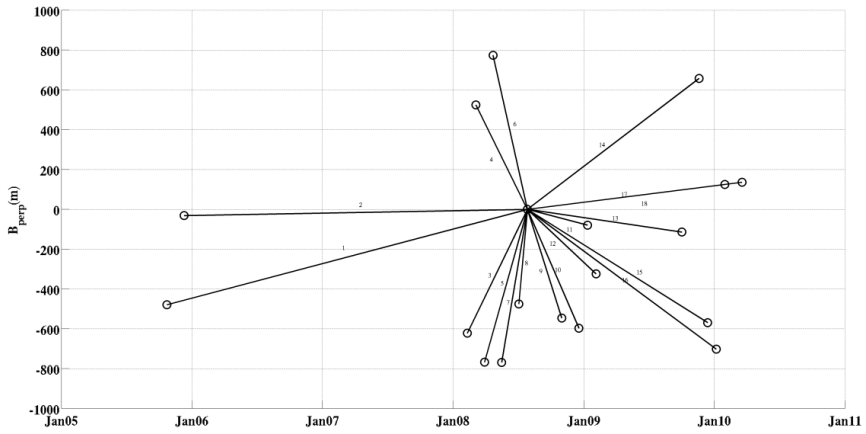

(*a*)

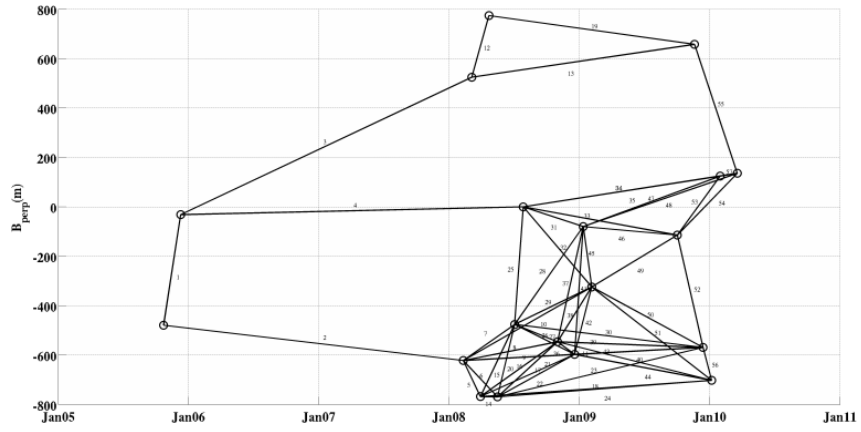

(*b*)

Figure 5.2 Baseline plots for (*a*) the PSI processing and (*b*) the small baseline processing. In both cases, perpendicular baselines are with respect to the master image used in the PS processing. Circles represent images and lines represent the interferograms formed.

After pre-processing, one can continue with the interferometric processing, as is visualized in the DORIS stage of the flowchart in figure 5.1. Computing interferograms requires first of all the coregistration and resampling of the slave to the master image. The coregistrations are performed in coarse and fine coregistration steps. The coarse coregistration step exploits orbit information as starting point, and then the slave image is subdivided into large windows and amplitude correlated with the master image. For every window, the translation with the highest correlation is kept. A coarse estimate is obtained by comparing the different translations in range and azimuth of the different windows. The result of the coarse coregistration is the starting point of fine coregistration step. Translation estimates at sub-pixel precision are obtained after oversampling and amplitude correlation between master and slave in the region where the maximum correlation at the pixel level was obtained. Finally, these estimates are used in estimation of the 2d coregistration polynomial which more details can be found in Kampes and Usai (1999).

Next, the slave is resample to the grid of the master image, and then the interferometric phase can be computed as explain in section 2.3.1. The interferometric phase φ is the sum of different phase contributions such as the reference surface, topography, deformation, atmosphere and noise. The reference surface can be removed using the position information with respect to the reference ellipsoid (WGS84). The topographic contribution can be corrected by using a Digital Elevation Model (DEM). The interferograms are then formed after subtraction of the reference surface and topography.

StaMPS-MTI

Persistent Scatterer processing using StaMPS forms the second processing block of the flowchart shown in figure 5.1. The change of selection parameters is done based on visual inspection of the wrapped and unwrapped interferograms (Hooper et al. 2007). During the initial processing step, the set of pixels were divided into a number of patches that partly overlap. The main reason for the patches is to reduce the required processing memory. The search for PS pixels is the search for pixels having a dominant scatterer in time, meaning that the phase should remain stable. An initial set of PS candidates can be selected based on amplitude dispersion. The latter is defined as the standard deviation of the amplitude divided by its mean (Ferretti et al. 2001). An amplitude dispersion value of 0.4 for PSI and 0.6 for SB resulted in a broad range of pixels, so

most of them not PS. The phase noise for the PS candidate pixels is estimated using an iterative approach (Hooper et al. 2007).

PS pixels were selected based on the pixel phase characteristics and by allowing maximum 20 random phase pixels/km^2. In the next processing step, additional weeding is performed in order to reduce noisy pixels. A pixel was rejected if the minimum phase noise standard deviation of all arcs of that pixel was larger than 1 radian. This in the first place reduces the noise and secondly additional weeding can be performed. During resampling, the new PS values as well as their variance are being estimated. The final set of PS pixels was obtained by allowing a maximum merging standard deviation of 0.45 radians.

StaMPS-MTI use iteration during the unwrapping in order to improve the unwrapping solution. Since unwrapping is an integration of the different fringes, unwrapping errors could be propagated into other regions of an interferogram. After unwrapping, an initial estimate is computed for the master atmosphere and the Spatially Correlated Look Angle (SCLA) error, based on the well unwrapped interferograms. This means that badly unwrapped interferograms need to be ignored, and identified by the user, in the estimation processes. Subsequently, the estimates for master atmosphere as well as the SCLA error are used to correct all wrapped interferograms. As last step in the StaMPS-MTI processing, the initial estimate of the SCLA error and master atmosphere is added back to the unwrapped signal.

5.3 Spatial patterns of Land subsidence

The mean deformation rates from the unwrapped time series are calculated using linear least squares. These estimates are relative to the area centered on benchmark (B52), for easy comparison with leveling. This benchmark is situated in a relatively stable area. To reduce the influence of noise associated with single scatters we take the average rate of pixels lying at a distance less than 100 m from each benchmark. Therefore, assume that the deformation signal does not change significantly over this distance as presented in figure 5.3. The scattering mechanism is assumed that it mainly depends on building type and orientation, so it does not vary over this distance. In order to determine the vertical deformation rate from line-of-sight, it is

simply divided by cosine of the incidence angle at scene center assuming that there is no significant horizontal displacement in the study area.

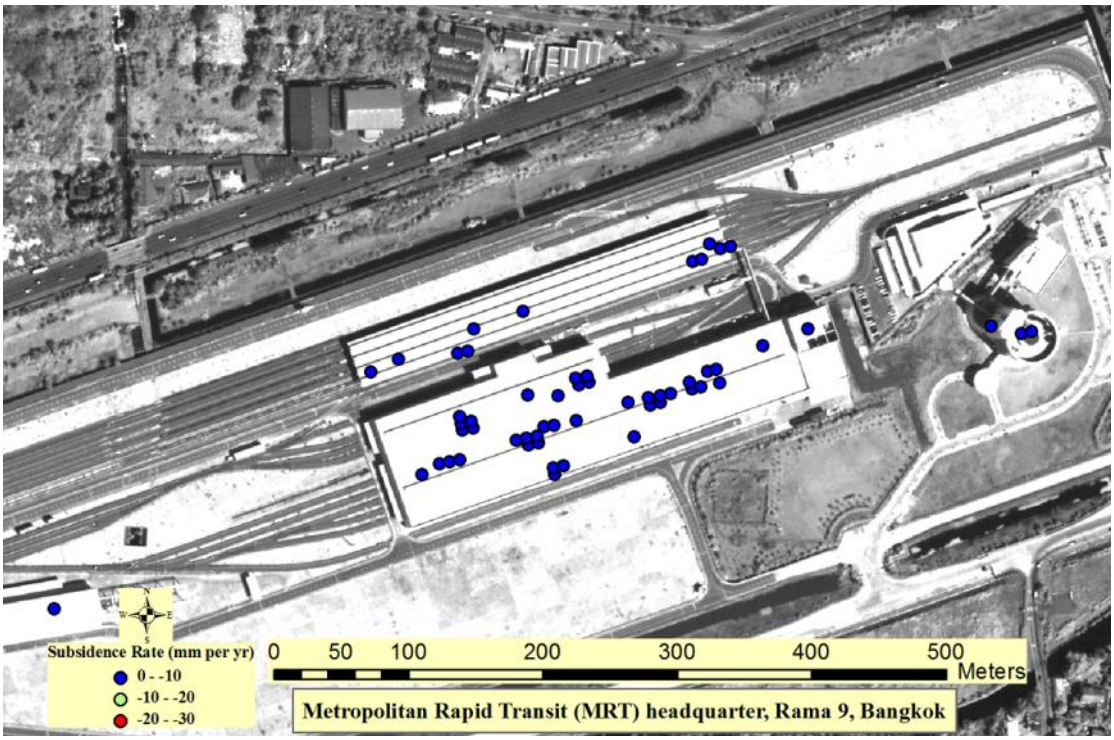

Figure 5.3 A small variation of scatters in an area within distance 100 m.

Figure 5.4(*a*) shows the results of this estimation. The average pixel density in the study area is 120 per km^2 and over 150 per km^2 in the urbanized areas. The standard deviations of the mean velocity in figure 5.4(*b*) are calculated by the percentile bootstrap method (Efron and Tibshirani, 1986). Most of the estimated subsidence rates have standard error less than 1 mm/yr. This means that, both atmospheric signal and unwrapping errors have a negligible contribution in the rate estimation; otherwise it would appear reflected when estimating the precision with bootstrapping. However, there are areas in the southwest and eastern part of the area where the standard deviations are up to 6 mm/yr (Figure 5.4(*b*)). This may be caused by atmospheric artifacts, unwrapping errors, or real deviations of the subsidence in these areas from linear behavior. The rates obtained for these areas should be regarded with caution.

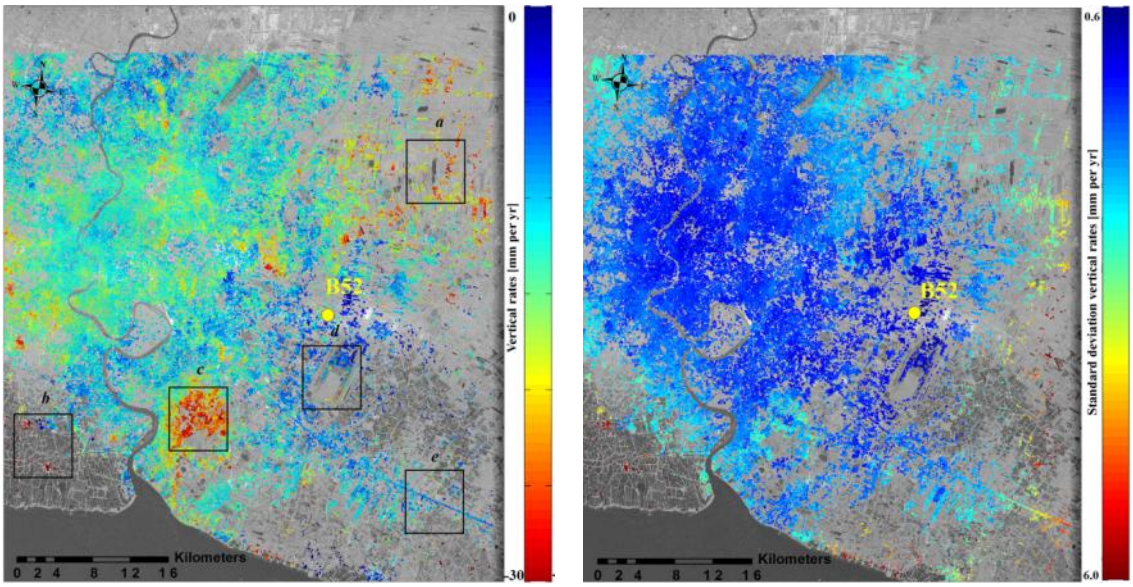

(*a*) (*b*)

Figure 5.4 (*a*): Subsidence rate in vertical direction (mm/yr) from InSAR time series analysis (*b*): Standard deviations of mean rates.

In order to explore the variation of subsidence in the study area, five areas that display different subsidence pattern were chosen, the locations of which can be found in figure 5.4(*a*). Figure 5.5(*a*) shows the agricultural Nongchok district of Bangkok, which includes a lake and paddy fields surrounded by villages. The subsidence rate in the area is between 10 and 30 mm/yr due to the over pumping of ground water for agriculture. This area is prohibited for groundwater pumping following the 'Groundwater Act for the Implementation of Groundwater Management Measurement' of the Department of Mineral Resources (Provincial Waterworks Authority, 2010). Figure 5.5(*b*) includes the coastal zone and southern neighboring provinces (Samut Prakarn, Na klua) in which severe flooding has occurred, probably caused by a combination of erosion and land subsidence (DMR, 2011). For this area we also find strong subsidence of ~25 mm/yr. These values must be treated with caution as the low density of PS may have compromised phase unwrapping. The area of Samut Prakarn-Thepharak in figure 5.5(*c*) shows subsidence rates that reflect the rapid development of an urban industrial zone in recent years. Figure 5.5(*d*) is located at the Suvarnabhumi airport. Here we detect the subsidence of the runway at a rate of 20 mm/yr. This contrasts with the slower deformation at the terminal building (0.5 mm/yr), which is built on piles resting on the sand layer. Finally, figure 5.5(*e*) shows the elevated expressway which is built on piles that stand on the sand layer around 21 m beneath ground surface, and appears to be very stable.

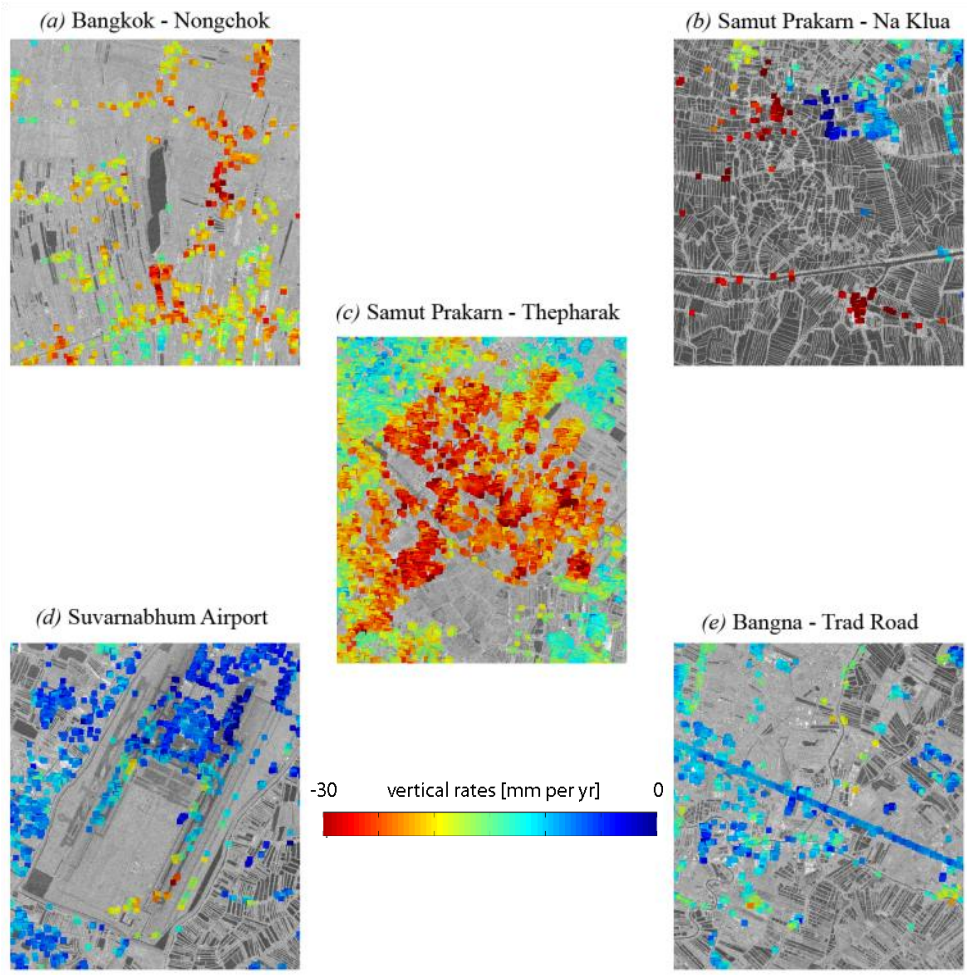

Figure 5.5 Subsidence rate (mm/yr) plotted on the mean radar amplitude. (*a*): Bangkok-Nongchok, (*b*): Samut Prakarn- Na klua, (*c*): Samut Prakarn-Thepharak, (*d*): Suvarnabhum Airport, (*e*): Bangna-Trad Road.

5.4 Validation with leveling

5.4.1 Subsidence rate

The subsidence rate from InSAR and leveling using B52 as a reference are compared in this section. First order geodetic leveling data is obtained from Royal Thai Survey Department (RTSD), respectively. The accuracy of the leveling survey is ±3 mm $\sqrt{K}$ for line leveling and ±4 mm $\sqrt{K}$ for loop leveling. K is the distance of a line or perimeter of a loop in kilometer. The 71 benchmarks attached to pillar or structures stand on top of sand layer are chosen to compare with InSAR results. The subsidence rates of all pixels within a 100 m radius of each benchmark are averaged. As explained above, the deformation caused by groundwater pumping over this

distance does not change significantly. Table 1 shows the velocity values estimated from both leveling and InSAR using least squares while the standard errors are estimated by bootstrap method. InSAR against leveling rates (v_{InSAR} and v_{lev} , respectively) were compared using the t-statistic (Fisher, 1925),

$$t = \frac{v_{InSAR} - v_{lev}}{\sqrt{\sigma_{InSAR}^2 + \sigma_{lev}^2}} \tag{5.1}$$

where the parameter t is a double-tailed Student distribution, and σ_{InSAR}^2 and σ_{lev}^2 are the InSAR and leveling rates variances, respectively. The critical value in hypothesis testing obtained from t-table is 1.97 by using a level of confidence of 95% at alpha equal to 0.05 and 128 for degree of freedom. The degree of freedom (df) for the test can be determined by the sum of the sampling in both InSAR and leveling $(n_1 + n_2)$ minus $2\left(df = n_1 + n_2 - 2\right)$. Thus, in this case, if a t-statistic calculated from the table 1 is less than this value, implying the InSAR and leveling rates are not statistically different, as represented by 0 in table 1. At 71 locations where leveling and InSAR data of the same period are available, the subsidence rates obtained from both methods found that 52 of 65 locations where InSAR results available within radius 100 m around leveling benchmarks are identical. B13, B49, B54, B69, and B71 have been rejected from the table 1 due to there are no InSAR results. B52 is the reference point, so the value of InSAR and leveling equal to 0 and it has been also rejected from the table.

Table 5.2 Comparison of subsidence rates between InSAR and leveling using t-test. The difference types of subsidence rate are +1 when InSAR faster than LEV, -1 when InSAR slower than LEV, 0 when InSAR equal to LEV using 1.97 as a critical value.

Official ID.	BM. ID.	InSAR (mm/yr)		LEV (mm/yr)		t-statistic	Difference Type
		v_{InSAR}	σ^2_{InSAR}	v_{lev}	σ^2_{lev}		
BM.10	**B1**	2.15	1.60	1.67	1.67	0.27	0
BM.11	**B2**	3.6	1.49	4.19	0.99	-0.37	0
BM.16	**B3**	0.86	1.45	2.9	0.83	-1.35	0
BM.17	**B4**	0.55	1.43	2.51	1.54	-1.14	0
BM.18	**B5**	7.58	1.80	0.66	0.92	4.20	+1
BM.20	**B6**	2.51	1.79	1.42	1.02	0.65	0
BM.28	**B7**	8.43	1.16	1.58	0.79	4.91	+1
BM.29	**B8**	2.46	1.41	1.46	0.56	0.71	0
BM.30	**B9**	3.03	1.46	0.78	0.89	1.47	0
BM.33	**B10**	1.55	1.54	3.57	0.61	-1.38	0
BM.38	**B11**	2.28	1.18	0.77	1.18	0.98	0
BM.40	**B12**	4.47	1.33	4.71	1.20	-0.15	0
BM.7	**B14**	2.53	1.43	3.46	1.32	-0.56	0
BM.8	**B15**	2.88	1.45	4.3	0.98	-0.91	0
BMA.106	**B16**	3.25	1.42	2.81	1.42	0.26	0
BMA.113	**B17**	3.02	1.50	2.48	1.01	0.34	0
BMA.115	**B18**	3.74	1.50	0.44	1.29	1.98	+1
BMA.124	**B19**	0.17	1.49	2.61	0.61	-1.68	0
BMA.140	**B20**	5.89	1.60	1.17	1.48	2.69	+1
BMA.155	**B21**	0.96	1.52	2.52	1.24	-0.94	0
BMA.156	**B22**	0.96	1.69	3.09	1.12	-1.27	0
BMA.157	**B23**	0.96	1.64	1.69	0.55	-0.49	0
BMA.159	**B24**	1.07	1.62	2.39	0.38	-0.93	0
BMA.160	**B25**	1.98	1.79	1.42	0.80	0.35	0

Official ID.	BM. ID.	InSAR (mm/yr)		LEV (mm/yr)		t-statistic	Difference Type
		v_{InSAR}	σ^2_{InSAR}	v_{lev}	σ^2_{lev}		
BMA.162	**B26**	6.83	1.60	6.18	1.53	0.37	0
BMA.178	**B27**	1.96	1.51	4.78	1.19	-1.72	0
BMA.206	**B28**	3.86	1.45	3.54	1.05	0.20	0
BMA.209	**B29**	4.26	1.50	4.51	2.21	-0.13	0
BMA.210	**B30**	4.03	1.46	3.52	1.09	0.32	0
BMA.215	**B31**	5.14	1.51	3.53	1.16	0.99	0
BMA.238	**B32**	3.47	1.66	5.18	1.68	-0.94	0
BMA.241	**B33**	4.42	1.53	3.22	2.02	0.64	0
BMA.242	**B34**	2.15	1.53	4.86	1.20	-1.64	0
BMA.255	**B35**	2.28	1.51	4.61	0.89	-1.50	0
BMA.257	**B36**	3.36	1.51	3.49	0.79	-0.09	0
BMA.277	**B37**	0.06	1.40	1.15	0.56	-0.78	0
BMA.284	**B38**	0.54	1.49	4.4	0.94	-2.48	-1
BMA.320	**B39**	0.8	1.56	7.48	1.65	-3.73	-1
BMA.322	**B40**	2.05	1.33	6.4	1.61	-2.54	-1
BMA.339	**B41**	5.73	1.50	0.06	0.60	3.91	+1
BMA.364	**B42**	10.12	1.20	1.99	0.81	5.73	+1
BMA.366	**B43**	7.36	2.08	0.66	0.52	4.16	+1
BMA.368	**B44**	0.87	1.33	1.09	0.64	-0.16	0
BMA.369	**B45**	6.75	1.79	0.62	0.65	3.92	+1
BMA.415	**B46**	5.95	1.66	3.17	2.30	1.40	0
BMA.424	**B47**	0.54	1.54	1.25	1.00	-0.45	0
BMA.434	**B48**	3.31	1.43	1.61	1.33	1.02	0
BMA.453	**B50**	2.43	1.49	1.8	0.44	0.45	0
BMA.454	**B51**	3.24	1.30	0.71	0.77	1.76	0
BMA.455	**B53**	3.1	1.06	1.4	1.00	1.18	0
BMA.502	**B55**	3.26	1.41	5.05	0.92	-1.17	0

Official ID.	BM. ID.	InSAR (mm/yr)		LEV (mm/yr)		t-statistic	Difference Type
		v_{InSAR}	σ^2_{InSAR}	v_{lev}	σ^2_{lev}		
BMA.510	**B56**	3.56	1.46	3.41	1.01	0.10	0
BMA.514	**B57**	5.04	1.38	3.67	0.72	0.95	0
BMA.533	**B58**	3.93	1.48	5.1	1.25	-0.71	0
BMA.547	**B59**	5.23	1.57	5.8	1.11	-0.35	0
BMA.612	**B60**	3.41	1.56	3.76	0.81	-0.23	0
BMA.613	**B61**	2.55	1.41	4.72	0.98	-1.40	0
BMA.618	**B62**	3.51	1.39	5.37	2.03	-1.01	0
BMA.619	**B63**	3.35	1.44	5.64	0.79	-1.53	0
BMA.622	**B64**	4.81	1.54	3.44	0.54	0.95	0
BMA.636	**B65**	6.46	1.80	2.77	0.84	2.27	+1
BMA.637	**B66**	8.71	1.51	3.44	1.05	3.29	+1
BMA.659	**B67**	1.27	1.46	4.14	1.23	-1.75	0
BMA.638	**B68**	4.08	1.53	3.68	0.68	0.27	0
BMA.682	**B70**	3.43	1.50	1.82	0.83	1.05	0

Most of the +1 category (B5, B7, B18, B20, B41, B42, B43, B45, B65, B 66) are found to be in suburban areas where building density are low. One possible explanation for these differences could be the nature of the scatterers contributing to the InSAR measurements. Double-bounce of radar echo from building to ground slab are expected to subside faster than, for example, roof-top scatterers, because buildings usually have deep foundations (see figure 5.6). The -1 category (B38, B39, B40) can be explained by phase unwrapping problem. In any case based on the t-test, the rates are performed; it seems that in most of the cases (80%), InSAR pixels seem to relate to the buildings. However, scatterer characterization is complex to assess and is beyond the scope of this study. The deformation regimes and their effect on single and double-bounce reflections are presented in Ketelaar (2009).

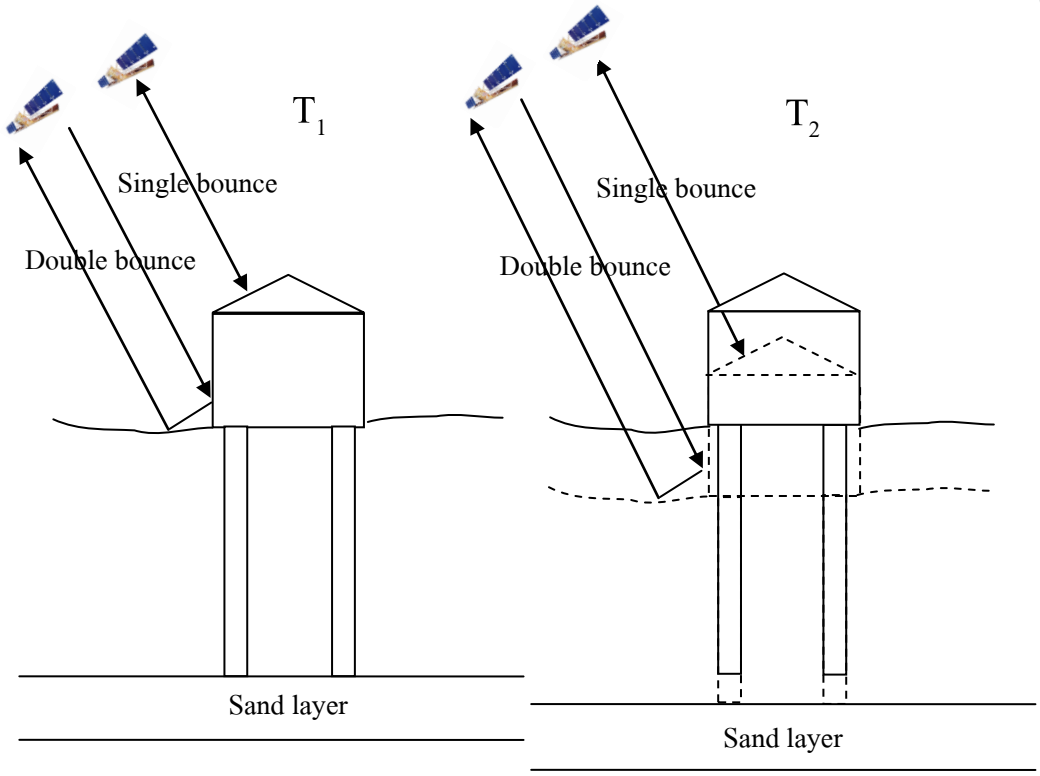

Figure 5.6 Scattering characteristics. (left) structure is affected by single and double bounce echoes at T1 and (right) faster subsiding of double bounce echo at T2 from building to ground slab contaminated into that of building because of the longer distance of radar echoes.

5.4.2 Time series

For a more detailed analysis, the time series from InSAR and leveling are also compared for the points selected base on rate results. Figure 5.7 shows the time series of the selected benchmarks for which subsidence rates from both techniques are in agreement. These benchmarks are B14, B21 and B27 (locations are shown in figure 5.10). Although the comparison is not entirely straight forward, because InSAR observations are acquired at different times to leveling, the two data sets can be said to agree at the 1-sigma error level.

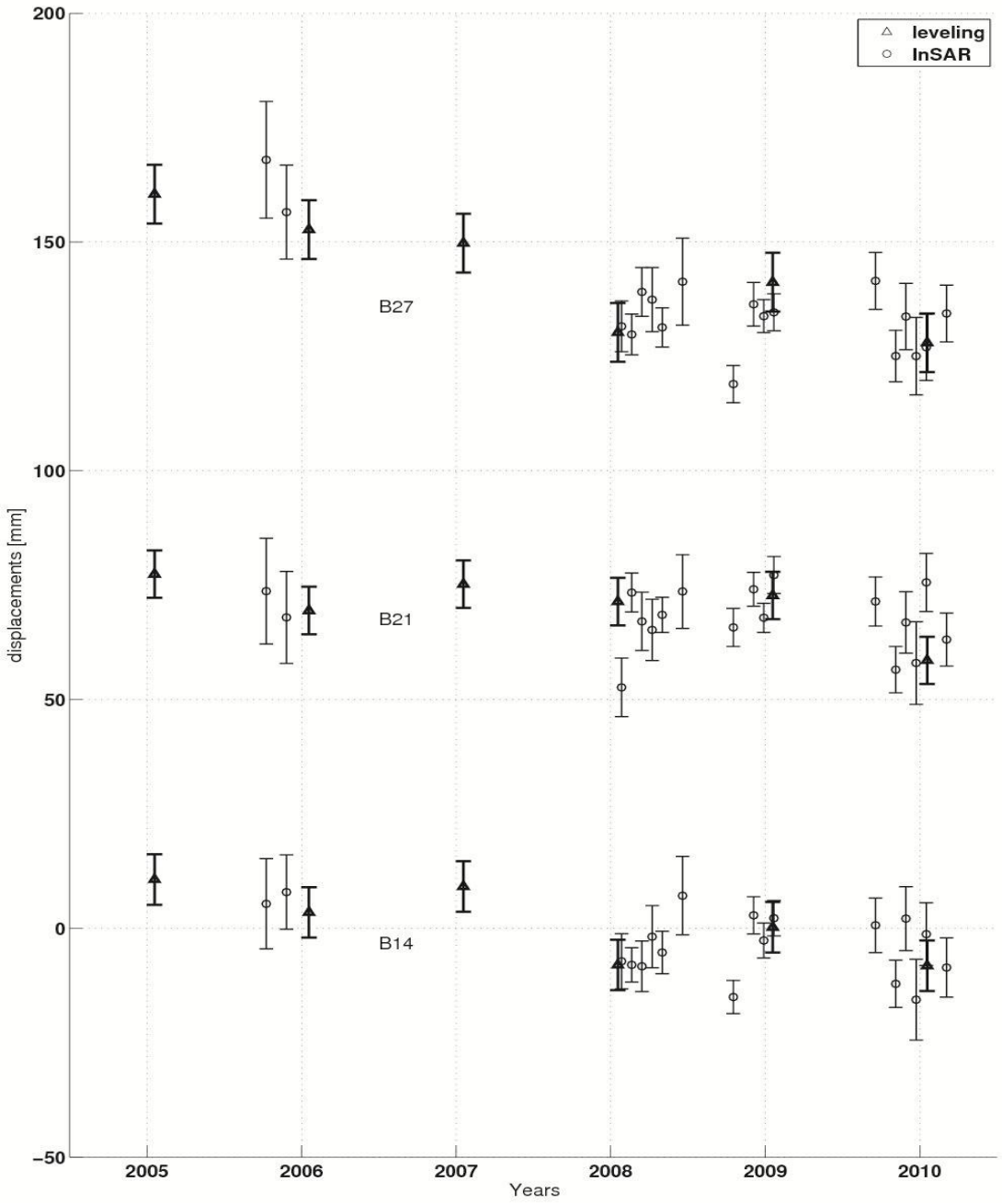

Figure 5.7 Displacement time series obtained from InSAR and leveling for three benchmarks for which the mean displacement rates are in agreement. Vertical offsets are added for visualization.

One example benchmark for which the rates from leveling and InSAR disagree is shown in figure 5.8. Although the measured displacements between the two techniques are in general agreement, there are strong non-linear motions detected by InSAR from 2009 on, which are not visible in the leveling data, perhaps due to the limited temporal sampling. The low number of scatterers near B7 and the potential contribution to the displacement estimates from double-bounce echoes, which express the displacement of the ground rather than the buildings, may be contributing factors, respectively leading to noisier estimates and a larger InSAR subsidence rate may also be contributing factors, leading to noisier estimates.

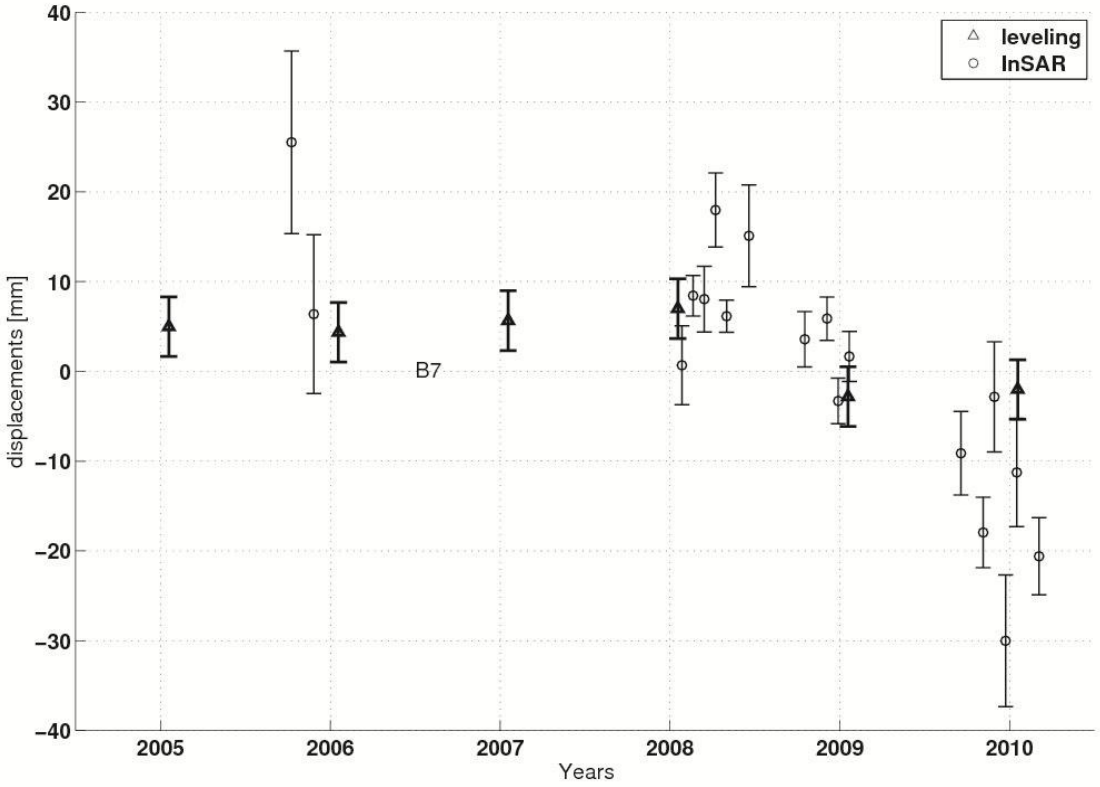

Figure 5.8 Displacement time series obtained from InSAR and leveling for benchmark B7, for which rates from the two techniques are not in agreement.

Figure 5.9 compares the distribution of pixels for B7 with a benchmark B27 where InSAR and leveling agree. Atmospheric delay also contributes to the noise for the InSAR time series. In fact, atmospheric noise was not subtracted due to the bad temporal sampling of SAR images and the inherent difficulty of separating it from non-linear motion. Selection of the reference point cannot be the cause of the differences between leveling and InSAR because otherwise all the time series would be affected.

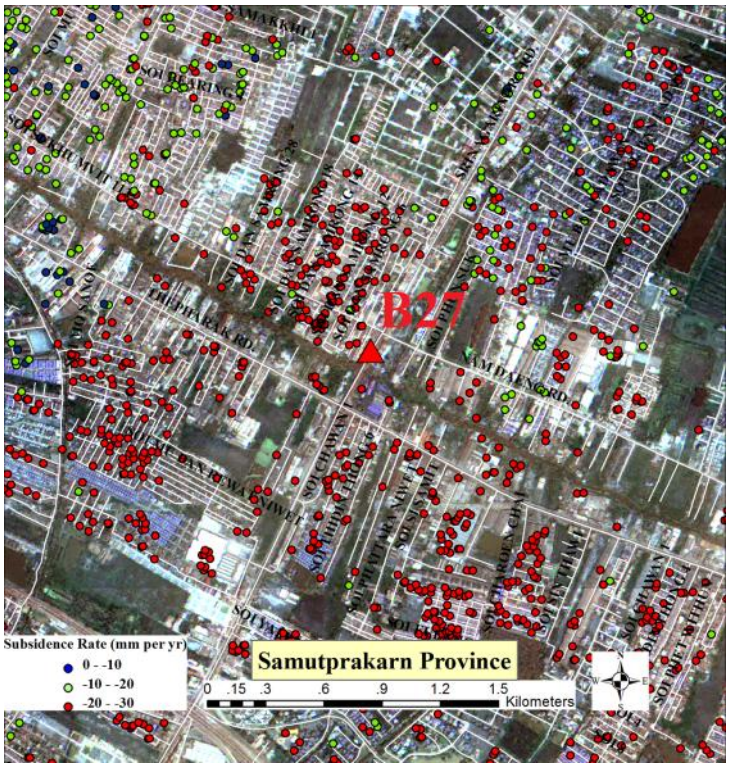

(*a*)

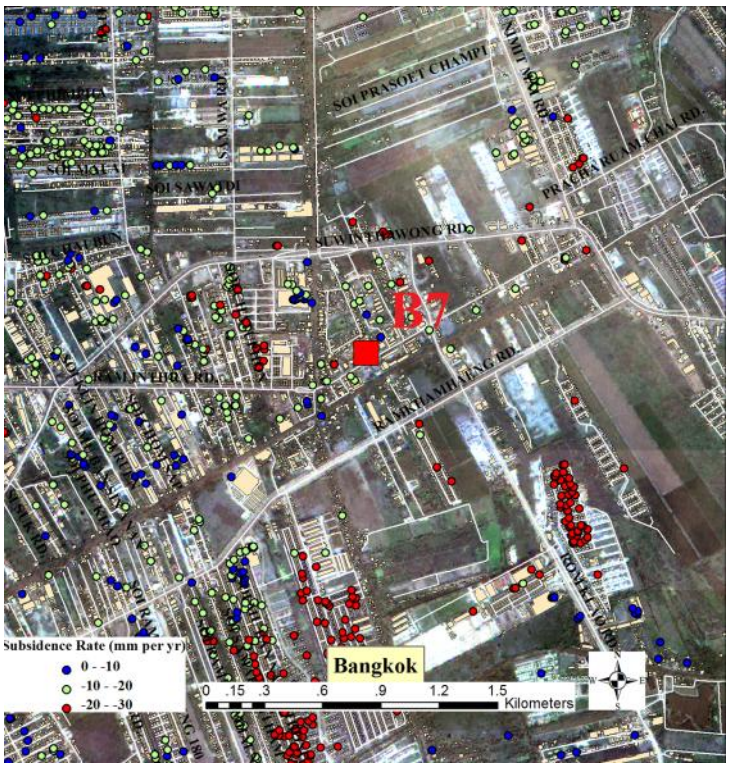

(*b*)

Figure 5.9 Subsidence rates in the neighborhood of two leveling benchmarks. (*a*) B27 is located in Thepharak, Samut Prakarn. (*b*) B7 is located in a rapid growing suburban area, Minburi, Bangkok

5.5 Comparison of interpolated rates

In the previous subsections, the mean rates and temporal pattern of displacement are generally in good agreement between leveling and InSAR. The spatial pattern of the deformation signal is explored in this section, through spatial interpolation. The inverse distance weighted interpolation technique determines cell values using a linearly weighted combination of a set of sample points. It depends on the inverse of the distance raised to a mathematical power, which is set to be 2 ("inverse square"). Figure 5.10 shows the spatial pattern of leveling and InSAR after spatial interpolation. In general, the map reveals similar patterns for both InSAR and leveling. InSAR provides a more detailed map due to the larger number of observations. Major differences occur mostly in areas where there is a lack of leveling benchmarks. For example, in Saphansung district and Ladkrabang district, Bangkok, a fast subsiding area has been detected with InSAR that is not revealed by leveling. The coastal zone in Amphoe Muang, Samutprakarn and the agriculture area in Amphoe Lam luk ka, Pathumthani have also been subsiding considerably rapidly at the rate of 20-30 mm/yr.

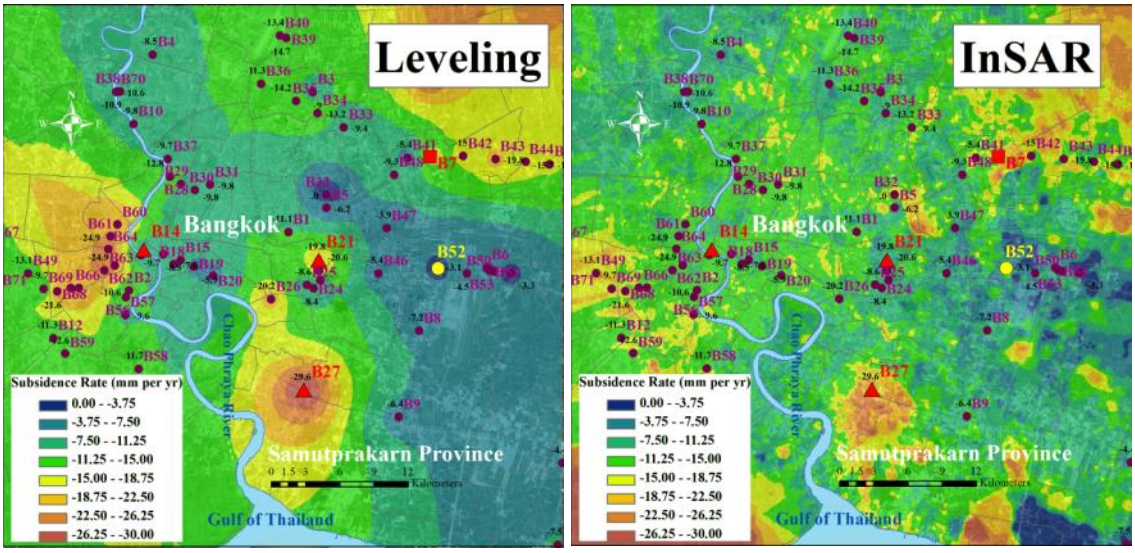

(*a*) (*b*)

Figure 5.10 Distribution pattern of subsidence from (*a*) leveling and (*b*) InSAR using inverse distance weighted interpolation. Point symbols represent leveling benchmarks, with red triangles indicating the benchmarks shown in figure 5.7 and the red square indicating the benchmark shown in figure 5.8. The yellow circle indicates the reference benchmark.

Finally, the spatial detailed subsidence patterns for the study areas can be contributed as a subsidence map in figure 5.11. The coverage area includes some part of Samut Prakarn, Nonthaburi, and Phatum thani.

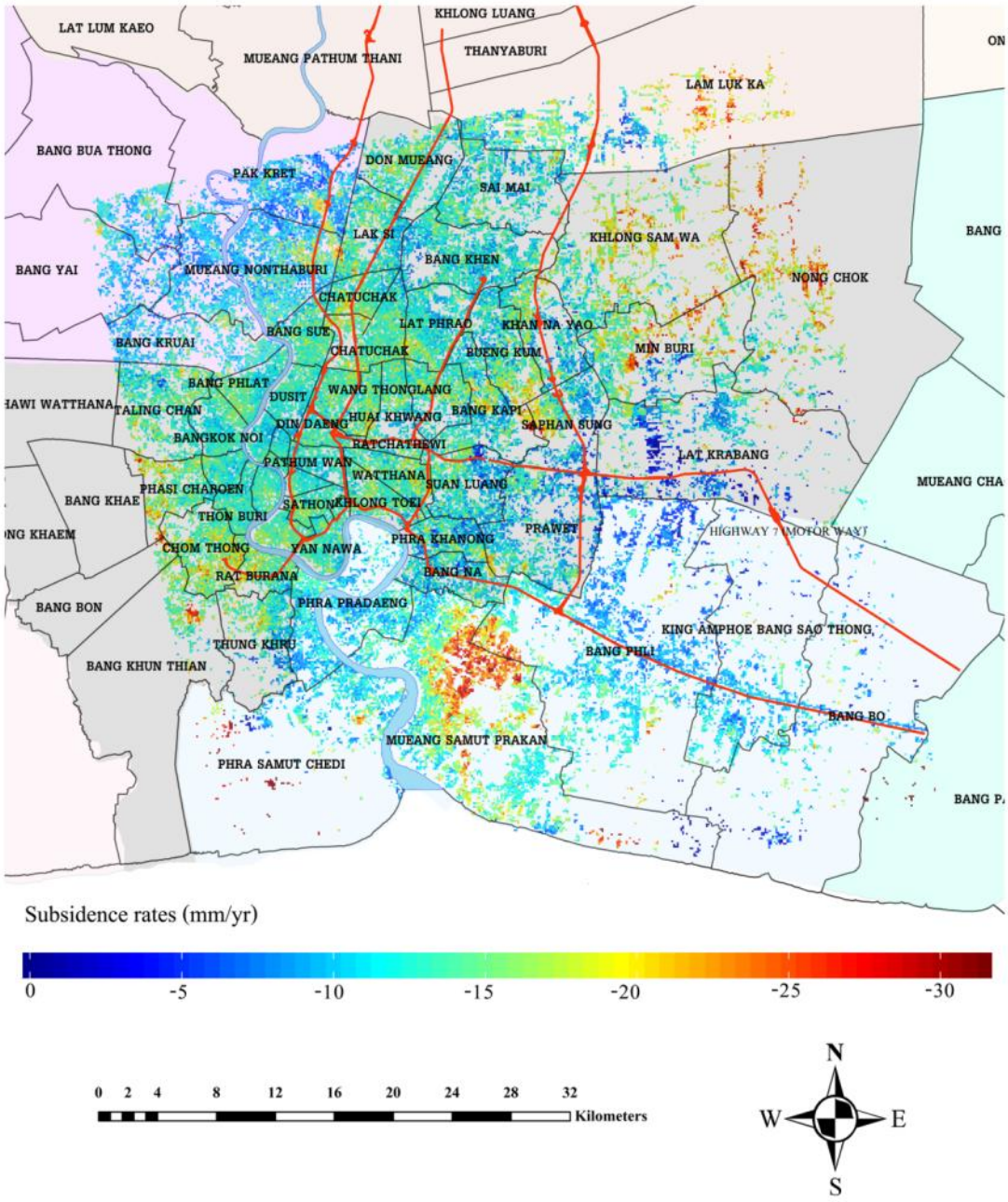

Figure 5.11 Land subsidence map of Bangkok from Radarsat-1 data in the period of 2005-2010 using InSAR time series analysis.

CHAPTER VI

CONCLUSIONS AND RECOMMENDATIONS

6.1 Summary

Chapter I of this thesis presents general information of background of land subsidence in Bangkok that it was first detected in the late 1960s and early 1970s. Monitoring of land subsidence has been performed using leveling. The motivation of the research is that the different characteristics of leveling and InSAR data can be integrated for subsidence monitoring, possibly resulting in more efficient monitoring strategies as complementary measurement techniques. A main objective is to apply a combination of two specific methods of InSAR namely Persistent Scatterer (PS) and Small Baseline (SB) to measure occurring subsidence in Bangkok and part of of Nothaburi, Pathumthani and Samutprakarn, for the period October 2005 until March 2010 from Radarsat-1 data.

The historical review and brief discussion on the applications of SAR Interferometry for measuring land deformation are presented in Chapter II. There are many applications for land deformation that InSAR can be applied such as earthquakes, volcanoes, landslides, and land subsidence. InSAR applications generally have been achieved by analyzing a single differential interferogram derived from one pair of SAR images (2-pass DInSAR). Though, this technique is appropriate for monitoring a large deformation signals compared to the errors sources in areas that do not continue from significant temporal surface changes. In areas with slow deformation rates such as land subsidence, a significant improvement of the decorrelation problem was obtained with the new methods called InSAR time series analysis.

Chapter III provides the background of land subsidence problem and the necessity for its monitoring in Bangkok and its vicinity areas. For Bangkok, it was in 1978 when subsidence was the first monitored by first-order leveling by the Royal Thai Survey Department (RTSD). For a very long time leveling data has been the only source from which subsidence is derived. The thesis has shown limitations of leveling survey network which includes frequent maintenance to prevent loss, location bias and costly and time-consuming operation. By using InSAR, some

problem of the leveling can be alleviated because InSAR has potential to provide surface deformation measurements at a significantly improved under-sampling and bias problem within millimeter-level accuracy over large areas.

InSAR time series analysis is a geodetic tool for deformation measurements to identify single pixel that is coherent over long time intervals. Therefore, the principle behind the technique is the search for permanent dominant scatterers as explained in Chapter IV for InSAR time series analysis with combined data set processing called Multi-temporal InSAR approach. The StaMPS-MTI approach requires both amplitude and phase analysis to estimate the PS probability for each pixel in the series of interferograms. Initially, the amplitude is analyzed to select PS candidates, and then estimate the PS probability of each candidate pixel through phase analysis by processing in a series of iterations. The phase unwrapping can then be used for displacement estimation.

The discussions of land subsidence rate comparing with leveling survey have been performed in Chapter V. The research has demonstrated the capability of InSAR time series analysis for monitoring subsidence. Further, it also shown that subsidence rates from InSAR are comparable to those derived from leveling data. Deformation rates have been estimated for the period 2005 until 2010 using 19 Radarsat-1 SAR images. Maximum rate of about 30 mm/yr can be seen in Amphoe Muang, Samutprakarn and Amphoe Lam luk ka, Pathumthani. Central Bangkok on the east of Chao Phraya river appears to be subsiding slowly at rates around 10 mm/yr or slower while in northern and western suburban areas are found to subside at rates between 10-20 mm/yr. InSAR also reveals fast subsiding areas in Saphansung district and Ladkrabang district, Bangkok which have been missed by leveling due to its under sampling problem.

The research has undergone comprehensive comparison of Subsidence rates estimated from InSAR and those estimated from leveling. In this comparison, all coherent targets detected by InSAR to 100 m from the benchmarks are averaged as representative of InSAR rate. Statistical test (t-test) of InSAR rates and leveling found that 52 of 65 locations are identical. The 10 locations where InSAR rates are larger than leveling are found to be in suburban areas where building density are low and possible larger opening between buildings. One possible explanation for these points could be the double-bounce of radar echo from building to ground slab to occur

and so faster subsiding ground slab contaminated into that of building. The 3 areas where InSAR rates are slower can be explained by phase unwrapping problem.

6.2 Conclusions

Until now, the principal source of information about land subsidence in Bangkok has come from annual leveling campaigns by the RTSD, which have been carried out since 1978. The leveling survey technique is a reliable technique, but the distribution of points in the leveling network is sparse. On the other hand, the results from InSAR provide a very high observation density with comparable accuracy. InSAR should, therefore, be considered as a complementary technique to leveling for monitoring land subsidence in Bangkok.

The application of time series InSAR approach that combines both persistent scatterer and small baseline methods detected approximately 300,000 pixels that can serve as monitoring points. These observations provide two orders of magnitude better spatial density than leveling making less bias results and more detailed pattern of the land subsidence.

In this research, it has further been demonstrated that InSAR can be utilized as a geodetic tool to monitor land subsidence. The average PS density in the Bangkok area is about 120 points/km^2, which is significantly higher than the leveling benchmarks density of less than 1 point/km^2. As a result, InSAR has largely overcome the under-sampling and bias problem of leveling technique. The higher temporal sampling of InSAR has also significant advantage. The 24 days revisit period of Radarsat-1 means 15 repeated acquisitions of images per year can be made while leveling of such a large area can be carried out at most once. However, leveling data remain necessary. A certain number of leveling points are still required as check points and for certain places where limitations of InSAR such as double-bounce and loss of coherence may provide unreliable rates.

6.3 Recommendations

It has been shown from this study that InSAR can be utilized as a geodetic tool with accuracy comparable to leveling. Recommendations are list below here as to further applications of InSAR time series analysis for slow-varying deformation.

- Applying time series InSAR for land subsidence in other areas where there are no monitoring network like Bangkok such as eastern seaboard or coastal provinces that may also be prone to problems caused by subsidence. Land subsidence is one cause of the problems for coastal erosion in the Gulf of Thailand. Aobpaet et al. (2011) presented the initial results of coastal zone subsidence using time series InSAR. The study reveals that the eastern coast of the inner Gulf of Thailand subsided with the maximum subsidence rate 23.6 mm/yr at golf course, Mueang Chon buri while the average subsidence rate of 10 mm/yr can be found at Laem Chabang deep-sea port. The other areas are applicable for time series InSAR for the fastest and most economic way to use.

- Applying time series InSAR for monitoring of other slow-varying deformation such as inter- or post-seismic motion. There are many successful stories using time series InSAR for inter- or post-seismic motion as review in chapter 2 sections 2.2.2.1. The ongoing project for post- seismic displacement of 2011 Mw6.8, Tarlay earthquake, Myanmar using time series InSAR technique is one of the interesting projects because the study area is very difficult to access using another geodetic tool and covering with dense vegetation. Thus, InSAR can be very interesting technique to measure active fault surface deformation.

- Further in-depth study of the 20% of PS points that rates do not agree with leveling survey as discussed in section 5.4.1 chapter 5. These differences could be the nature of scatterers contributing to InSAR measurements. Ground scatterers (ground to wall reflections) are expected to subside faster than that, for example, roof-top scatterers, because buildings usually have deep foundations. The scatterer characteristic is very complex to assess and it should be considered and included for future monitoring.

- 13 ALOS-PALSAR L-band data available over Bangkok area from 2007-2010 would be interesting to study the dense vegetated area neighboring Bangkok. The relative high coherence in an interferogram will allows easier unwrapping aiding further statistical investigations on the spatial properties of the atmospheric signal.

- The first German radar satellite mission, TerraSAR-X and COSMO-SkyMed of Italian space agency are X-band SAR data available with high spatial resolution and short revisit time for 11 days and 16 days (same satellite), respectively. Moreover, the revisit time of COSMO-SkyMed can be up to 1 day interval using COSMO-SkyMed 2 and 3. Thus, the main benefit of short revisit period is the abilities to get build time series more rapidly than others satellites and to produce more interferograms for the more reliable of atmospheric and orbital estimation.

REFERENCES

Akagi, T., 1979, Some land subsidence experiences in Japan and their relevance to subsidence in Bangkok, Thailand. Geotechnical Engineering, 10: 1-48.

Amelung, F., Galloway D., Bell J., Zebker H., and Laczniak R., 1999, Sensing the ups and downs of Las Vegas: InSAR reveals structural control of land subsidence and aquifer system deformation. Geology, 27(6): 483-486.

Aobpaet, A., Trisirisatayawong, I., Hoopper, A.J., 2011, Coastal Zone Deformation over Eastern Inner Gulf Of Thailand Using Multi-Temporal InSAR Method. In Proceedings of the 32nd Asian Conference on Remote Sensing. Taipei, Taiwan.

Asian Institute of Technology (AIT), 1995, Artificial recharges subsidence control, Bangkok Thailand. Final technical report, School of Civil Engineering, Asian Institute of Technology, Bangkok, Thailand. Submitted to the International Development Research Center.

Asian Institute of Technology (AIT), 1981, Investigation of land subsidence caused by deep well pumping in the Bangkok area: Comprehensive report 1978–1981. Research report no. 91. Submitted to the Office of the National Environment Board. Bangkok:

Askne, J.I.H., Dammert, P.B.G., Ulander, L.M.H., and Smith, G., 1997, C-band repeat-pass interferometric SAR observations of the forest. IEEE Transactions on Geoscience and Remote Sensing, 35: 25-35.

Balasubramaniam, A.S., Oh, E.Y.N, Bolton, M.W., Bergado, D.T. and Phienwej, N., 2005, Deep well pumping in the Bangkok plain and its influence on ground improvement development with surcharge and vertical drains. Ground Improvement, 9(4): 149-162.

Baran, I., 2004, Advanced Satellite Radar Interferometry for Small-Scale Surface Deformation Detection. PhD Thesis. Curtin University of Technology, Australia.

Beavan, J., Motagh, M., Samsonov, S., Fielding, E. and Celentano, A., 2011, Coseismic and postseismic deformation analysis of the 2010 Mw 7.1 Darfield and 2011 Mw 6.3 Christchurch earthquakes in New Zealand from combined GPS and InSAR observations. In Proceedings of the FRINGE Workshop 11, 19-23 September 2011. ESA-ESRIN. Frascati (Rome), Italy.

Bekaert, D., 2010, InSAR time series analysis of the 2006 slow slip event on the Guerrero Subsidence Zone, Mexico. Master Thesis. Delft University of Technology, The Netherlands, 116p.

Berardino, P., Fornaro, G., Lanari, R. and Sansosti, E., 2002, A new algorithm for surface deformation monitoring based on small baseline differential SAR interferograms. IEEE Transactions on Geoscience and Remote Sensing, 40(11): 2375-2383.

Bontebal, M., 2001, Land subsidence in Bangkok. Available online at: http://www.unescap.org/esd/water/urbangeology/land/background.asp (accessed 25 August 2010)

Brand, E.W., and Paveenchana, T., 1971, Deep-well Pumping and Subsidence in the Bangkok Area. In 4th Asian Regional Conference on Soil Mechanics and Foundation Engineering., Bangkok, 1: 1-7.

Buapeng, S., and Foster, S., 2008, Controlling Groundwater Abstraction and Related Environmental Degradation in Metropolitan Bangkok -Thailand. Available online at: http://siteresources.worldbank.org/INTWAT/Resources/GWMATE_CP_20_Bangkok.pdf (accessed 25 July 2012).

Buckley, S., Rosen, P., Hensley, S., and Tapley, B., 2003, Land subsidence in Houston, Texas measured by radar interferometry and constrained by extensometers, Journal of Geophysics Research, 108(B11).

Carnec, C., Massonnet, D., and King, C., 1996, Two examples of the application of SAR Interferometry to sites of small extent, Geophysics Research Letter, 23, : 3579-3582.

Cetin, E., Meghraoui, M. Cakir, Z., Akoglu, A., Mimouni, M.O., and Chebbah, M., 2012, Seven years of post- seismic deformation following the 2003 Mw = 6.8 Zemmouri earthquake (Algeria) from InSAR time series. Geophysics Research Letter, 39(L10307), doi:10.1029/2012GL051344.

Chatterjee, R.S., Fruneau, B., Rudant, J.P., Roy, P.S., Frison, P.L., Lakhera, R.C., Dadhwal, V.K. and Saha, R., 2006, Subsidence of Kolkata (Calcutta) City, India during the 1990s as observed from space by Differential Synthetic Aperture Radar Interferometry (D-InSAR) technique. Remote Sensing of Environment, 102: 176-185.

Chen, C., and Zebker, H., 2001, Two-dimensional phase unwrapping with use of statistical models for cost functions in nonlinear optimization, Journal of the Optical Society of America A, 18: 338–351.

Colesanti, C., Ferretti A., Prati C., and Rocca F., 2003, Monitoring landslides and tectonic motions with the Permanent Scatterers technique, Engineering Geology, 68, 3-14.

Cox, J.B., 1968, A review of engineering properties of the recent marine clays in Southeast Asia. AIT research report no. 6. Bangkok: Asian Institute of Technology.

Crosetto, M., Arnaud, A., Duro, J., Biescas, E. and Agudo, M., 2003, Deformation monitoring using remotely sensed radar interferometric data. In Proceedings of the 11th FIG Symposium on Deformation Measurements, Santorini, Italy.

Department of Groundwater Resources, 2007, The report of the groundwater and land subsidence and guidelines for the management of groundwater in the Bangkok metropolitan area. Available online at: http://www.dgr.go.th/hilight/file/report50.pdf (accessed 25 July 2012).

Department of Ground Water Resources (DGR), 2004, Mathematical modeling on effects of mitigation measures to excessive groundwater use in Bangkok area. A technical report by Kasetsart University submitted to DGR, Bangkok, Thailand.

Department of Mineral Resources, 2011, Status of Coastal Geo-Environment in Thailand. Available online at: http://www.dmr.go.th/ewtadmin/ewt/dmr_web/main.php?filename=coastal_En (accessed 26 June 2011).

Dixon, T., Amelung F., Ferretti A., Novali F., Rocca F., Dokka R.and others., 2006, New Orleans subsidence: space geodesy and Hurricane Katrina Flooding. Nature, 441: 587-588.

Duc N.A., 1999, Updating and analysis of Bangkok land subsidence caused by deep well pumping with emphasis on shallow soil settlement, Master Thesis. Asian Institute of Technology, Bangkok, Thailand.

Edward, W., 1976, Soil Compressibility and Land Subsidence in Bangkok. Publication n°121 of the International Association of Hydrological Sciences, Proceedings of the Anaheim Symposium, California, USA.

Efron, B. and Tibshirani, R., 1986, Bootstrap methods for standard errors, confidence intervals, and other measures of statistical accuracy. Statistical Science, 1(1): 54-77.

Evans, D., Farr, Zebker, T.H. and Mouginis-Mark, P., 1992, Radar interferometry studies of the Earth's topography, EOS, Transaction of American Geophysical Union, 73(553): 557-558.

Ferretti, A., Prati, C. and Rocca, F., 2001, Permanent scatterers in SAR interferometry. IEEE Transactions on Geosciences and Remote Sensing, 39(1): 8-20.

Ferretti, A., Rocca, F., and Prati, C., 2000, Nonlinear subsidence rate estimation using permanent scatterers in differential SAR Interferometry. IEEE Transactions on Geoscience and Remote Sensing, 38(5): 2202-2212.

Fielding, E.J., Lundgren, P.R., Burgmann, R., Funning, G.J., 2009, Shallow fault-zone dilatancy recovery after the 2003 Bam earthquake in Iran. Nature, 458, doi:10.1038/nature07817.

Fielding, E., Bloom R., and Goldstein R., 1998, Rapid subsidence over oil fields measured by SAR interferometry. Geophysics Research Letter, 27: 3215-3218.

Fisher, R.A., 1925, Applications of Student's distribution. Metron, 5: 90-104.

Fornaro, G. and Sansosti, E., 1999, A two-Dimentional Region Growing Least Square Phase Unwrapping Algorithm for Interferometric SAR Processing. IEEE Transactions on Geoscience and Remote Sensing, 37(5): 2215-2226.

Franceschetti, G., and Lanari, R., 1999, Synthetic Aperture Radar Processing. CRS Press, New York, USA: 307.

Friedrich, K., David, A., Geraint, C., Javier, D., Johanna, G., Susanne, H., Arne, H.R., Dodid, M., 2010, Detection of land subsidence in Semarang, Indonesia, using stable points network (SPN) technique. Environmental Earth Sciences, 60 (5): 909–921. doi:10.1007/s12665-009-0227-x.

Fujiwara, S., Rosen, P., Tobita, M., and Murakami, M., 1998, Crustal deformation measurements using repeat-pass JERS-1 synthetic aperture radar interferometry near the Izu Peninsula, Japan, Journal of Geophysical Research, 103: 2411-26.

Gabriel, A.K., Goldstein, R.M., Zebker, H.A., 1989, Mapping small elevation changes over large areas: differential radar interferometry. Journal of Geophysical Research, 94 (B7): 9183-9191.

Gabriel, A.K. and Goldstein, R.M., 1988, Crossed Orbit Interferometry: Theory and Experimental Results from SIR-B. Journal of Geophysical Research, 9(5):857-872.

Galloway, D.L., Jones, D.R., and Ingebritsen, S.E., 2000, Measuring land subsidence from space: U.S. Geological Survey Fact Sheet 051-00, 4p.

Galloway, D., Hudnut, K., Ingebritsen, S., Phillips, S., Peltzer, G., Rogez, F., and Rosen, P., 1998, Detection of aquifer system compaction and land subsidence using interferometric synthetic aperture radar, Antelope Valley, Mojave Desert, California, Water Resources Research, 34: 2573-2585.

Ghiglia, D.C., and Pritt, M.D., 1998, Two-dimensional phase unwrapping: Theory, Algorithms and Software, Wiley, New York.

Goldstein, R.M., 1995, Atmospheric limitations to repeat-track radar interferometry. Geophysical Research Letters, 22(18): 2517–2520.

Goldstein, R.M., Zebker, H.A., and Werner, C.L., 1988, Satellite radar interferometry: two-dimensional phase unwrapping, Radio Science, 23(4): 713-20.

Graham, L.C., 1974, Synthetic Interferometer Radar for Topographic Mapping. Proceeding of the IEEE, 62(2): 763-768.

Haley&Aldrich Inc., 1970, Effect of Deep Well Pumping on Land Subsidence in Bangkok, part of "Master Plan, Water Supply and Distribution, Metropolitan Bangkok, Thailand". 4, Report by Camp, Dresser & Mckee Inc., submitted to Metropolitan Water Works Association, Bangkok.

Hanssen, R.F., 2001, Radar Interferometry: Data Interpretation and Error Analysis. Kluwer Academic Publishers, Dordrecht, The Netherlands, 301p.

Hanssen, R.F., 1998, Atmospheric Heterogeneties in ERS Tandem SAR Interferometry. Delft University Press, Delft, The Netherlands. 155p.

Hernandez, B., Cotton, F., Campillo, M., and Massonnet, D., 1997, A comparison between short term (co- seismic) and long term (one year) slip for the Landers earthquake: measurements from strong motion and SAR interferometry, Geophysical Research Letters, 24, 1579-82.

Hilley, G., Bürgmann R., Ferretti A., Novali F., and Rocca F., 2004, Dynamics of slowmoving landslides from Permanent Scatterer Analysis, Science, 304: 1952-1955.

Hoffmann, J., Zebker H., Galloway D., and Amelung F., 2001, Seasonal subsidence and rebound in Las Vegas Valley, Nevada, observed by synthetic aperture radar interferometry, Water Resources Research, 37(6): 1551-1566.

Hooper, A., 2009, A Statistical-Cost Approach to Unwrapping the Phase of InSAR time Series. In Proceedings of the FRINGE 2009 Workshop, 30 November-4 December 2009, ESA ESRIN, Frascati (Rome), Italy.

Hooper, A., 2008, A multi-temporal InSAR method incorporating both persistent scatterer and small baseline approaches. Geophysical Research Letters, 35(L16302), 5p., doi:10.1029/2008GL034654.

Hooper, A., Segall, P. and Zebker, H., 2007, Persistent scatterer interferometric synthetic aperture radar for crustal deformation analysis, with application to Volcáno Alcedo, Galapagos. Journal of Geophysical Research, 112(B07407), doi:10.1029/2006JB004763.

Hooper, A., 2006, Persistent Scaterrer Radar Interferometry for Crustal Deformation Studies and Modeling of Volcanic Deformation. PhD thesis, Stanford University, 3219289, 124p.

Hooper, A., Zebker, H., Segall, P., and Kampes, B., 2004, A new method for measuring deformation on volcanoes and other natural terrains using InSAR persistent scatterer. Geophysical Research Letters, 31(L23611).

Japan Institute of Irrigation and Drainage (JIID), 1999, Water resources laws in Thailand. Bangkok: JICA, DEDP, and JIID.

Ishimaru A. 1978, Wave Propagation and Scattering in Random Media. Academic Press.

Japan International Cooperation Agency (JICA), 1995, The study on management of groundwater and land subsidence in the Bangkok Metropolitan Area and its vicinity. Report submitted to the Department of Mineral Resources. Bangkok: JICA.

Just, D. and Bamler, R., 1994, Phase statistics of interferograms with applications to synthetic-aperture radar. Applied Optics, 33(20): 4361-4368.

Kampes, B., 2006, Radar interferometry: Persistent Scatterer Technique. Earth and Environmental Science, Springer Netherlands.

Kampes, B.M., 2005, Displacement Parameter Estimation Using Permanent Scatterer Interferometry. PhD thesis, Delft University of Technology, The Netherlands.

Kampes, B., and Usai, S., 1999, Doris: The Delft Object-oriented Radar Interferometric Software. Paper presented at ITC 2nd ORS Symposium, Int. Inst. for Geoinf. Sci. and Earth Obs., Enschede, Netherlands.

Ketelaar, G., 2009, Satellite Radar Interferometry: Subsidence Monitoring Techniques. Dordrecht :Springer, The Netherlands, 270p.

Kuehn, F., Margane, A., Tatong, T. and Wever, T., 2004, SAR-Based Land Subsidence Map for Bangkok, Thailand. Zeitschrift für Angewandte Geologie, Germany.

Li, F., and Goldstein, R., 1990, Studies of multi-baseline space-borne interferometric synthetic aperture radars, IEEE Transactions on Geosciences and Remote Sensing, 28(1): 88- 96.

Loffeld, O., and Krämer, R., 1999, Phase Unwrapping for SAR Interferometry. In Proceedings of IGARSS'99, Hamburg, Germany: 1715-1717.

Lu, Z., Masterlark, T. and Dzurisin, D., 2005, Interferometric Synthetic Aperture Radar (InSAR) Study of Okmok Volcano, Alaska, 1992-2003: Magma Supply Dynamics and Post-emplacement Lava Flow Deformation, Journal of Geophysical Research, 110(B02403), doi:10.1029/2004JB003148.

Lu, Z., Fatland R., Wyss M., Li S., and Eichelberer, J., 1997, Deformation of New Trident volcano measured by ERS-1 SAR interferometry, Kalmia National Park, Alaska, Geophysical Research Letters, 24: 695-98.

Lyons, S., and Sandwell, D., 2003, Fault creep along the southern San Andreas from interferometric synthetic aperture radar, permanent scatterers, and stacking. Journal of Geophysical Research, 108(B1): 2047-2070.

Madsen, S., Zebker, H. and Martin, J., 1993, Topographic mapping using radar interferometry: processing techniques. IEEE Transactions on Geosciences and Remote Sensing, 31(1), 246-256.

Marinkovic, P., Ketelaar, G. van Leijen, F. and Hanssen, R., 2008, In-SAR quality control: Analysis of five years of corner reflector time series. In Proceedings of the FRINGE 2009 Workshop, 26-30 November 2007, ESA ESRIN, Frascati (Rome), Italy.

Massonnet, D., and Feigl, K.L., 1998, Radar interferometry and its application to changes in the earth's surface. Reviews of Geophysics, 36(4): 441-500.

Massonnet, D., Holzer T., and Vadon H., 1997, Land subsidence caused by the East Mesa geothermal field, California, observed using SAR interferometry, Geophysical Research Letters, 24: 901-904.

Massonnet, D., and Feigl, K., 1995a, Discrimination of geophysical phenomena in satellite radar interferograms, Geophysical Research Letters, 22(12): 1537-1540.

Massonnet, D., and Feigl, K., 1995b, Satellite radar interferometric map of the co- seismic deformation field of the M = 6.1 Eureka Valley, California, earthquake of May 17, 1993, Geophysical Research Letters, 22(12): 1541-1544.

Massonnet, D., Briole, P., and Arnaud, A., 1995, Deflation of Mount Etna monitored by space-borne radar interferometry, Nature, 375: 567-570.

Massonnet, D., Feigle, K., Rossi, M. and Adragna, F., 1994, Radar interferometric mapping of deformation in the year after the Landers earthquake, Nature, 369: 227-230.

Massonnet, D., Rossi, M., Carmona, C., Adragna, F., Pletzer, G., Feigle, K., and Rabaute, T., 1993, The displacement field of the Landers earthquake mapped by radar interferometry. Nature, 364: 138-142.

Massonnet, D., 1993, Radar interferometry: limits and potential. IEEE Transactions on Geosciences and Remote Sensing, 31(2): 455-464.

Ng, A.H-M., Chang, H-C., Zhang, K., Ge, L. and Rizos, C., 2009, Land subsidence monitoring in Australia and China using satellite interferometry, Observing Our Changing Earth, International Association of Geodesy Symposium (AIG), 133, Springer Berlin Heidelberg,: 743-750.

Nutalaya, P., 1981, Investigation of Land Subsidence caused by Deep Well Pumping in the Bangkok Area. Comprehensive report 1978-1981, submitted to National Environmental Board, Asian Institute of Technology, Bangkok.

Perissin, D., 2008, Validation of the Submetric Accuracy of Vertical Positioning of PSs in C-Band. IEEE Transactions on Geosciences and Remote Sensing Letters, 5(3): 502-506.

Phien-wej, N., Giao, P.H. and Nutalaya, P., 2006, Land subsidence in Bangkok, Thailand. Engineering Geology, 82: 187-201. (RTSD pers. comm., 2010)

Pletzer, G., Hudnut, K. and Feigl, K., 1994, Analysis of co- seismic surface displacement gradients using radar interferometry: new insights into the Landers earthquake, Journal of Geophysical Research, 99(B11): 21971-21981.

Prati, C., Rocca F., Monti Guarnieri, A. and Pasquali P., 1994, Report on ERS-1 SAR Interferometric Techniques and Applications, ESA report n.3-7439/92/HGE-I, Dipartimento di Elettronica-Politecnico di Milano.

Premchit, J., 1978, Analysis and simulation of land subsidence with special reference to Bangkok. Dissertation no. d37, School of Civil Engineering, Asian Institute of Technology, Bangkok, Thailand.

Price, E., and Sandwell, D., 1998, Small-scale deformations associated with the 1992 Landers, California, earthquake mapped by synthetic aperture radar interferometry phase gradients, Journal of Geophysical Research, 103: 27001-27016.

Ramnarong, V., 1999. Evaluation of groundwater management in Bangkok: Positive and negative. In Proceedings of the XXVII IAH Congress on Groundwater in the Urban Environment, ed. John Chilton, Rotterdam: A. A. Balkema: 51-62.

Ramnarong, V., Buapeng, S., Chootnatut, S., Loupensri, A., 1998. Groundwater and land subsidence crisis in Bangkok metropolitan and vicinity. Technical Report, vol. 3/1998. Department of Mineral Resources, Bangkok, Thailand.

Ramnarong, V., and Buapeng, S., 1991, Mitigation of groundwater crisis and land subsidence in Bangkok. Journal of Thai Geosciences, 2: 125–137.

Rosen, P., Hensley, S., Zebker, H., Webb, F., and Fielding, E., 1996, Surface deformation and coherence measurements of Kilauea Volcano, Hawaii, from SIR-C radar interferometry. Journal of Geophysical Research, 101: 23109-23125.

Rott, H., Nagler, T., and Rocca, F., 2003, InSAR techniques and applications for monitoring landslides and subsidence, in: T. Benes (ed.), In Proceedings of EARSeL Assembly Geoinformation for European-wide Integration, Prague, June 2002, Millpress, Rotterdam 25-31, 2003.

Saejeng, N., 2007, Application of Geographic Information System for Risk area of Land subsidence in Nakornpathom Province. M.Sc. Thesis, Mahidol University: 105.

Sandwell, D.T. and Price, E. J., 1998, Phase gradient approach to stacking interferograms, Journal of Geophysical Research, 103(B12): 30,183-30,204.

Scharroo R. and Visser, 1998, Precise orbit determination and gravity field improvement for the ERS satellites. Journal of Geophysical Research, 103(C4): 8113-8127.

Schmidt, D.A. and Burgmann, R., 2003, Time-dependent land uplift and subsidence in the Santa Clara valley, California, from a large interferometric synthetic aperture radar data set. Journal of Geophysical Research, 108(B9): 2416- 2428.

Singhroy, V., Mattar K., and Gray L., 1998, Landslide characterization in Canada using interferometric SAR and combined SAR and TM images. Advances in Space Research, 2(3): 465-476.

Spagnalini, U., 1995, 2-D Phase Unwrapping and Instantaneous Frequency Estimation, IEEE Transactions on Geosciences and Remote Sensing. 33(3): 579-589.

Stramaglia, S., Nico, G., Lovergine, F. and Guerriero, L., 1999, InSAR Phase Unwrapping Algorithm Based on Mean-Field Theory. In Proceedings of IGARSS'99, Hamburg, Germany: 1345-1347.

Strozzi, T., Tosi, L., Wegmüller,U., Werner. C., Teatini, P., and Carbognin, L., 2003, Land Subsidence Monitoring Service in the Lagoon of Venice. In Proceedings of International Geosciences and Remote Sensing Symposium, Toulouse, France.

Tarchi, D., Casagli, N., Fanti, R., Leva, D., Luzi, G., and Pasuto, A., 2003, Landslide monitoring by using ground-based SAR interferometry: an example of application to the Tessina landslide in Italy, Engineering Geology, 68: 15-30.

Teatini, P., Tosi, L., Strozzi, T., Carbognin, L., Wegmüller, U., Rizzetto, F., 2005, Mapping regional land displacements in the Venice coastland by an integrated monitoring system. Remote Sensing of Environmental, 98(4): 1-11, doi:10.1016/j.rse.2005.08.002.

Thatcher, W., and Massonnet D., 1997, Crustal deformation at Long Valley Caldera, eastern California, 1992-1996 inferred from satellite radar interferometry Journal of Geophysical Research, 24: 2519-22.

Trisirisatayawong, I., Hooper, A., Aobpaet, A., 2011, Co-seismic Displacement of 24-March-2011 Mw 6.8 Mong Hpayak Earthquake, Myanmar. In Proceeding of the FRINGE Workshop 11, 19-23 September 2011, ESA-ESRIN, Frascati (Rome), Italy.

Tsang, L., Kong J.A. and Ding K.H., 2000, Scattering of Electromagnetic Waves, Theories and Applications. Wiley-Interscience, 445 pages.

Ulaby, F.T., Moore, R.K. and Fung, A.K., 1982, Radar Remote Sensing and Surface Scattering and Emission Theory, Vol. II, Microwave Remote Sensing, Active and Passive, Addison-Wesley Publishing Company, Reading, Massachusetts, 609p.

Usai, S., Hanssen, R., 1997, Long time scale InSAR by means of high coherence features. In Proceedings of the 3rd ERS Symposium on Space at the service of our Environment, Florence, Italy, 14-21 March, European Space Agency.

van der Kooij, M., Hughes, W., Sato, S., and Poncos, V., 2006, Coherent target monitoring at high spatial density: Examples of validation results. In Proceeding of the FRINGE Workshop 05, 28 November-2 December 2005, ESA-ESRIN, Frascati (Rome), Italy.

Wadge, G., Scheuchl, B., Cabey, L., Palmer, M.D., Riley, C., Smith, A., Stevens, N.F., 2010, Operational use of InSAR for volcano observatories: experience from Montserrat. In Proceeding of the FRINGE Workshop 09, 30 November-4 December 2009, ESA-ESRIN, Frascati (Rome), Italy.

Wang, T., Perissin, D., Rocca, F., Liao, MS., 2011, Three Gorges Dam stability monitoring with time-series InSAR image analysis. China Earth Science, 25(5): 720–732. doi:10.1007/s11430-010-4101-1.

Werner, C., Wegmuller, U., Strozzi, T. and Wiesmann, A., 2003, Interferometric point target analysis for deformation mapping. In Proceedings of the International Geoscience and Remote Sensing Symposium (IGARSS), 21-25 July 2003, Toulouse, France.

Wicks, C., Thatcher, W., and Dzurisin, D., 1998, Migration of fluids beneath Yellowstone caldera inferred from satellite radar interferometry. Science, 282(5388): 458-462.

Woodhouse, I.H., 2006, Introduction to Microwave Remote Sensing. Boca Raton: CRC Press Taylor&Francis Group, 370p.

Worawattanamateekul, J., 2006, The Application of Advanced Interferometric Radar Analysis for Monitoring Ground Subsidence: A Case Study in Bangkok. Ph.D Thesis, Technical University of Munich, Germany, 169p.

Zebker, H., Amelung F., and Jonsson S., 2000, Remote sensing of volcano surface and internal processes using radar interferometry, AGU Geophysical Monograph, 116: 179-205.

Zebker, H.A., Rosen, P.A. and Hensley S., 1997, Atmospheric effects in interferometric synthetic aperture radar surface deformation and topographic maps. Journal of Geophysical Research, 102(B4): 7547–7563.

Zebker, H.A., Rosen, P.A., Goldstein, R.M., Gabriel, A., and Werner, C.L., 1994, On the derivation of co- seismic displacement fields using differential radar interferometry: The Landers earthquake. Journal of Geophysical Research, 99(B 10): 19, 617-19,643.

Zebker, H.A., and Villasenor, J., 1992, Decorrelation in interferometric radar echoes. IEEE Transaction on Geosciences Remote Sensing, 30(5): 950–959.

Zebker, H.A. and Goldstein, R.M., 1986, Topographic mapping from interferometric synthetic aperture radar observations. Journal of Geophysical Research, 91(B5): 4993-4999.

BIOGRAPHY

Anuphao Aobpaet was born in 1977 in Chumporn province, Thailand, and grew up in the town of Langsuan. In March 2000, he received B.Eng in Civil Engineering from Mahanakorn University of Technology, Bangkok, Thailand. He earned Master of Engineering (M.Eng) in Geographic Information Systems from the University of Colorado at Denver, USA., in 2005, with the master thesis entitled 'Groundwater Data Model in South Platte River Basin, Colorado', respectively. After graduated from the University of Colorado, he returned to Thailand in 2006 and joined Earth Observation Center, The Geo-Informatics and Space Technology Development Agency, Ministry of Science and Technology as the position in satellite data product generation engineer. He attended PhD. Program in Survey Engineering at Chulalongkorn University since 2007.